UNIVERSITY OF PIEMONTE ORIENTALE

Department of Translational Medicine
Ph.D. Program in Medical Sciences and Biotechnology
XXXV Cycle

Thesis for Doctoral Degree

"Characterizing the Role of Host's Immune Mechanisms in Coronavirus Pathogenesis"

Coordinator:

Prof.ssa Marisa Gariglio

Tutor(s):
Prof. Cinzia Borgogna
Prof. Vincenzo Cantaluppi

Candidate:
Dott.ssa Shikha Chandel
Matricola: 012688

Contents

SUMMARY

Coronaviruses are positive sense, single-stranded RNA viruses known to cause mild to severe respiratory diseases. The current COVID-19 pandemic has highlighted the need to identify the different molecular mechanisms and antiviral cellular host antagonists involved in the coronavirus pathogenesis. IFI16, a member of the PYHIN family, is an antiviral restriction factor known to restrict several DNA viruses like human papillomavirus, human cytomegalovirus, and herpes simplex virus type 1. Recently, its role in restricting RNA virus replication has also been established.

IFI16 belongs to a PYHIN family, which is entirely lost in bats, the only mammals capable of sustained flight, and are also a natural reservoir for several deadly viruses in the world, including coronaviruses. The evolutionary loss of the PYHIN family in bats highlights that an impaired innate immune system might be a potential explanation for their ability to host several pathogenic viruses without facing any casualties. IFI16 is abundantly present in other mammalian species. Thus, we proposed that IFI16 might have an antiviral role in coronavirus pathogenesis. We used two bat-derived coronaviruses- low pathogenic (NL63) and highly pathogenic (SARS-CoV-2) to analyze IFI16 involvement in modulating the host innate immune response in IFI16 WT and IFI16 KO-HaCaT cells.

We found an increase in the induction of innate immune response in NL63-infected IFI16 KO-HaCaT cells. However, the infection rate in HaCaT cells was insufficient to provide any conclusions. Thus, we switched to a different cell line, LLC-MK2, which is an efficient study model for studying both viruses. We noticed the induction of IFI16 upon both NL63 and SARS-CoV-2. We also observed that NL63 dampens the innate immune response in LLC-MK2 cells.

Moreover, we have identified the nuclear to cytoplasmic localization of IFI16 and its co-localization with the NL63 nucleoprotein. However, the antiviral role of IFI16 in this context is yet to be established. We are currently working on characterizing these experiments in the newly established IFI16KO-LLC-MK2. IFI16 is a crucial regulator for identifying and responding to invading pathogens and maintaining a homeostatic balance of host cells. Deepening our understanding of IFI16's involvement in triggering abnormal inflammatory reactions in hCoV-infected human epithelial cells can help develop novel therapeutic approaches for hCoV-related disease pathologies.

1. INTRODUCTION

1.1 Coronaviruses

1.1.1 Background

Coronaviruses are RNA viruses widely distributed among humans and other animals and are known to cause acute and persistent respiratory infections (Xin, Hayes, Susanna, & Patrick, 2019). Members of this family were isolated in the early 1930s for causing infectious bronchitis in chickens, transmissible gastroenteritis in pigs, and severe hepatitis and neurological diseases in mice. In the 1960s, it was identified that these and specific human respiratory viruses had shared characteristics that merited them to be together in the same group (Masters & Perlman, 2013). The most distinctively common feature of these viruses, uncovered by electron microscope, was a widely spaced, club-shaped spike protruding from the surface of the virion. Morphologically these spikes were different from the surface projections of ortho- and paramyxoviruses. The ring-like appearance of viral points was depicted as the appearance of the solar corona, prompting the name given to this new virus group (Almeida et al., 1968).

Coronaviruses were mainly studied because they provide unique models for viral pathogenesis and cause the significant economic burden of respiratory and gastrointestinal diseases in domestic animals. In humans, two coronaviruses, 229E and OC43, were known to cause substantial cases of the common cold (Masters & Perlman, 2013). However, the situation changed dramatically in 2002 with the severe acute respiratory syndrome (SARS) in southern China, a devastating new human disease caused by a hitherto unknown coronavirus (Drosten et al., 2003).

The rapid spread of SARS caused a global pandemic, leading to more than 8000 confirmed cases with a mortality rate of 10% (Xin, Hayes, Susanna, & Patrick, 2019). Although the SARS pandemic ended in 2003, the viral outbreak stimulated the research in understanding coronaviruses, which by 2005 led to the discovery of two additional widespread human coronaviruses, NL63 (Van der Hoek et al., 2004) and HKU1 (Woo, et al., 2005), which caused mild, self-limiting upper respiratory infections with occasional cases of lower respiratory infections in humans.

Almost a decade after the SARS outbreak, a Middle East respiratory syndrome coronavirus (MERS-CoV) appeared around 2012 in the Arabian Peninsula, a highly fatal human pathogen with an even higher mortality rate of approximately 40% (Xin, Hayes, Susanna, & Patrick, 2019). In December 2019, a new SARS-like human coronavirus named SARS-CoV-2 was detected in Wuhan, Hubei Province, China, responsible for causing COVID-19 disease. The

timeline of discovering different human coronaviruses is shown in Fig.1. With the rapid spread of the virus in China and internationally, the world health organization (WHO) announced SARS-CoV-2 as a pandemic on March 11, 2020 (Kesheh, Hosseini, Soltani, & Zandi, 2022). Since 2004, significant breakthroughs have been seen in the zoonotic origins of SARS and MERS research. Soon after the pronouncement of COVID-19 as a global pandemic, coronavirus research took a revolutionary turn in understanding viral pathogenesis, prevention, and treatment.

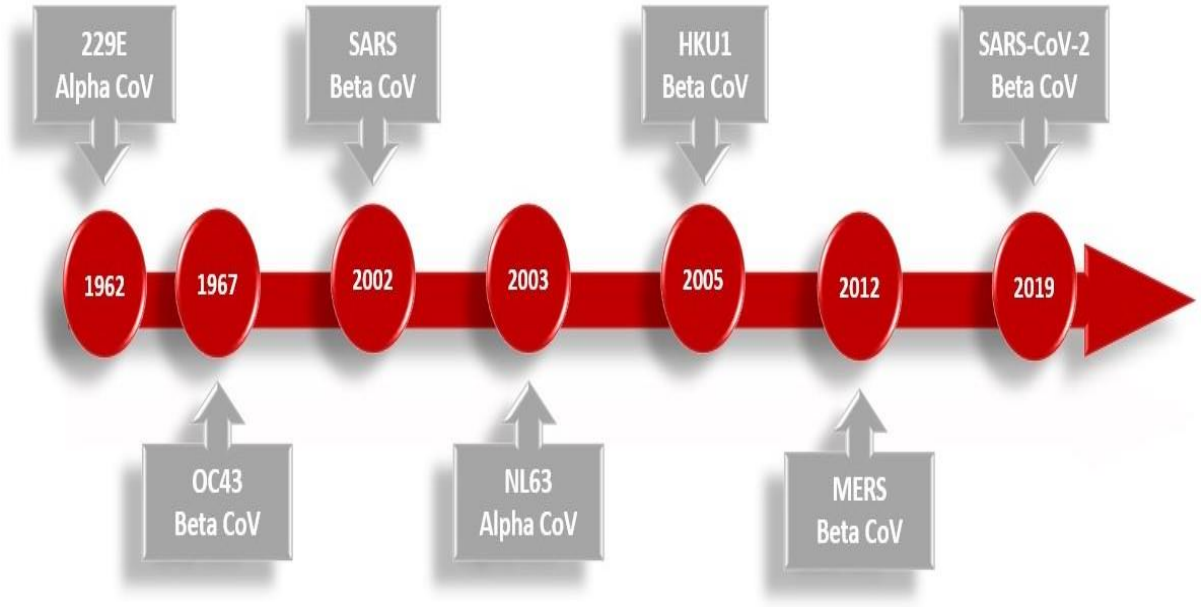

Fig.1. Timeline of coronaviruses discovered in human history. 229E was the first identified coronavirus capable of infecting humans. OC43 was the second identified hCoV. SARS was the first highly pathogenic hCoV which triggered the research in coronaviruses and led to the identification of NL63 and HKU1. After seven years, another coronavirus occurred in the middle east, a novel coronavirus named MERS. In 2019, another novel coronavirus called SARS-CoV-2 was found that caused COVID-19 pandemic (Image source Biorender)

Due to the inherently high mutation rate and high recombination frequency, coronaviruses establish quick adaptations to new host receptors, which enables them to overcome the interspecies barrier. Epidemiologists predict that in the future, there will likely be another spillover event that will impose a threat to public health. Despite the global collaborations and advancements made in healthcare because of the COVID-19 pandemic, there are still limited

therapies and preventive strategies like vaccines and antivirals for such emerging zoonotic pathogens, thus, leaving fewer treatment options for fatal human infections. The ongoing COVID-19 pandemic and the continuation of the existing gap in therapeutic and preventive options for coronavirus-related infections initiated the research concept of this project which focuses on identifying the underlying host innate immune mechanisms upon coronavirus infection.

1.1.2 Classification and general features

Coronaviruses are the largest virus group within the order of *Nidovirales* in the family *Coronaviridae, Arteriviridae, and Roniviridae* (Masters & Perlman, 2013). They are highly conserved in genomic organization and comprise a 3' nested sub-genomic mRNA. The *Coronaviridae* family is grouped into two subfamilies, i.e., *Coronavirinae* and *Torovirinae*. Based on their phylogenetic characteristics, the *Coronavirinae* subfamily is categorized into four genera-*Alphacoronavirus, Betacornavirus*, *Gammacornavirus,* and *Deltacoronavirus.* The *Betacoronavirus* is further classified into five lineages: *Embecovirus, Sarbecovirus, Merbecovirus, Nobecovirus,* and *Hibecovirus* (Xin, Hayes, Susanna, & Patrick, 2019). Only *alphacoronaviruses* and *betacoronaviruses* are mammalian, while *gammacoronaviruses* and *deltacoronaviruses* are avian viruses, but some are capable of infecting mammals (Cui, Li, & Shi, 2019). A phylogenetic relationship of human coronavirus is shown in Fig.2.

Coronaviruses can be either highly pathogenic or low pathogenic, depending on their infectivity. hCoVs like 229E, NL63, OC43, and HKU1 infect the upper respiratory tract, cause mild to moderate respiratory infections in healthy individuals, and are considered low pathogenic. On the other hand, SARS-CoV, MERS-CoV, and SARS-CoV-2 are categorized as highly pathogenic because these CoVs infect the lower respiratory tract, cause fatal illnesses like acute lung injury (ALI), severe pneumonia, or acute respiratory distress syndrome (ARDS), causing high morbidity and mortality rate in infected individuals (Chen, et al., 2020).

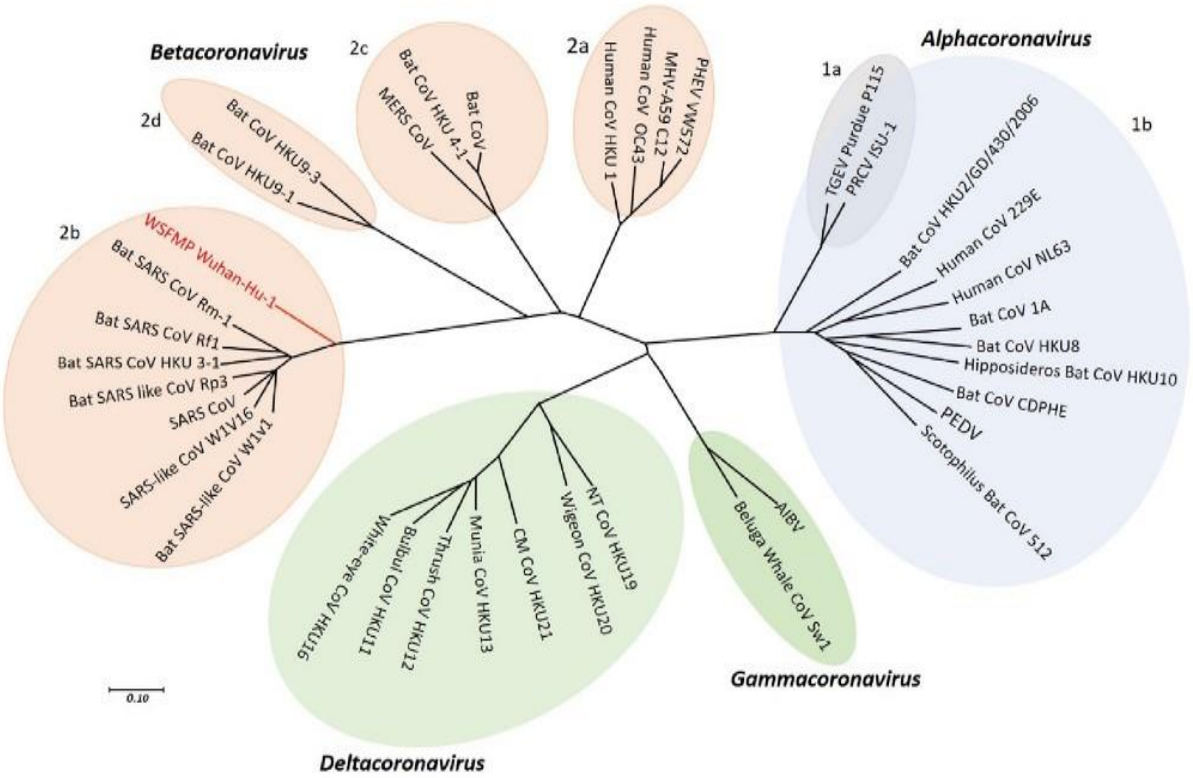

Fig.2. Phylogenetic relationship of coronaviruses. The viruses are grouped into four genera. Aplhacoronavirus (blue), betacoronavirus (peach), gammacoronavirus (olive green), and deltacoronavirus (light green). Each group is clustered into subgroups- 1a and 1b (alphacoronavirus) and 2a, 2b, 2c, and 2d (betacoronaviruses). The image is adapted from Shereen, Khan, Kazmi, Bashir, & & Siddique, 2020)

1.1.3 Origin and evolution of human coronaviruses

Most human and animal coronaviruses have originated from different bat species. Recent advancements in coronavirus research identified that bats harbor more than 200 novel coronaviruses (Banerjee, Kulcsar, Misra, Frieman, & Mossman, 2019). Except for hCoV-HKU1 and OC43, NL63, 229E, SARS, MERS, and SARS-CoV-2 have bats as their natural host, where all the hCoVs are supposedly transmitted through an animal-to-human spillover event using intermediate animal hosts (Fig.3) (Islam, et al., 2021). hCoV-229E, OC43, NL63, and HKU1 are endemic viruses contributing to 1/3rd of the common cold and mild to moderate respiratory illness globally for over five decades.

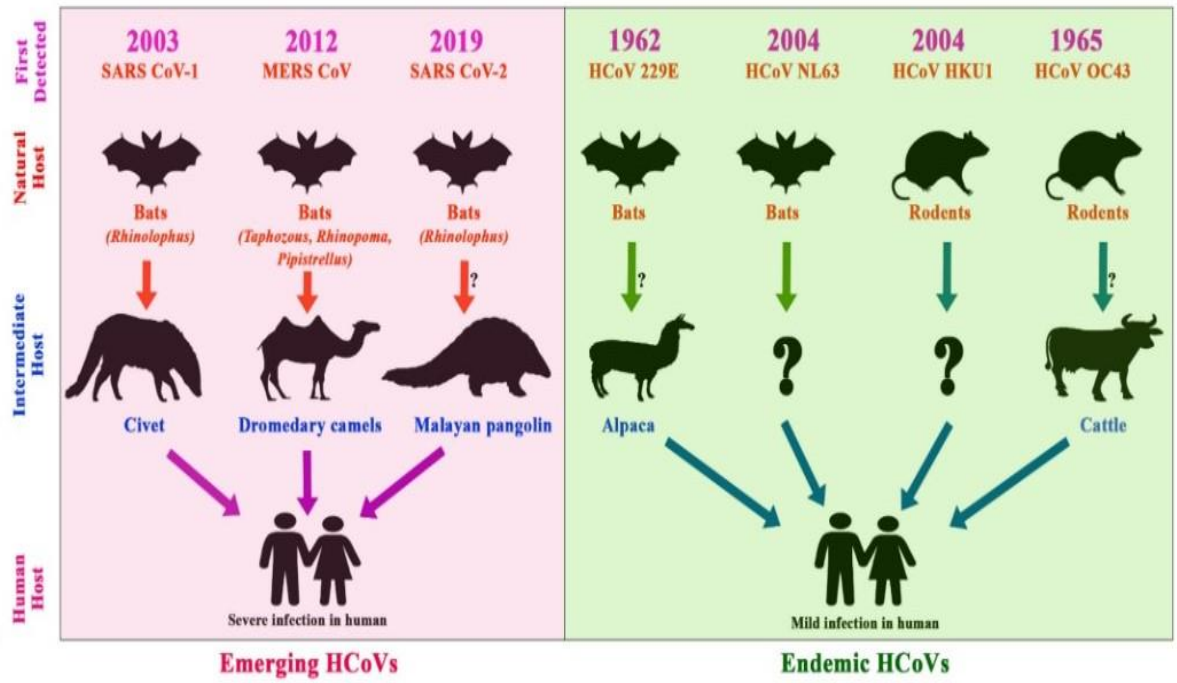

Fig.3. The emergence of human coronavirus and spillover mechanisms. Arrows show the viral transmission route from animal to human through intermediate hosts (Adapted from Islam, et al., 2021)

Before the emergence of SARS, coronaviruses were not considered highly pathogenic to humans. After SARS-CoV-2, a newly emerged coronavirus responsible for COVID-19 diseases that infected more than 630 million people with >6.5 million deaths globally (World Health Organization, 2022), coronaviruses are now considered a threat to public health. The genomic sequence analysis of the large number of newly identified CoVs indicates a high diversity based on phylogenetic and evolutionary rates, highlighting their potential to cross interspecies barriers (Miranda, Silva, Igrejas, & Poeta, 2021). There is a high likelihood of future zoonotic outbreaks like COVID-19. Therefore, understanding the molecular mechanisms of coronavirus pathogenesis and the innate immune response is essential to prevent adverse outcomes from such events.

1.1.4 Coronavirus structure and genome organization

The coronavirus virions are ~120nm in diameter, roughly spherical, and moderately pleomorphic. They comprise four structural proteins- Spike (S), envelope (E), Membrane (M),

and Nucleocapsid (N) (Fig.4), which are essential in viral replication and maintaining viral structure (Xin, Hayes, Susanna, & Patrick, 2019).

S-protein is a large transmembrane trimeric globular protein (Beniac, Andonov, Grudeski, & Booth, 2006) ranging from 3.5- 4.7 kbps, generally described as club or petal-shaped. It emerges from the virion surface like a stalk with a bulb-like distal terminus and gives characteristic crown-like morphology to the virion. Spike is heavily N-glycosylated and comprises two functionally distinct subunits, i.e., N-terminal S1 and C-terminal S2 domains, which facilitate receptor binding and viral entry (Li, Luk, Lau, & Woo, 2019). The S-protein is highly variable at the amino acid and nucleotide levels.

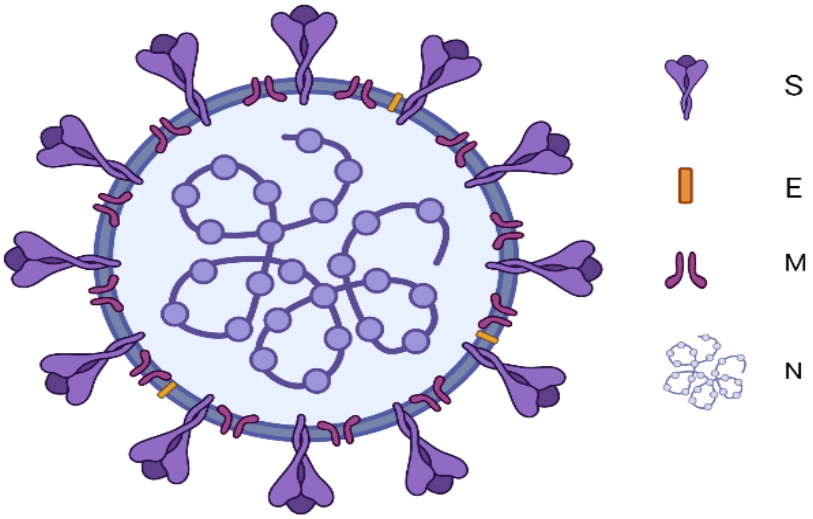

Fig.4. Schematic illustration of the structure of coronavirus virion. S-spike, E-envelope, M-membrane, and NP- nucleocapsid protein (Image source Biorender)

E-protein is a small polypeptide, 0.2 kbps, found in small amounts in the viral envelope. E-protein is present in all wild-type coronaviruses. Although it is not essential, however, is critical for viral infection (Deng & Baker, 2021).

M-protein is moderately conserved in all coronavirus genera. It is an integral glycoprotein, size 0.6-0.7 kbps, and is the highly abundant structural protein in the viral envelope. Both M and E-proteins play a role in viral assembly and determining the shape of the viral envelope (Deng & Baker, 2021).

N-protein is 1.1-1.3 kbps in size, resides inside the virion, is heavily phosphorylated, and is the only protein constituent of the helical nucleocapsid. The N-protein plays a protective role in viral genome packaging and ensures timely replication and effective transmission (Otieno, Cherry, Spiro, Nelson, & Trovao, 2022). Some *betacoronaviruses* have a fifth structural protein called hemagglutinin esterase (HE), which acts as a co-factor to spike and assists in viral attachment to the host cell. It is not essential for *in vitro* viral replication; however, it might affect *in vivo* production of infectious virions and viral tropism.

The coronavirus genome is a positive sense, single-stranded RNA, approximately 26-32kb in size. Coronaviruses contain a 5'-cap structure and 3'-poly(A) tail and are the largest among all RNA viruses (Lee, et al., 2021). The genome of all coronaviruses follows a similar order- downstream to the 5'-2/3rd of the genome comprises leader sequence and open reading frames 1a/b (ORF1a/b). The 3'-1/3rd of the genome contains a nested set of subgenomic RNA, encoding structural proteins (S-E-M-N) and accessory proteins (Fig.5). The coronavirus genome includes untranslated regions (UTRs) next to 5' and 3' ends. A standard transcriptional regulatory sequence (TRS) is present at the beginning of each structural and accessory protein gene (Li, Luk, Lau, & Woo, 2019).

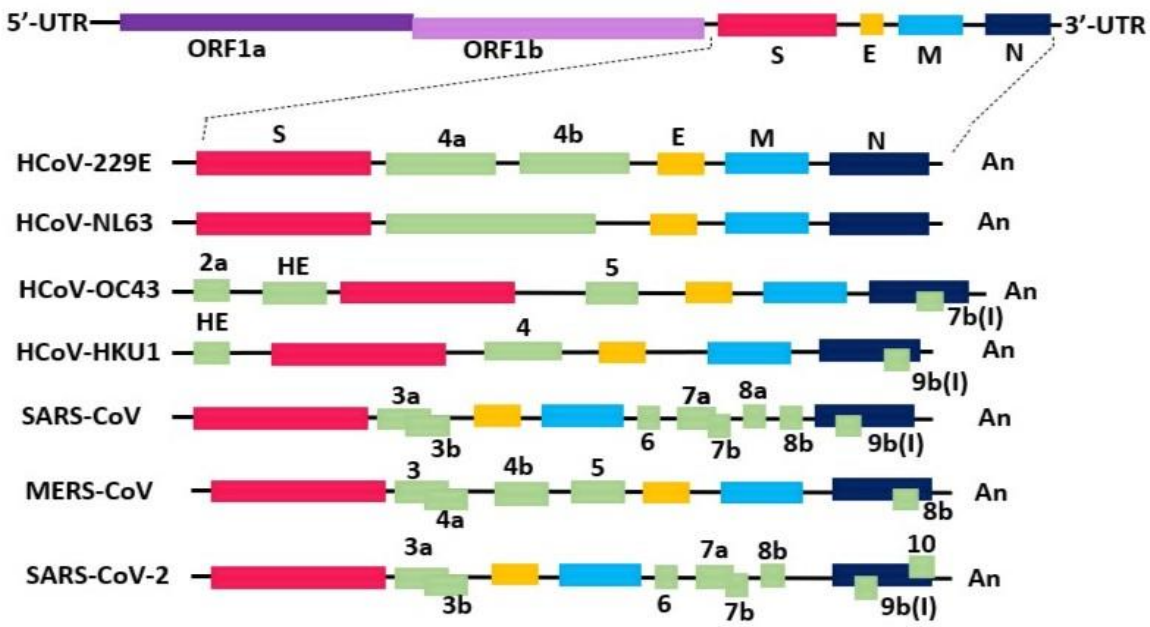

Fig.5. A schematic representation of the complete genome of seven different human coronaviruses (hCoVs). The replicase gene comprises two open reading frames (ORFs)- 1a and 1b. The extended regions downstream show the genome of two alphacoronaviruses (299E and NL63) and five betacoronaviruses (OC43, SARS, MERS, and SARS-CoV-2). Relative to

the basic genes-spike (S), envelope (E), membrane (M), and nucleocapsid (N), the sizes and positions of accessory genes are shown.

The translation of ORF1a/b encodes two co-peptides, i.e., pp1a and pp1ab, which are cleaved by self-encoding proteases to form 16 non-structural proteins (nsps), which associate together to form replicase-trasncriptase complex (RTC). The RTC amplifies the genomic RNA (gRNA) and synthesizes sub-genomic mRNAs. Besides that, the 3'-end contains additional ORFs designated to encode a variable number of accessory proteins, depending on the virus genus (Forni, Cagliani, Clerici, & Sironi, 2017). These accessory proteins are non-essential for *in vitro* viral replication but allegedly serve a modulatory role in unfolded protein response (UPR), DNA synthesis, cellular apoptosis, and innate immunity interactions.

1.1.5 Coronavirus lifecycle

Coronaviruses employ several host factors to infect a cell, whose expression patterns determine the viral tropism. Viral replication inside a cell (Fig.6) depends on multiple strategies incorporated by the virus to ensure virion attachment, membrane fusion, genome replication, assembly, and virion release (Malone, Urakova, Snijder, & Campbell, 2022). Successful completion of the viral life cycle inside a cell extensively relies on host infrastructure and metabolism.

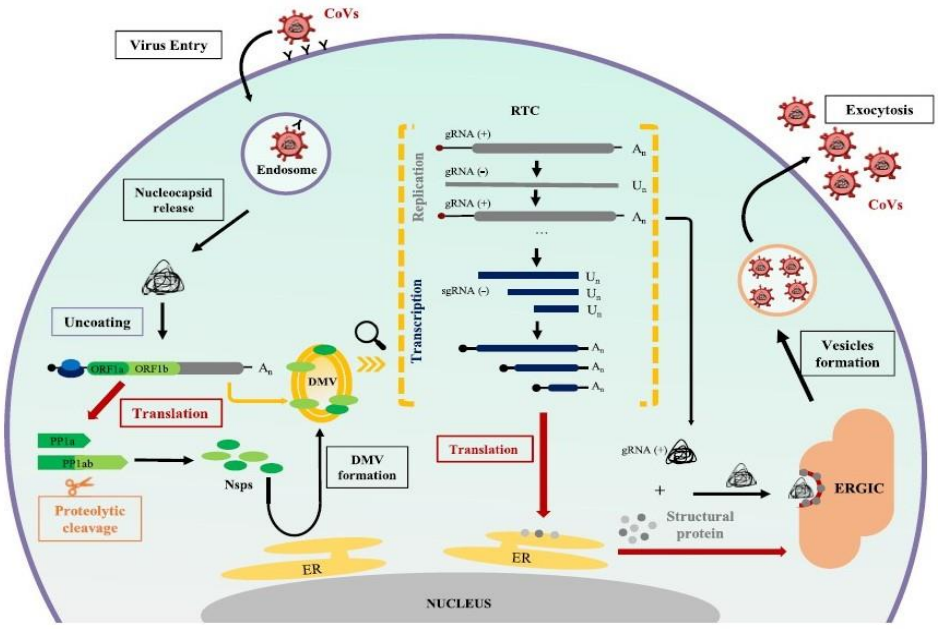

Fig.6. An overview of the coronavirus lifecycle. A spike-mediated attachment to host cell receptors allows the viral particle entry into the cell, followed by the uncoating of gRNA

undergoing direct translation in the cytoplasm forming 16 non-structural proteins (nsps) required for proteolytic cleavage, viral replication transcription complex (RTC) formation, and mRNA translational control. The double membrane vesicles (DMV), derived from the endoplasmic reticulum (ER), support the genomic replication and transcription of sgRNAs. Viral assembly (gRNA and structural proteins) occurs at ERGIC, and the newly synthesized virons exit the cell by exocytosis (Adapted from de Breyne, et al., 2020).

Virion entry and membrane fusion: The coronavirus interaction between the host cell and virion initiates with the attachment of viral S protein to specific cellular receptors. The viral Spike protein and host receptor interaction determine the species range and tissue tropism. The S1 subunit of S proteins plays an essential role in spike-mediated protein binding to the host receptors. Among coronaviruses, the S1 subunit is highly variable and thus is partly responsible for the dynamic host range (Walls, et al., 2017). Coronaviruses display complex patterns in receptor recognition, and diversity in receptor deployment is their prominent feature (Li F. , 2016). Different cellular receptors for human coronaviruses are orderly listed in Table 1.

Following the receptor binding, viral transmembrane fusion proteins called fusogen mediate fusion among the viral envelope and host cell membrane. Generally, depending on the structure, there are four classes of viral-membrane fusion proteins- class I, class II, class III, and class IV. Class I is rich in α-helix prefusion trimers, and class II is rich in β-sheet prefusion homo or hetero-dimers. On the other hand, class III is a combination of both α-helix and β-sheet prefusion fusogen, while class IV fusion is a cell-cell, viral-encoded, small fusion protein, oligomerizing to fuse membranes (Podbilewicz, 2014). The S protein of coronaviruses is a class I fusion protein with functional similarity to other RNA viruses like HIV, Ebola, and influenza, requiring protease cleavage for fusion activity. Host proteases like transmembrane proteases/serine sub-family member 2 (TMPRSS2), cathepsin B, cathepsin L, furin, trypsin, and elastase are known to be involved in the cleavage of coronavirus S protein (Kirchdoerfer, et al., 2016).

Table 1. Cellular receptors for pathogenic human coronaviruses.

Viruses	**Receptor**	**Reference**
229E	Human aminopeptidase N (APN.)	(Artika, Dewantari, & Wiyatno, 2020)

NL63	Heparan sulfate proteoglycan and Angiotensin-converting Enzyme 2 (ACE2)	(Hofmann, et al., 2005)
HKU1	9-O-Acetylate sialic acid (9-O-Ac-Sia)	(Gaunt, Hardie, Class, Simmonds, & Templeton, 2010)
OC43	9-O-Acetylate sialic acid (9-O-Ac-Sia)	(Masters & Perlman, 2013)
SARS-CoV	Angiotensin-converting Enzyme 2 (ACE2)	(Li F. , 2016)
MERS-CoV	Dipeptidyl peptidase 4 (DPP4)	(Raj, et al., 2013)
SARS-CoV-2	Angiotensin-converting Enzyme 2 (ACE2)	(V'kovski, Kratzel, Steiner, Stalder, & Thiel, 2021)

Membrane fusion, an essential event in the coronavirus lifecycle, occurs after receptor binding. Depending on the protease availability, the virus entry and membrane fusion can occur through two routes, i.e., early and late pathways. The virus can fuse through an early pathway if plasma membrane fusion proteases are available. Exogenous, membrane-bound proteases like furin or TMPRSS2 can stimulate an early fusion pathway, while clathrin and non-clathrin-mediated endocytosis of coronaviruses lead to a late fusion pathway in the absence of plasma membrane proteases. Notably, membrane fusion is a non-spontaneous process requiring high energy to bring membranes together, and viral fusion protein plays an essential role as a catalyst providing the energy required in this process (Tang T. , Bidon , Jaimes, Whittaker, & Daniel, 2020).

Genome replication: It is the most vital part of coronavirus biology. As the largest group of RNA viruses, coronaviruses require an RNA synthesis machinery for their RNA replication, achieved by employing complex mechanisms that include several proteins encoded by both the cellular host and the viral genome. Coronaviruses encompass evolutionary conserved genomic sequences encoding proteins essential for viral replication and expression. The proteins like RNA-dependant R.N.A. polymerases (RdRp), chymotrypsin-like proteases, RNA helicases, metal binding proteins, and papain-like proteases are conserved sequence motifs encoded by genes located in ORF1 in the 5'-end of the coronavirus genome *(Artika, Dewantari, & Wiyatno, 2020)*.

After the viral attachment and membrane fusion, the viral nucleocapsid is released to the host cell cytoplasm through an uncoating process and initiates the replication cycle. The

positive (+) stranded viral genome serves as mRNA to start the synthesis of the complementary negative (-) strand, which is further used as a template to synthesize another (+) stranded RNA template through continuous transcription. In the continuous transcription, ORF1ab translates into pp1a and pp1b, which through proteolytic cleavage, forms 16 nsps, leading to the formation of RTC.

Additionally, coronaviruses, through a discontinuous transcription process, synthesize multiple short (-) stranded RNA, which serve as a template to synthesize numerous (+) stranded sub-genomic RNA (sgRNA), encoding structural (S, E, M, and N) and other accessory proteins (Chen, et al., 2020). Most RNA viruses replicate in the host cytoplasm and have no access to host polymerases. Thus, the viruses encode their own polymerase, which is essential to their transcription and replication. For RNA viruses, RdRp is the most conserved and essential component of the viral replication machinery (Gaurav & Al-Nema, 2019).

Virion assembly and release: A common feature of (+) RNA viruses is their RTC assembly, closely associated with forming membrane rearrangements to develop virus replication organelle. The RTCs are interconnected, double-membrane vesicles (DMVs) obtained from the endoplasmic reticulum (ER), providing the environment for effective transcription and translation (Doyle, Hawes, Simpson, Adams, & Maier, 2019). Most enveloped virus assembly occurs at the host cell plasma membrane; however, for coronaviruses, virus assembly and budding occur at the endoplasmic reticulum-Golgi intermediate compartment (ERGIC). An intracellular trafficking signal transports M, E, and S proteins to the assembly site. The efficiency of viral protein integrating into coronavirus virion depends on protein trafficking and protein-protein interaction at ERGIC (Woo, Lee, Lee, Kim, & Cho, 2019).

The coronavirus M protein is the central organizer for virion formation and mediates most of the protein-protein interactions required for viral assembly. The N protein plays a fundamental role in viral self-assembly, where its prime function is to form helical ribonucleocapsid from the viral genome. The cis-regulatory protein element called packaging signal (PS) encoded in the viral RNA plays a role in packaging the viral genome into ribonucleocapsid. After encapsulation of the viral genome, all the structural proteins assemble to form a mature virion which is then transported to the cell surface and released into extracellular space through cell lysis or exocytosis (Fehr & Perlman, 2015).

1.2 NL63

NL63, first isolated in 2004 from a 7-month-old infant with bronchiolitis (Hoek, et al., 2004), is an alphacoronavirus known to cause comparatively severe respiratory infections such as pneumonia and bronchitis in young children (Fielding, 2011). Generally, 10-15% of all upper respiratory tract infections are caused by coronaviruses, accounting for significant hospitalization (Carbajo-Lozoya, et al., 2014). The NL63 infection, in most cases, only involves the upper respiratory tract. It causes mild symptoms like fever, cough, sore throat, and rhinitis. However, it can also cause severe clinical infections in children younger than 18, immunocompromised individuals and elderly (Hoek, Pyrc, & Berkhout, 2006).

Research on international studies suggests that NL63 is responsible for causing 1-10% of acute respiratory diseases (Abdul-Rasool & Fielding, 2010). This number might be an underestimation because diagnostic tests for hCoV screening are infrequent. Notably, NL63 can co-infect with more respiratory viruses like respiratory syncytial virus (RSV), influenza A, and parainfluenza virus. Around 11-41% of coronavirus-detected samples were positive for other respiratory viruses (Carbajo-Lozoya, et al., 2014). NL63 and two other "common cold" coronaviruses (229E and OC43) are responsible for causing 10-30% of yearly common cold cases during the winter season (Pyrc, Berkhout, & van der Hoek, 2007).

The NL63 is a capped, polyadenylated, single-stranded RNA genome of 27.55 kb. It shares genetic similarities with other members of the coronavirinae subfamily. As discussed previously, the NL63 lifecycle is like other coronaviruses with shared genetic similarities. Despite that, a detailed analysis of NL63 has revealed some unique features. For instance, unlike other alphacoronaviruses that use aminopeptidase N to gain access inside cells, NL63 utilizes the metallocarboxyl peptidase angiotensin receptor 2 (ACE2), the same receptor used by some *betacoronaviruses* (including SARS-like CoVs) (Pyrc, Jebbink, Berkhout, & Hoek, 2004).

ACE2 is a type I membrane protein, a homolog of the ACE protein, and is a critical enzyme of the renin-angiotensin system (RAS) that controls blood pressure (Hofmann, et al., 2005). Being a negative regulator of the RAS system, ACE2 inactivates angiotensin II and acts as an antagonist of ACE functions by degrading Ang II and its consequent vasoconstrictive effects. The presence of ACE2 in the lung, heart, kidneys, and intestine explains the critical aspect of SARS-CoV tropism and the likelihood of its central role in spreading infection. However, whether the virus interaction with ACE2 is associated with disease induction is unclear (Hu,

Liu, & Lu, 2021). Thus, understanding the viral pathogenesis of a low pathogenic NL63 that utilizes the same receptor as highly pathogenic SARS might shed some insights into this question.

The NL63 infection process initiates after the virus binds to the cellular membrane via heparan sulfate proteoglycans (Milewskaa, et al., 2018), facilitating the spike protein-mediated recognition and interaction with the entry receptor ACE 2 (Li, et al., 2007). The viral glycoprotein specificity to its receptors determines the cell types that can be infected, and the variety of permissive cells directs the outcome in viral pathogenesis. NL63 employs the same cellular receptor and infects the same target cells as SARS-CoV (Milewskaa, et al., 2018). However, NL63 induces a mild to moderate effect compared to its highly pathogenic counterpart.

On the contrary, NL63 infection in infants and immunocompromised adults causes severe respiratory tract infections (RTI), suggesting its potential to be pathogenic in a weakened immune system. Possibly, NL63 lacks a specific pathogenicity factor, which is present in other highly pathogenic CoVs. This pathogenic factor might be encoded by one or more accessory genes found in SARS-CoV, while only one accessory gene exists in the NL63 genome (Hofmann, et al., 2005). Although the function of human coronavirus accessory genes is not entirely recognized, they might play a role in determining viral replication and pathogenicity.

Another possible explanation for apparent differences in pathogenicity could be the interaction with ACE2. The NL63 S protein binds to ACE2 with lesser affinity than the SARS-CoV S protein. Researchers have already identified the amino acid residues essential for interaction in SARS-CoV (Mathewson, et al., 2008). In NL63, it was discovered that the N-terminal region of S protein, corresponding to the receptor-binding domain (RBD), contains a unique 179 amino acids domain that is not present in other coronaviruses. It represents the most variable region of the NL63 genome and is likely to have a role in immune evasion (Pyrc, Berkhout, & van der Hoek, 2007) (Hoek, et al., 2003).

Considering the differences in amino acid residues, which might be responsible for differential binding affinity to ACE2 in NL63 and SARS-CoV, it is fair to say that spike protein might play a partial role in virus-induced pathogenicity. In this regard, the variants of NL63 that binds with higher affinity to ACE2 and cause severe diseases can evolve and mutate, given the continued existence of NL63 in human populations, highlighting a possible threat to public

health. Therefore, understanding the pathogenic behavior of NL63 and identifying the different innate immune markers in viral sensing is essential to develop future antiviral treatments and therapies against coronaviruses.

1.3 SARS-CoV-2

SARS-CoV-2 is a *betacoronavirus* that shares 79% genome sequence identity with SARS-CoV and 50% with MERS-CoV but causes comparatively milder infection and has a lower mortality rate (Lu, et al., 2020). Unlike MERS and SARS, which were mainly associated with nosocomial spread, SARS-CoV-2 transmits at a much broader rate within the community (Petrosillo, Viceconte , Ergonul, Ippolito, & Petersen, 2020).

The phylogenetic analysis of the novel coronavirus revealed that despite having bats as a common wild reservoir, SARS-CoV-2 underwent a different evolution route than SARS and MERS. Genomic comparison among SARS and SARS-CoV-2 has revealed that there are 27 different mutations in the genes encoding for viral Spike protein, responsible for receptor binding and cellular entry, which might be a possible explanation for the lower pathogenicity of SARS-CoV-2 (Petrosillo, Viceconte , Ergonul, Ippolito, & Petersen, 2020).

The SARS-CoV-2 mediated clinical manifestations and lethality of infection are highly variable and depend on many factors, including patient age and comorbidities such as diabetes and hypertension. In most cases, infected individuals remain asymptomatic or manifest influenza-like symptoms such as fever, sore throat, weakness, olfactory and taste dysfunction, and headache. The case fatality rates are highest among 80 years or older and lowest among 0-9 years. People older than 80 have a twenty times higher risk of COVID-19-related mortality than 50-59 years old (Bickler, et al., 2021). About 10-15% of infected persons without early treatment develop a severe disease, which might become lethal in critical cases (Martellucci, et al., 2020).

The SARS-CoV-2 genome is approximately 30 kb long and follows the same genomic order as other coronaviruses. Like SARS-CoV and NL63, SARS-CoV-2 also uses ACE2 as a receptor to gain cellular entry. After receptor binding, the virions enter the cell through fusion at the cellular or endosomal membrane, depending on the available host proteases. The virus entry occurs through early or late fusion pathways. The transmembrane serine protease 2 (TMPRSS2) dependent cleave of S protein triggers the viral entry at the cellular membrane

through early fusion. In contrast, endocytic internalization of the virus occurs through late fusion pathways where cathepsin L cleaves the viral spike protein in the endosome to initiate the genome release in the cytoplasm (Tang T. , Bidon, Jaimes, Whittaker, & Daniel, 2020).

The variation in the cellular protease activity can modulate the relative efficiency of SARS-CoV-2 entry in ACE2-expressing cells. However, this feature is not present in NL63, where viral entry is not dependent on cathepsins' activity (Huang, et al., 2006). In SARS, it is well established that the favorable mutations in the RBD of S-protein strengthen its receptor binding affinity and thus increase pathogenicity. The scenario was assumed to be the same in SARS-CoV-2, but there were no amino acid substitutions in RBD interacting directly with ACE2. On the contrary, there were six mutations seen in SARS-CoV-2 RBD. Analysts predict that a single nucleotide mutation in the SARS-CoV-2 RBD, if occurred, can enhance the viral pathogenicity (Bickler, et al., 2021).

Considering the status of SARS-CoV-2, which continues to circulate and infect the human population, researchers believe in three possible scenarios for its future. First, the ongoing manifestations of the severe disease combined with high levels of infection could foster further evolution of the virus. Second, it could transition to a seasonal epidemic disease such as influenza. Third, it could transition to an endemic disease like other human coronavirus infections with a much lower disease impact than influenza or SARS-CoV-2 (Telenti, et al., 2021).

Over the last two decades, three coronavirus spillover mechanisms have occurred, increasing the likelihood of a future pandemic being an RNA virus, most likely a coronavirus. The COVID-19 pandemic has implicated the need to study the role of the innate immune system and viral escape mechanism in coronavirus pathogenesis to provide preparedness for such an event, if it happens, in the future to prevent the likelihood of adverse outcomes from the disease burden.

1.4 Host-Pathogen Interactions and Immune Defense Mechanisms

Host-pathogen interaction is a highly dynamic process commencing between microbial pathogens and cellular hosts during all stages of infections, from pathogenic invasion to its spread (Jo, 2019). Upon pathogenic infiltration, the innate immune system reacts to pathogen-associated molecular patterns (PAMPs) and initiates immediate host inflammatory and antimicrobial defense (Beutler, 2004). Innate immune cells activate sophisticated intracellular

signaling pathways through innate immune receptors comprising membrane-bound or cytosolic receptors (Akira, Uematsu, & Takeuchi, 2006). Host innate immune activation triggers the induction of numerous effector molecules, involving cytokines, chemokines, and anti-microbial proteins, to fight against invading pathogens and parasites (Kawai & Akira, 2010).

After receptor-mediated entry into the cells, coronaviruses encounter different innate immune defenses and activate the adaptive immune system components. Innate immunity offers the first line of protection against foreign invasions through antigen-nonspecific mechanisms, while adaptive immunity is target-specific, providing antibody-mediated or T-cell-mediated defense (Mueller & Rouse, 2008). This project was partly involved in characterizing the persistence of neutralizing antibodies (immunological memory, a cardinal defense feature of adaptive immunity) among the SARS-CoV-2 infected and recovered individuals, which is successfully published and discussed in 2.1 PART-A (Published Results). However, the primary aim of this project is to characterize the innate immune mechanisms and the host-pathogen interactions against NL63 and SARS-CoV-2 infection in epithelial cells. Therefore, this section mainly discusses the host's innate immune response against coronavirus infection and viral invasion mechanisms.

Adequate activation of innate immunity depends on “pathogen-associated molecular patterns (PAMPs) or damage-associated molecular patterns (DAMPs)” identification by pattern recognition receptors (PRRs). PAMPs are conserved molecular structures exclusively expressed by microbes, while DAMPs are molecules released from cells upon inflammation or infection (e.g., uric acid, ROS, heat shock proteins, DNA, RNA) (Turvey & Broide, 2010). Different immune cells such as dendritic cells, epithelial cells, macrophages, monocytes, and neutrophils express PRRs like Toll-like receptors (TLRs), nucleotide-binding oligomerization domain- (NOD-) like receptors (NLRs), retinoic acid-inducible gene- (RIG-) I-like receptors (RLRs), and AIM2-like receptors (ALRs) (Akira, Uematsu, & Takeuchi, 2006).

Upon recognition by either PAMP or DAMP, PRRs recruit adaptor proteins to initiate multiple kinase-dependent complicated signaling pathways, leading to downstream activation of essential transcription factors and promoting the production of type I/III interferons (IFNs). These IFNs induce an antiviral state by producing several interferon-stimulating genes (ISGs) to antagonize viral replication (Fung & Liu, 2019). Type-I IFNs are essential in initiating the

host antiviral response and are activated by two significant pathways-RLRs and TLRs. TLR3, 7, and 8 can sense single- and double-stranded RNA in endosomal compartments, and cytoplasmic RLRs- melanoma differentiation-associated gene 5 (MDA5) and RIG-I, recognize intracellular non-self RNAs possessing specific patterns of secondary structures or biochemical modifications (Kasuga, Zhu, Jang, & Yoo, 2021).

TLRs utilize two adaptor proteins, MyD88 (myeloid differentiation primary response 88) and TRIF (TIR-domain-containing adapter-inducing IFN-β), for signal transduction. On the other hand, RLRs first undergo conformational changes to expose their caspase activation and recruitment domains (CARDs) to bind to the signaling adaptor molecule mitochondria antiviral signaling protein (MAVS) (Kawai & Akira, 2006). MyD88, TRIF, and MAVS recruit other ubiquitin ligases- TNF receptor-associated factor (TRAF) 3 and TRAF6, which initiate downstream signaling pathways that ultimately result in the activation of the transcription factors IRF3, IRF7, and NF-κB, promoting type-I IFNs and pro-inflammatory cytokines induction (Kawai & Akira, 2006).

Coronaviruses like SARS, MERS, and SARS-CoV-2 are detected by TLR3/7 and RIG-I/MDA5. Generally, activation of TLR3/7 results in the nuclear translocation of NK-kB and IRF3, whereas RIG-I/MDA5 results in IRF3 activation, which triggers the type I IFN induction and other pro-inflammatory cytokines such as IL-1, IL-6, and TNF-α (Lee, Channappanavar, & Kanneganti, 2020). The regulated type-I IFN induction provides defense against SARS, MERS, and SARS-CoV2 by enhancing the clearance of viral pathogens. However, some coronaviruses remain highly pathogenic because of different virus evasion mechanisms, suppressing the IFN response (Felsenstein, Herbert, McNamara, & Hedrich, 2020). Different innate immune pathways involved in coronavirus sensing are shown in Fig.7.

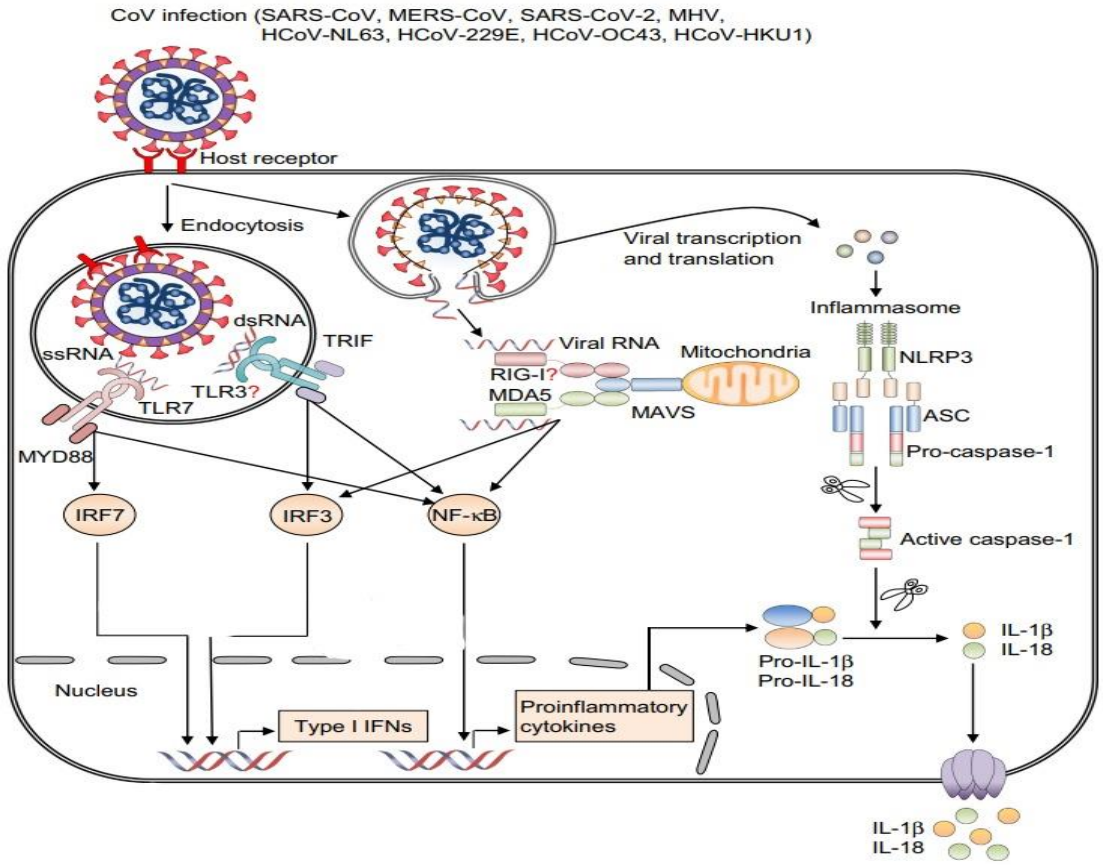

Fig.7. Innate immune sensing pathways in CoV infection. After CoV infection, TLR3 and 7 recognize the single- or double-stranded RNA and, through downstream signaling, induce the activation of NF-κB to produce pro-inflammatory cytokines and phosphorylation of IRF3 and IRF7 to drive type I IFN production. RIG-I and MDA5 recognize the cytosolic viral RNA and associate with adaptor protein MAVS to activate NF-κB and IRF3 phosphorylation. Different pro-inflammatory cytokines can also activate and induce an inflammatory response upon CoV infection (adapted from Lee, Channappanavar, & Kanneganti, 2020).

Mild hCoVs like 229E induce a high amount of type I IFNs. Other hCoVs like SARS, MERS, and SARS-CoV-2 utilize different structural and non-structural proteins to escape recognition by PRRs, inhibiting the induction of type I/III IFNs, blocking IFN (α,β) receptor (INFAR) signaling and directly suppress the effector function of ISGs (Zhuang, Liu, Sun, Li, & Jincun, 2022). The three highly pathogenic hCoVs interfere with the early innate immune response affecting RNA sensing, type I IFN production, and signal transducer and activator of transcription (STAT)-1/2 activation.

The severe cases of SARS-CoV-2 infection were related to inhibited or delayed IFN response, contributing to viral pathogenesis. Lack of IFN production in the early stages of infection affects the viral clearance mechanisms, allowing continuous viral replication. Consequently, high viral titers induce a hyperinflammatory state known as cytokine storm (CS) characterized by the presence of vast amounts of pro-inflammatory cytokines, including IL-1, 2, 6, 7, 8, 10, 12, 17 and 18, TNF-α, IFN-γ, granulocyte colony-stimulating factor (G-CSF), and monocyte chemoattractant protein-1 (MCP-1). The pathogenic infiltration of the immune system causes tissue damage, coagulation, and vascular homeostasis, resulting in capillary leak syndrome, thrombosis, and disseminated intravascular coagulation, eventually causing ARDS, multiorgan failure, and death (Yang, et al., 2021).

Viral nsps cause the IFN antagonism; for example, SARS-CoV-2 NSP1 blocks phosphorylation and nuclear translocation of IRF3, impairing the type I IFN transcription (Kumar, et al., 2021). Similarly, SARS-CoV and NL63 NSP3, which contain papain-like protease domains (PLPs), suppress IFN-β production by blocking the assembly or stability of STING dimers, essential for downstream signaling (Sun, et al., 2012). Besides NSPs, several accessory proteins contribute to IFN suppression through different mechanisms. SARS-CoV and SARS-CoV-2 ORF3a downregulate the induction of type I IFN receptor (IFNAR1) (Minakshi, et al., 2009) and inhibit STAT1 phosphorylation, respectively (Xia, et al., 2020), ORF3b of both viruses impair nuclear translocation of IRF3 (Konno, et al., 2020); and ORF4b of MERS-CoV suppresses NF-κB translocation into the nucleus (Canton, et al., 2018).

hCoVs have evolved other mechanisms to escape PPR recognition. For example, the use of DMVs to hide nascent viral RNA, mimicking eukaryotic mRNAs to shield recognition of PAMPs on the viral genome, and inhibiting the formation of stress granules (SG), that provide a pool of substrates for different PRRs, such as RIG-I and MDA5 (Li, et al., 2021). Because of high adaptability to a new host and adaptation of new evasion mechanisms, there is a need to establish a deeper understanding of the immune antagonizing mechanism used by coronaviruses.

1.5 IFI16 in Antiviral Innate Immunity

γ-IFN-Inducible protein 16 (IFI16), an absent in melanoma 2 (AIM2)-like receptor (A.L.R.), is a member of the PYHIN protein family (Bawadekar, de Andrea, Gariglio, & Londolfo, 2015), and a regulator of several biological processes like DNA damage responses,

apoptosis, cell growth, and regulation of cell differentiation. PHYIN proteins are IFN-inducible factors exclusively expressed in mammals and play an essential role in immune sensing and inflammasome activation.

The number of PYHIN proteins varies among different species. Humans encode four PHYIN proteins- AIM2, IFI16, IFN-Inducible protein X (IFIX), and Myeloid Nuclear Differentiation Antigen (MNDA), which are involved in innate immune sensing pathways (Fig.8). Structurally, these proteins have a common N-terminal pyrin domain (PYD) followed by one or two 200-amino acids, DNA binding HIN domains (Bosso, et al., 2020). Because of their pathogen recognition and self-DNA binding ability, HIN-200 domains classify as PRRs, while PYD binds to pro-apoptotic speck protein ASC, activating procaspase-1 during pathogenic DNA sensing, followed by the secretion of IL-1β (Bawadekar, de Andrea, Gariglio, & Londolfo, 2015).

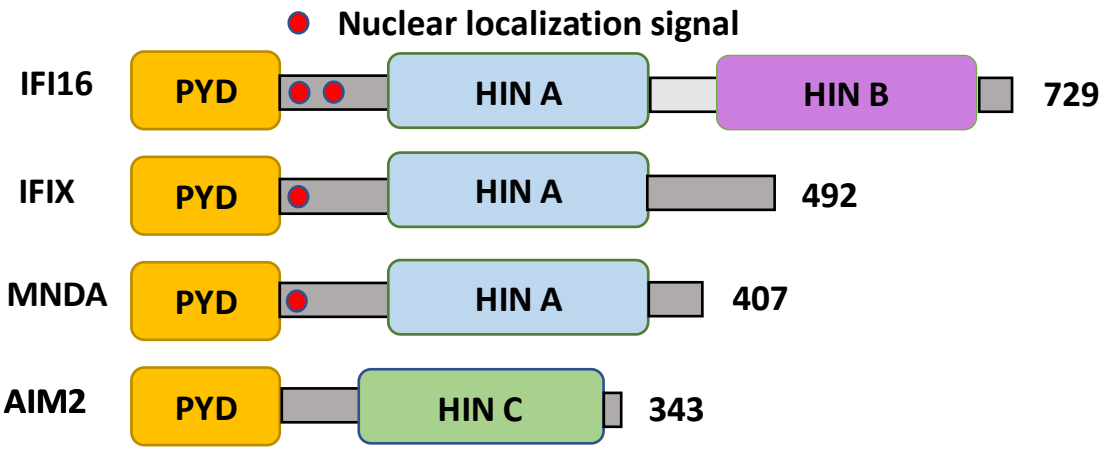

Fig.8. The human PYHIN protein family. Each PYHIN family member possesses an N-terminal pyrin domain (PYD) and one or more HIN domains, classified as HIN A, HIN B, and HIN C. All PYHIN proteins, except AIM2, harbor at least one nuclear localization signal (NLS).

PYHIN proteins are now recognized as viral inhibitors, serving as antiviral restriction factors. IFI16 can suppress viral transcription of herpes-, retro-, papilloma-, cytomegalovirus, and hepatitis viruses through various mechanisms, including epigenetic modifications and interference with the transcription factor Sp1 (Bosso & Kirchhoff, 2020). While in humans, PYHIN proteins are crucial antiviral restriction factors, in bats, the entire PYHIN gene family,

along with other essential proteins of innate immunity, are either genetically or functionally lost (Zhang, et al., 2012) (Ahn, Cui, Irving, & Lin-FaWang, 2016).

The genetic changes and the loss of the PYHIN locus are hypothesized as evolutionary modifications to ensure the unique ability of bats, as mammals, to fly great distances. Flying is a high-energy metabolic process that releases large amounts of reactive oxygen species (ROS), damaged DNA, and other known danger signals to trigger inflammasome activation. Bat has evolved to develop a unique immune system that limits flight-induced excessive inflammation, which has also enabled them to develop a state of tolerance against several deadly viruses, like filoviruses (Ebola and Marburg), paramyxoviruses (Hendra and Nipah), and severe acute respiratory syndrome-like coronaviruses (SARS-CoV, MERS-CoV, and SARS-CoV-2) (Luis A. D., et al., 2013).

Infected bats exhibit no or little signs of disease, even with high viral titers in tissue or sera, whereas the same viruses frequently cause aberrant innate immune responses in humans (Irving, Ahn, Goh, & Anderson, 2021). Considering the antiviral role of PYHIN proteins and the loss of its entire locus in bats might explain the abundance of viruses detected in bats. Only the PYHIN family can drive mass-inflammasome activation as a response to invading pathogens, and its deletion might have an asymptomatic impact, as seen in bats (Ahn, Cui, Irving, & Lin-FaWang, 2016).

Since IFI16 is the protein of interest, this section further discusses its role as an antiviral restriction factor in innate immunity. Already shown in Fig.8, IFI16 has two DNA-sensing HIN domains (A and B) separated by a spacer region (Unterholzner, et al., 2011) (Jiang, et al., 2021) and a protein-protein interacting PYD (Dell'Oste, et al., 2015). Because it contains a nuclear localization signal (NLS), IFI16 was initially considered a nuclear protein. However, evidence suggests that IFI16 can also be detected in the cytoplasm of cells, even though molecular mechanisms regulating IFI16 redistribution between nuclear and cytolytic compartments are only partially understood (Dell'Oste, et al., 2015).

IFI16 can recognize pathogen-derived nucleic acids in the nucleus and cytoplasm. Depending on the type of viral infection, IFI16 can translocate to the cytosol and trigger IFN transcription through the cyclic guanosine monophosphate-adenosine monophosphate (cGAMP) synthase (cGAS)-STING pathway. IFI16 moves to the cytoplasm during infection of different viruses such as Epstein-Barr virus (EBV), herpesvirus type 1 (HSV-1), and

cytomegalovirus (CMV) (Dell'Oste, et al., 2014). In Kaposi Sarcoma herpesvirus (KSHV) infection, IFI16 and ASC procaspase-1 redistribute to the cytoplasm, forming a functional inflammasome which leads to caspase-1 activation and secretion of IL-1β (Zheng, Liwinski, & Elinav, 2020).

The role of IFI16 in sensing DNA viruses is well-characterized, but its function during RNA virus infections remains partially unknown. A recent study showed that IFI16 could inhibit influenza A virus (IAV) replication in cooperation with RIG-I (Jiang, et al., 2021). RIG-I is a member of the RIG-I-like receptors (RLRs) family and serves as a cytoplasmic sensor of pathogen-associated molecular patterns (PAMPs) for RNA viruses. RIG-I activation induces an intracellular immune response characterized by type I IFN production and antiviral gene expression aimed at controlling virus infection (Loo & Jr, 2011).

A recent study mentioned that IFI16 could enhance RIG-I transcription during IAV infection and interact with RIG-I protein, increasing the sensitivity of RIG-I signaling. IAV infection upregulates IFI16 expression and directly interacts with the viral RNA genome (Jiang, et al., 2021). Another study reported the potential role of IFI16 in pyroptosis in alveolar epithelial cells infected by IAV, suppressing cell-to-cell viral transmission. The precise mechanisms are unknown, but it is thought that IFI16-induced programmed cell death starts with the interaction between IFI16 and viral RNA, which predominantly occurs in the nucleus (Mishra, et al., 2022).

Another recent research has shown that IFI16 can inhibit the viral replication of other RNA viruses. IFI16 directly interacts with chikungunya virus (CHIKV) genomic RNA, acting as an antiviral restriction factor and inhibiting its replication and maturation (Kim, et al., 2020). Also, IFI16 can efficiently restrict the replication of porcine reproductive and respiratory syndrome virus 2 (PPRSV-2) by directly binding MAVS and promoting MAVS-mediated IFN-I production (Chang, et al., 2019).

Considering the involvement of IFI16 as an antiviral in RNA viruses, we hypothesized that IFI16 might exert similar functions also during the infection of other RNA viruses, including coronaviruses. Despite the few studies highlighting the critical role of IFI16 in RNA virus pathogenesis, its role as an RNA virus sensor is poorly understood and requires further studies. Currently, there are no studies on understanding the role of IFI16 in coronavirus infection, highlighting the scope and uniqueness of this project.

2. AIMs

2.1 PART-A (Published Results)

COVID-19, in a short time, became a global health crisis, imposing unprecedented challenges to develop diagnostic and therapeutic tools to control and treat the pandemic. Studies have shown that the majority of COVID-19-infected individuals develop neutralizing antibodies (nAbs) against the spike (S) glycoprotein within the first two weeks after the onset of symptoms (Nguyen, et al., 2020) (Bayarri-Olmos, et al., 2021). These antibodies have a protective effect against infection in animal models. However, the duration of serological response and the extent of the protective effect of such antibodies in infected individuals is not fully characterized. Quantitative determination of virus nAbs is considered a good correlate of protection (CoP) (Mercado, et al., 2020). Some studies have suggested that after 3-4 months post-infection, there is a rapid decline in humoral response (Roltgen, et al., 2020) (Marot, et al., 2021). On the contrary, some longitudinal studies have shown the persistence of NAbs up to 8-10 months post-infection, indicating a possibility that such SARS-CoV-2 NAbs can also be a CoP against emerging variants (Dan, et al., 2021) (Pradenas, et al., 2021).

Since the information on the long-term dynamics of NAbs is limited, this study aimed:

i) To assess the longitudinal profile of neutralizing antibodies against SARS-CoV-2 Spike and receptor binding domains (RBD).

The results of the above-discussed aspects of the persistence of nAbs in SARS-CoV-2 infected individuals are thoroughly discussed in the attached manuscript as listed below:

Griffante, G., Chandel, S., Ferrante, D., Caneparo, V., Capello, D., Bettio, V., et al. persistence of neutralizing antibodies to SARS-CoV-2 in first wave infected individuals at ten months post-infection: the UnIRSA cohort study. Viruses. 2021;13:2270.

2.2 PART-B (Unpublished Results)

Bat's immune system has evolved to limit the flight-induced collateral damage caused by the by-products of elevated metabolic rate, enabling bats to be the ideal reservoir hosts for various viruses, including coronaviruses (Zhang, et al., 2012) (Luis A. D., et al., 2013). Bats have lost the PYHIN protein family locus, which contains sensory proteins for recognizing the intracellular self and foreign DNA molecules that trigger inflammasome and IFN response (Ahn, Cui, Irving, & Lin-FaWang, 2016). IFI16, a PYHIN protein family member, plays a role in innate immunity, acting as a DNA sensor and a viral restriction factor in inflammasome signaling (Bawadekar, et al., 2015). While IFI16 activity against DNA viruses is already known, few studies have demonstrated its antagonistic role against RNA viruses, including IAV (Jiang, et al., 2021), CHIKV (Kim, et al., 2020), and porcine reproductive and respiratory syndrome virus 2 (PPRSV-2) (Chang, et al., 2019). Considering this information and the lack of studies on the involvement of IFI16 in coronavirus pathogenesis, this project aims to test the hypothesis that ***"IFI16 is also a key regulator of the host response to hCoV infection in human epithelial cells and that therapeutic modulation of this pathway may impact hCoV replication/infectivity."***

To prove this hypothesis, the work described in this thesis focuses on two main objectives

i) Is IFI16 involved in hCoV sensing and the ensuing immunopathogenic response?

ii) Can IFI16 depletion/inactivation restore a more tolerant and balanced host reaction resembling that found in bats?

This proposal aims to characterize the mechanisms of IFI16-mediated restriction of hCoV human epithelial cells. The project aims to answer specific research questions: i) Is IFI16 involved in hCoV sensing and the ensuing immunopathogenic response? ii) Can IFI16 depletion/inactivation restore a more tolerant and balanced host reaction resembling that found in bats? To provide mechanistic insights into the IFI16-hCoV interplay, we will: 1) Determine the molecular events involving IFI16 in hCoV sensing; 2) Characterize the host response and signaling pathways triggered by IFI16-mediated sensing of hCoVs; 3) Assess the impact of IFI16-driven signaling pathways on hCoV replication and evaluate their potential use as therapeutic targets.

Characterizing the molecular machinery involved in host-virus interaction and controlling inflammation is crucial for identifying druggable targets. Thus, the results obtained from this thesis will deepen our understanding of IFI16's involvement in triggering abnormal inflammatory reactions in hCoV-infected human epithelial cells and help develop novel therapeutic approaches for not just hCoV-related diseases but also other RNA virus diseases.

3. MATERIALS AND METHODS

3.1 Cell lines and viruses

Experiments were performed on different cell lines, including rhesus monkey kidney LLC-MK2 (ATCC: CCL-7) cells, wild-type (WT), and IFI16 knockout (KO) keratinocytes HaCaT cells generously provided by Professor Leonie Unterholzner (University of Edinburgh, UK), and Vero E6 cells kindly provided by John Hiscott (Pasteur Institute, Rome). Dulbecco's Modified Eagle's Medium (DMEM) was used as a culture media for all the cells along with additional supplements, i.e., 10% fetal bovine serum (FBS), 100 U/ml penicillin (P), 100 μg/ml of streptomycin (S) and 0.05mM glutamine (G) as supplements.

The human coronavirus strain NL63 (NR-470, also referred to as Amsterdam I, Bei Resources) was kindly provided by Lucia Nencioni (University of Rome, La Sapienza, Rome, Italy). NL63 was proliferated in LLC-MK2 and Caco-2 cells at 34 °C in a humidified 5% CO_2 incubator and titrated by the standard plaque assay method on LLC-MK2 cells, as described later.

All the experiments on SARS-CoV-2 have been performed in collaboration with Serena Delbue (*Università degli Studi di Milano La Statale*). SARS-CoV-2 was isolated from a nasal-pharyngeal swab positive for SARS-CoV-2. The isolated SARS-CoV-2 strain belongs to the B.1 lineage, carrying the characteristic spike mutation D614G. The B.1 lineage is the sizeable European lineage, whose origin roughly corresponds to the Northern Italian outbreak in early 2020. The complete nucleotide sequence has been deposited at GenBank and GISAID (accession Nos. MT748758.1 and EPI_ISL 584051, respectively).

3.2 IFI16 knockout cell line

For the generation of gene-specific knockouts in LLC-MK2 cells, the CRISPR/Cas9 system was employed. A lentiviral CRISPR/Cas9 vector 54 carrying a Cas9 gene (codon-optimized nuclear-localized) is fused to the puromycin resistance gene at the N-terminal via the T2A ribosome-skipping sequence. The vector also contains a human U6 promotor sequence to drive the expression of gRNA, containing a gene-specific crRNA (CRISPR RNA) fused to the trcrRNA (trans-activating RNA) and a terminator sequence. For IFI16 KO, the cloned gene-specific crRNA sequence is 5'-GTACCAACGCTTGAAGACC-3.'

Vesicular stomatitis virus G (VSV-G)-pseudotyped lentiviral vector-based clustered regularly interspaced short palindromic repeats (lenti-CRISPR) virions were created by transfecting HEK293T cells with the following plasmids: CRISPR/Cas9 vector and virapower

mix (pLP1, pLP2-REV, VSV-G). Viral supernatants were collected after 72 h and used to transduce LLC-MK2 cells by infection in the presence of 10 ug/ml Polybrene. Transduced cells were selected with increasing dosages of puromycin (1g/ml, 2.5 g/ml, 5mg/ml, 7.5mg/ml, and 10 mg/ml) for 14 days post-transduction. After selection, the successful KO was confirmed using qPCR and immunoblotting. A reference sequence (WT cells) was used as a control.

3.3 NL63 production and titration

For the virus production, monolayers of LLC-MK2 cells were infected with NL63 at MOI (multiplicity of infection) 0.01. The flasks were incubated at 34°C, 5% CO2, followed by a change of media 24h post-infection, and the virions were harvested from the supernatants of infected cells on days 5-6 after a visible cytopathic effect (CPE). Flasks were frozen at -80°C and thawed for harvesting, ensuring the release of virions attached to the cellular surface. After scraping the cells from the flask, cells and supernatant were centrifuged at 2000 rpm for 10 min. Cleared supernatant was filtered using a 0.45um sterile filter, aliquoted, and stored at -80°C for further use.

The virus yield was assessed by titration on fully confluent LLC-MK2 cells in 96-well plates. LLC-MK2 cells were seeded one day before infection in 96-well plates, reaching confluency at the time of infection. The supernatant containing virions was serially diluted in DMEM, 10% FBS, and 1% PSG. The infected wells were centrifuged at 2000 rpm for 30 minutes and then incubated at 34 °C for 2h, allowing the virions attachment and cellular entry. After incubation, cells were washed with 1XPBS and overlaid with 0.8% methylcellulose. The plates were incubated at 34°C and 5% CO_2. Overlays were removed on day 6 and stained with a 0.2% crystal violet solution for 30 minutes, shaking under the dark. Plaques were counted using a light microscope. Viral titers were expressed in terms of plaque-forming units per ml (PFU/ml).

3.4 SARS-CoV-2 titration

For the SARS-Cov-2 plaque assay, 7.5 x 10^5 Vero E6 cells per well were plated in a 6-well plate in DMEM with 10% FCS and 1x penicillin/streptomycin. After 24h, 100 plates forming a unit per mL (PFU mL^{-1}) of a previously titrated SARS-CoV-2 isolate were added to $MISMA_2$ (from 30 to 10 ng µL) serially diluted in DMEM and incubated for 1 hour before adding to confluent Vero cells. Cell supernatants were discarded after 2 hours, and 0.3% agarose (3 µg mL^{-1}) dissolved in DMEM was added to each well. After 72 hours, cells were stained with

methylene blue (0.4 g L-1) upon agarose removal. Viral plaques were counted, and the results were expressed as Plaque Forming Unit (PFU) mL^{-1} (Parisi, et al., 2021).

3.5 NL63 and SARS-CoV-2 infection

Sub-confluent LLC-MK2 cells and confluent WT and IFI16 KO-HaCaT cells were infected with the appropriate MOI, and virus absorption was allowed for 2-8 hours before changing media. Every infection with NL63 was performed at MOI1 in a BSL2 facility, while with SARS-CoV-2 at MOI3 in a BSL3 facility. Both viruses were incubated at 34°C and 5% CO2 incubators. For the viral kinetics, cells were infected with the respective virus, incubated at 34°C and 5% CO2 incubators, followed by changing media at 2 hours post-infection (h.p.i.), supernatants and cells were collected at different time points from 12h.p.i. to 5 days post-infection (d.p.i.), with a corresponding mock, centrifugation at 2000 rpm for 5 minutes. The supernatants were then stored at -80°C for later use.

3.6 FACS analysis

For FACS analysis, cell pellets were harvested and resuspended in 100 ul FACS buffer (1xPBS, 1%FBS, 1 mM EDTA). After centrifugation at 2000rpm for 5min, the supernatant was discarded. The pellet was fixed in 100ul of 4% PAF for 10 min at room temperature. Following the centrifugation at 2000 rpm for 5minn, cells were washed twice in 200 ul FACS buffer and permeabilized in 200 ul of 0.1 Triton-X in 1X PBS. The cells were incubated at room temperature (RT) for 20 min, centrifuged, and washed in FACS buffer twice. The cells were then incubated in the dark at 4°C with NL63 NP Antibody (1:100 in 3% BSA in 1xPBS) for 1 h. After triple washing in FACS buffer, cells were incubated in the dark with Alexa green IgG secondary antibody and incubated at 4°C for 1 h. Cells were centrifuged twice and resuspended in 250ul FACS buffer. The cell sorting for NP-positive cells was performed using Attune NxT Flow Cytometer.

3.7 RNA extraction and quantification

For gene expression analysis, cells were treated with 500 µL TRIzol Reagent to disrupt cells and cell components without altering RNA's integrity during homogenization. Following the 10 minutes of incubation at RT, 100 µL of chloroform (TRIzol 1:5) was added to each sample, followed by a 10-minute incubation at room temperature. Samples were centrifuged at 12000g for 15 min at 4°C to allow phase separation forming aqueous and organic phases

containing RNA and protein, respectively. The upper transparent phase containing RNA was recovered, and 250 µL of isopropanol (isopropanol: TRIzol 1:2) was added to each sample. After gentle pipetting and 10 minutes of incubation at room temperature, samples were incubated for 10 min at RT Samples were centrifuged for 10 minutes at 4°C at 12000 rpm to allow RNA precipitation.

After obtaining the RNA pellet, supernatants were removed, and RNA pellets were washed with 500 µL 70% ethanol followed by 5 min centrifugation at 7500g at 4°C. Then, supernatants were removed, pellets were left to air dry for 15-20 minutes to remove the excess ethanol, and resuspended in 10 µL nuclease-free water. The RNA samples were quantified using the *ThermoScientific NanoDrop spectrophotometer*. The photometric nucleic acid measurement depends on the intrinsic absorption properties of DNA or RNA. In an absorption spectrum measurement for nucleic acids, the light absorption peaks at 260 nm. The signal is measured by the spectrophotometer and expressed as absorbance values of the sample. Initially, a blank (1 µL distilled water) was run to perform RNA quantification, followed by 1 µL of each sample. The software converted the absorbance values of each sample in RNA concentration, measured in ng/µL.

3.8 DNase treatment and retrotranscription

To remove genomic DNA, RNA extracts were treated using the *TURBO DNA-free™ Kit*, agreeing to the manufacturer's instruction (Invitrogen). For cDNA synthesis, *SensiFAST cDNA Synthesis Kit* was used according to the manufacturer's instructions (Meridian Bioscience). The total RNA of each sample was mixed with 4 µL 5X TransAmp Buffer and 1 µL Reverse Transcriptase; DNase/RNase free-water was used to reach the final volume of 20 µL. Reverse transcription was performed using the *C100 Touch Thermal Cycler* (Bio-Rad Laboratories) following the conditions for retrotranscription as 25 °C for 10 min, 42 °C for 15 min, and 85 °C for 5 min.

3.9 Real-Time qPCR

The viral cDNA (1 µL per sample) was amplified in a 20 µL reaction mixture containing 10 µL SensiFast SYBR (Bioline) 1 µL forward primer, 1 µL reverse primer, and 7 µL water. Primers used for qPCR assay for NL63 genomic and sub-gnomic genes are shown in Table 2. The reaction conditions consisted of an enzyme activation cycle of 30 s at 95°C, 40 cycles of 10 s denaturation at 95°C, and 10s annealing at 60°C. The conditions used for the amplification

of subgenomic mRNAs were the following: 3 min initial denaturation at 95°C in step 1, denaturation for 30 s at 95°C in step 2a, 30 s primer annealing at 47°C in step 2b, and 25 s extension at 72°C in step 2c, a 40 cycle repeat for step 2, followed by 5 min final extension at 72°C and infinity hold at 4°C in step 3. The PCR products were checked on 1% agarose gels (1X Tris-acetate EDTA [TAE] Buffer) and visualized using *ChemiDoc Touch Imaging System* (Bio-Rad).

The presence of SARS-CoV-2 *N1* and *ORF1ab* gene in cells was evaluated through AgPath-ID One-Step RT-PCR assay (ThermoFisher, Waltham, MA, USA), using the 7500 Real-Time PCR system (ThermoFisher Scientific, Waltham, MA, USA). The sequence for primers and probes is described in table 3. The reaction mix was conducted in a final volume of 25 µL, containing 1× RT-PCR buffer (2×), 0.4 µM of each primer, 0.1 µM of the probe, 1× RT-PCR Enzyme mix (25×), and five µL of heat-inactivated cell medium.

The standard curve was constructed using a serially diluted plasmid pEX-A128-nCoV_all (Eurofins, Luxemburg), containing part of the SARS-CoV-2 genome (3×10^7–3×10^1 copies/µL). Samples were analyzed in duplicate, and negative control was added. The limit of detection was three copies per reaction. To confirm SARS-CoV-2 active replication, SARS-CoV-2 subgenomic RNA (sgRNA) was amplified utilizing AgPath-ID One-Step RT-PCR assay. Real-time quantitative reverse transcription (qRT)-PCR analysis was achieved on a CFX96 real-time system (Bio-Rad). Calculation of ΔCt between genomic RNA (gRNA) and sgRNA was performed at each time point in infected cells as follows: ΔCt = Ct (sgRNA) − Ct (gRNA).

3.10 Digital droplet PCR

The viral cDNA from the supernatants of NL63-infected LLC-MK2 cells was processed for the ddPCR reaction using QX200 2X ddPCR Evagreen Supermix (Bio-Rad), 200nM forward and reverse primers targeting transcripts of N gene (Table-2). The droplets were generated using the Bio-Rad QX200 Droplet generator. The reactions were run on a CFX96 real-time system (Bio-Rad) and analyzed with a QX200 plate reader using the Quanta Soft Analysis software (Bio-Rad).

3.11 Primers

The list of primers and probes used to detect viral transcription inside the cells for NL63 and SARS-CoV-2 and the induction of innate immune sensors are shown in table 2.

Table 2. List of primers sequences used to quantify genomic, sub-gnomic (sg) mRNA levels for NL63, SARS-CoV, type I/III IFNs, and ISGs.

	Gene	**Primer**
NL63	*N* Forward	AGGACCTTAAATTCAGACAACGTTCT
	N Reverse	GATTACGTTTGCGATTACCAAGACT
	ORF1ab Forward	TGTTGTAGTAGGTGGTTGTGTAACATCT
	ORF1ab Reverse	AATTTTTGTGCACCAGTATCAAGTTT
	sg N Forward	TAAAGAATTTTTCTATCT ATAGATAG
	sg N Reverse	TACGCCAACGCTCTTGAAC
SARS-CoV-2	sgLeader	5′-CGATCTCTTGTAGATCTGTTCTC-3′.
	N Forward	GACCCCAAAATCAGCGAAAT
	N Reverse	TCTGGTTACTGCCAGTTGAATCTG
	Probe	ACCCCGCATTACGTTTGG TGGACC-BHQ1
	ORF1ab Forward	GTGARATGGTCATGTGTGGCGG
	ORF1ab Reverse	CARATGTTAAASACACTATTAGCATA
	Probe	CAGGTGGAACCTCATCAGGAGATGC-BHQ1
Housekeeping	*GAPDH* Forward	TCACCACCATGGAGAAGGC
	GAPDH Reverse	GCTAAGCAGTTGGTGGTGCA
Type I/III IFNs	IFNβ forward	GTCTCCTCCAAATTGCTCTC
	IFNβ reverse	ACAGGAGCTTCTGACACTGA
	IFNλ1 forward	CGCCTTGGAAGAGTCACTCA
	IFNλ1 reverse	GAAGCCTCAGGTCCCAATTC
ISGs	*IFIT1* Forward	TTGCCTGGATGTATTACCAC
	IFIT1 Reverse	GCTTCTTGCAAATGTTCTCC
	Mx1 Forward	AGGACCATCGGAATCTTGAC
	Mx1 Reverse	TCAGGTGGAACACGAGGTTC

3.12 Protein extraction and quantification

Whole-cell protein extracts were obtained using 100 µL cell lysis buffer containing 150 mM NaCl, 50 mM Tris-HCl pH 8, 1% NP40, 0,5% sodium deoxycholate, 0,1% SDS, with the addition of protease inhibitors (25 µL/mL, Sigma-Aldrich). The samples were homogenized for 1 hour at 4°C under rotation and then centrifuged at 14000g for 10 min at 4°C. The supernatant was collected in a micro-centrifuge tube and quantified. Protein quantification was done using Bradford Method.

The Bradford assay converts the red dye to blue after binding to the proteins. The protein-dye complex causes a spectral shift in the maximum absorption of the dye from 465 to 595 nm.

The increase in absorbance at 595 nm wavelength is proportional to the amount of dye bound to the protein, giving the protein concentration in the sample. Bovine serum albumin (BSA) was used to calibrate the assay by preparing six serial dilutions of protein diluted with PBS1X to final concentrations of 1, 2.5, 5, 10, 15, 30 μg/μL (2 μL of cell lysis Buffer were added in each dilution). Test tubes were prepared by adding 2 μL sample, 498 μL PBS, and 500 μL Bradford Reagent. Two blanks were obtained by adding 498 μL PBS, 2 μL RIPA Buffer, and 500 μL Bradford Reagent. Absorbance readings were measured at 595 nm using a spectrophotometer, and the standard curve was used to provide a relative measurement of the protein concentration of each sample.

3.13 Western Blot

For protein analysis, protein extracts were dissolved in *Laemmli Sample Buffer 4X* (0.02% bromophenol blue, 8% β-mercaptoethanol, 250mM-HCl, 8% SDS, 40% Glycerol) and heated at 95°C for 5 min for protein denaturation. Proteins were separated by their molecular weight under denaturing conditions using ReadyGels (7.5%; Bio-Rad). The samples (20 μL) and a molecular weight ladder (7 μL) were loaded into appropriate wells; gels were initially run at 80V until the complete separation of the marker's bands and then at 200V. Proteins were transferred from the SDS-polyacrylamide gels to nitrocellulose membranes using *Trans-blot Turbo Blotting System* according to the manufacturer's instruction (Bio-Rad).

Membranes were stained with Ponceau stain to confirm the transfer. To visualize the proteins, membranes were washed thrice with TBS-T 1X (10mM Tris-HCl, pH 7.5, 100mM NaCl, 0.1% Tween-20). To minimize any unspecific interaction of the Antibody, membranes were blocked in 10% non-fat dry milk dissolved in TBS-T 1X for 1 hour. Overnight incubation of membranes with primary antibodies was done at 4°C on a rocker in the dark. Table 4 lists the primary antibodies used for the experiments. Then, the membranes were washed thrice in TBS-T 1X to eliminate unbound antibody residues, followed by incubation with the respective species-specific secondary Antibody (Anti-rabbit diluted 1:2000; Anti-mouse diluted 1:4000). Proteins were detected using the instrument *ChemiDoc Touch Imaging System* (Bio-Rad). Using Image Lab software (Bio-Rad Laboratories Srl), images were analyzed, and band density was calculated using the densitometry application on the software.

3.14 Immunofluorescence

Cells were fixed with 4% paraformaldehyde (PAF) for 10 min at room temperature for immunofluorescence analysis. Permeabilization was accomplished with 0.5% Triton X-100 in PBS 1X for 20 min on ice to enable antibodies to cross the cellular membranes. Using 1% Normal Goat Serum (NGS) in PBS 1X for 30 min at room temperature, cells were blocked to reduce the unspecific binding of antibodies to non-target structures, and cells were incubated all night with the primary Antibody (diluted in a blocking solution). After, several washings were performed with PBS 1X + 0.05% Tween-20 to remove the unbound Antibody, and then 1-hour incubation with a secondary antibody in the dark was performed; in addition, 4',6-diamidino-2-phenylindole (DAPI) was added to stain cells' nuclei. After a few washes, coverslips were mounted on slides using an anti-fade mounting medium and visualized using the Multiphoton Microscope Leica TCS SP8 (Leica Microsystems, Wetzlar, Germany). The Images were analyzed using the Leica Application Suite X (L.A.S. X).

3.15 Immunoprecipitation

Uninfected or NL63-infected cells (MOI1) were washed with 1× PBS and lysed in cell lysis buffer (same as protein extraction). Following the manufacturer's protocol (Novex by Life Technologies), Proteins (100 µg) were incubated with 4 µg of specific antibodies against NL63 NP (Sino Biological) or with rabbit IgG pre-immune Antibody (NRI01; Cell Sciences) as a negative control at RT for 1 h with rotation. Immune complexes were collected using magnetic beads, washed three times using wash buffer, and resuspended in elution buffer along with 10 ul of NuPAGE LDS sample buffer (4x LDS 2.4ul + 6.5 ul ddH_2O), boiled for 10 min at 70^0C, and resolved on an SDS-PAGE gel to assess protein binding by Western blotting.

3.16 Antibodies

A list of antibodies used for western blot (WB) and immunofluorescence (IF) is given in Table 3.

Table 3. List of antibodies and their dilutions used for western blot (WB) and immunofluorescence (IF)

Antibody (Company name, location)	**Dilution WB.**	**Dilution IF**
Rabbit MAb anti-RIG-I (*Millipore*)	1:1000	
Mouse MAb anti-IFI16 (Santa-Cruz)	1:1000	1:600
Rabbit PAb anti-IFI16 (*in-house made*)	1:1000	1:200

Rabbit MAb anti-NL63 NP (*Sino Biological*)	1:2000	1:200
SARS-CoV-2 NP (Genetex)	1:1000	1:200
Mouse MAb anti-GAPDH (*Proteintech*)	1:10000	

3.16 Statistical analysis

All statistical tests were performed using Graph-Pad Prism version 7.00 for Windows (GraphPad Software). The data are stated as mean ± standard deviation (SD). For comparisons consisting of two or more groups, means were compared using two-tailed Student's t-tests or one-way or two-way ANOVA followed by Bonferroni's post-tests. Differences in P value < 0.05 were considered statistically significant.

4. RESULTS

PART-A (Published Results)

viruses

MDPI

Brief Report

Persistence of Neutralizing Antibodies to SARS-CoV-2 in First Wave Infected Individuals at Ten Months Post-Infection: The UnIRSA Cohort Study

Gloria Griffante [1], Shikha Chandel [1], Daniela Ferrante [1], Valeria Caneparo [1,2], Daniela Capello [1,3], Valentina Bettio [1,3], Cinzia Borgogna [1], Chiara Aleni [1], Salvatore Esposito [1], Andrea Sarro [1], Alessandra Vasile [1], Marco Comba [1], Tommaso Testa [1], Gianmarco Cotrupi [1], Marco De Andrea [2,4], Sara Bortoluzzi [1] and Marisa Gariglio [1,2,*]

[1] Department of Translational Medicine, University of Piemonte Orientale, 28100 Novara, Italy; gloria.griffante@uniupo.it (G.G.); shikha.chandel@uniupo.it (S.C.); daniela.ferrante@med.uniupo.it (D.F.); valeria.caneparo@med.uniupo.it (V.C.); daniela.capello@med.uniupo.it (D.C.); valentina.bettio@med.uniupo.it (V.B.); cinzia.borgogna@med.uniupo.it (C.B.); 20032401@studenti.uniupo.it (C.A.); 20017042@studenti.uniupo.it (S.E.); andrea.sarro@uniupo.it (A.S.); 20034878@studenti.uniupo.it (A.V.); marco.comba@uniupo.it (M.C.); tommaso.testa@uniupo.it (T.T.); 20034824@studenti.uniupo.it (G.C.); sara.bortoluzzi@uniupo.it (S.B.)
[2] Center for Translational Research on Autoimmune and Allergic Disease (CAAD), University of Piemonte Orientale, 28100 Novara, Italy; marco.deandrea@unito.it
[3] UPO Biobank, University of Piemonte Orientale, 28100 Novara, Italy
[4] Department of Public Health and Pediatric Sciences, University of Turin, 10126 Turin, Italy
* Correspondence: marisa.gariglio@med.uniupo.it

Citation: Griffante, G.; Chandel, S.; Ferrante, D.; Caneparo, V.; Capello, D.; Bettio, V.; Borgogna, C.; Aleni, C.; Esposito, S.; Sarro, A.; et al. Persistence of Neutralizing Antibodies to SARS-CoV-2 in First Wave Infected Individuals at Ten Months Post-Infection: The UnIRSA Cohort Study. *Viruses* **2021**, *13*, 2270. https://doi.org/10.3390/v13112270

Academic Editor: Caijun Sun

Received: 27 August 2021
Accepted: 8 November 2021
Published: 12 November 2021

Publisher's Note: MDPI stays neutral with regard to jurisdictional claims in published maps and institutional affiliations.

Abstract: Longitudinal mapping of antibody-based SARS-CoV-2 immunity is critical for public health control of the pandemic and vaccine development. We performed a longitudinal analysis of the antibody-based immune response in a cohort of 100 COVID-19 individuals who were infected during the first wave of infection in northern Italy. The SARS-CoV-2 humoral response was tested using the COVID-SeroIndex, Kantaro Quantitative SARS-CoV-2 IgG Antibody RUO Kit (R&D Systems, Bio-Techne, Minneapolis, USA) and pseudotype-based neutralizing antibody assay. Using sequential serum samples collected from 100 COVID-19 recovered individuals from northern Italy—mostly with mild disease—at 2 and 10 months after their first positive PCR test, we show that 93% of them seroconverted at 2 months, with a geometric mean (GeoMean) half-maximal neutralization titer (NT50) of 387.9. Among the 35 unvaccinated subjects retested at 10 months, 7 resulted seronegative, with an 80% drop in seropositivity, while 28 showed decreased anti-receptor binding domain (RBD) and anti-spike (S) IgG titers, with a GeoMean NT50 neutralization titer dropping to 163.5. As an NT50 > 100 is known to confer protection from SARS-CoV-2 re-infection, our data show that the neutralizing activity elicited by the natural infection has lasted for at least 10 months in a large fraction of subjects.

Keywords: SARS-CoV-2; COVID-19; Neutralizing humoral response

1. Introduction

Severe acute respiratory syndrome coronavirus 2 (SARS-CoV-2) infection is associated with the development of variable levels of antibodies (Abs) with neutralizing activity, which can protect against infection in animal models [1–3]. However, the duration of the serological response in infected subjects and the extent to which such Ab response may be protective against reinfection [4] have still to be fully characterized.

Given the short time SARS-CoV-2 has been studied, information on long-term antibody dynamics is still limited. In this regard, quantitative titer determination of virus-neutralizing Abs (nAbs) is considered an excellent correlate of protection (CoP). Initial reports pointed to a rapid decline in the humoral response within 3–4 months post-infection [5–7]. More recently, longitudinal studies assessing mid-term kinetics of SARS-CoV-2 infection showed persistent neutralizing antibody responses for up to 8–10 months [8–10], leading to the possibility that nAbs to SARS-CoV-2 may also represent a CoP from emerging SARS-CoV-2 variants of concern.

The aim of this study was to assess the longitudinal profile of anti-spike (S) IgG and anti-recombinant receptor binding domain (RBD) Abs as well as the SARS-CoV-2 neutralizing activity of sera from 100 individuals who were infected during the first wave of SARS-CoV-2 infection in Italy. Although a decline in both IgG levels and neutralizing activity was observed overtime, most of the study subjects still retained a neutralizing activity above the cut-off value (i.e., GeoMean NT50, the reciprocal dilution inhibiting 50% of the infection) of 100, which is considered to be effective in reducing the risk of reinfection [11], [12].

2. Material and Methods

2.1. Ethical Statement

Participants were involved and consented under the UPO Biobank study and ethical governance approved by the Ethics Committee of "Maggiore della Carità" Hospital (protocol 427/CE; study No. CE 84/20).

2.2. Human Subjects, Sample, and Data Collection

Blood samples were obtained from individuals enrolled in the UnIRSA (Unveiling the Immune Response against SARS-CoV-2) cohort study. An observational study was carried out on a cohort of 100 individuals with real-time reverse-transcriptase-polymerase chain reaction (rRT-PCR)-confirmed SARS-CoV-2 infection from nasopharyngeal swab that dated from 14th March, 2020 to 17th May, 2020, thus corresponding to the first wave of infection in Italy. Patient recruitment commenced in May 2020 and continued until June 2020. Recruited patients were followed up until February 2021. The inclusion criteria were (i)one positive rRT-PCR test for SARS-CoV-2 followed by two consecutive negative tests performed 24 h apart, that fulfilled the administrative definition of recovery from COVID-19 as established by the Italian Ministry of Health on February 28th, 2020, (ii)age ≥ 18 years, (iii)absence of an immunosuppressive conditions, and (iv)willingness to provide an informed consent. At blood sample collection, an ad-hoc questionnaire was administered to collect data, including socio-demographic characteristics, biometric data (e.g., weight, height, body mass index), and presentation of SARS-CoV-2 infection.

The study participants were stratified according to COVID-19 disease severity as follows: (i)asymptomatic patients, reporting no symptoms, (ii)symptomatic patients, disclosing at least one symptom of those indicated in Table 1 without the need of hospitalization, and (iii)hospitalized patients, requiring hospital assistance due to the severity of COVID-19.

Table 1. Characteristics of the study population with SARS-CoV-2 infection.

	n = 100
Age at COVID-19 diagnosis (years) median (IQR)	46.5 (33.5,52.8)
BMI, kg/m^2 Median (IQR)	24.2 (21.9,28.1)
Sex, n (%)	
female	77 (77)
male	23 (23)

Occupation, n (%)	
Physician or paramedical staff	74 (74)
Others	26 (26)
Comorbidities, n (%)	
No comorbidities	53 (53)
allergy	29 (29)
hypertension	14 (14)
autoimmune diseases	13 (3)
asthma	5 (5)
cancer	3 (3)
diabetes	3 (3)
heart disease	2 (2)
Reported Symptoms, n (%)	
No symptoms	16 (16)
asthenia	57 (57)
anosmia	55 (55)
muscle ache	53 (53)
fever	52 (52)
ageusia	49 (49)
headache	47 (47)
cough	44 (44)
diarrhea	35 (35)
runny nose	28 (28)
dyspnea	24 (24)
chest pain	22 (22)
skin manifestations	14 (14)
palpitations	13 (13)
Severity, n (%)	
asymptomatic	16 (16)
symptomatic	74 (74)
hospitalized	10 (10)
Median (IQR) days between positive PCR and first antibody test (M2)	51 (43,56)
Median (IQR) days between positive PCR and second antibody test (M10)	293 (287,303)
Vaccinated (among 71 subjects with second antibody test), n (%)	36 (50.7)
One dose, n (%)	21 (29.6)
Two doses, n (%)	15 (21.1)
Median (IQR) days between vaccination (single dose) and second antibody test (M10)	15 (11,18)
Median (IQR) days between vaccination (second dose) and second antibody test (M10)	8 (3,10)

A retrospective chart review was performed on hospitalized participants. Samples were coded and then de-identified prior to analysis. Other efforts to maintain the confidentiality of participants consisted in labeling samples with coded identification numbers. All the data

were recorded on the REDCap (https://www.project-redcap.org/, accessed on 11 November 2021) web application in compliance with current General Data Protection Regulation (GDPR) and Italian legislation on the protection of sensitive data and privacy.

2.3. Quantitative Determination of Anti-SARS-CoV-2-Specific Abs

To perform quantitative determination of anti-SARS-CoV-2 Abs, the COVID-SeroIndex, Kantaro Quantitative SARS-CoV-2 IgG Antibody RUO Kit (R&D Systems, Bio-Techne, Minneapolis, MN, USA), which comprises two serial direct enzyme-linked immunosorbent assays (ELISA), was employed. The immunoassays were used and interpreted following the manufacturer's instructions. Briefly, an initial ELISA was performed to test the reactivity of Abs raised against the recombinant receptor binding domain (RBD) of the SARS-CoV-2 spike protein from the first virus isolate Wuhan-Hu-1 [13,14]. Results were expressed as cut-off index (CI) calculated as the ratio of the corrected sample OD value to the corrected positive control optical density (OD) value. CI values > 0.7 were considered positive. In the quantitative ELISA against the full-length SARS-CoV-2 spike protein (S), the Ab concentration of samples was calculated using a four-parameter logistic (4-PL) curve fit. Values below the limit of quantification (LoQ) of 3.2 AU/mL were considered negative.

2.4. SARS-CoV-2-Specific Neutralizing Antibody Assay

Vero E6 and Vero E6-TMPRSS2—kindly provided by John Hiscott, Pasteur Institute Rome—were cultured in Dulbecco's modified Eagle's medium (DMEM) supplemented with 10% fetal calf serum (FCS) (Sigma-Aldrich, Milan, Italy). The replication-competent vesicular stomatitis virus r(VSV)-eGFP-SARS-CoV-2-SΔ21 was a kind gift from Sean P.J. Whelan (Washington University School of Medicine, USA) [15]. To grow this virus, Vero E6 cells were infected with a low Multiplicity of Infection (MOI) (0.01) and maintained at 34 °C from then on. Cell supernatants were harvested upon visualization of extensive cytopathic effect and cell detachment at approximately 24 h post-infection (hpi). Upon viral RNA extraction and amplification by RT-PCR, the *spike* gene was sequenced every time the virus was harvested. The virus was titrated by flow cytometry. Serum samples were heat-inactivated at 56 °C for 30 min. Indicated dilutions of sera were incubated with rVSV-SARS-CoV-2-SΔ21 at an MOI of 0.05 for 1 h at 37 °C. Ab-virus complexes were added to Vero E6-TMPRSS2 cells in 96-well plates and incubated at 34 °C for 24 h. Subsequently, cells were fixed in 4% formaldehyde (Millipore Sigma) containing DAPI for 15 min on ice, when fixative was replaced with PBS. Images were acquired using Cytation 5 Cell Imaging Multi-Mode Reader (BioTek) in both the DAPI and GFP channels to visualize nuclei and infected cells (i.e., eGFP-positive cells). The raw images (2 × 2 montage) were acquired using 4X objective, processed, and stitched using the default setting.

2.5. Statistical Analysis

Normally distributed data were represented as mean and standard deviation (SD), whereas data following a non-normal distribution were represented as median and interquartile range (IQR). Categorical variables were summarized as counts and percentages. Differences in medians were evaluated using the Mann–Whitney's U test and Wilcoxon Rank signed-rank test for pairwise comparisons. The Kruskal–Wallis test along with the Dunn test for multiple comparisons was used to compare more than two groups. The Bonferroni correction method was applied.

The Spearman's correlation coefficient was used to compute correlation between quantitative variables. A two-sided p-value < 0.05 was considered statistically significant. Images and raw data were processed, and the NT50 (the reciprocal dilution inhibiting 50% of

the infection) was calculated by plotting and fitting the log of serum dilution versus response to a 4-parameters equation using the Gen5 v3.0 software. Data were processed using Prism software (GraphPad Prism v6.0) and STATA v16 (College Station, TX, USA).

3. Results

3.1. Patient Selection and Magnitude of the Antibody Response to SARS-CoV-2 at Two Months after the First Positive PCR Test (M2)

From 21st May to 19th June 2020, 100 individuals (77 female, 23 male) who were infected by SARS-CoV-2 during the first wave of infection in Italy were enrolled in this study (Table 1). Their median age was 46.5 years (IQR 33.5,52.8). All study subjects had an RT-PCR-confirmed SARS-CoV-2 infection. While most of these COVID-19 patients (74%) experienced mild-to-moderate disease or did not report any symptoms (16%), 10% of them required hospitalization without the need of intensive care unit (ICU)-level care.

All patients provided an initial blood sample defined as M2 (approximately two months post-infection), which was taken at a median number of 51 days (interquartile range, IQR 43, 56) from the first positive PCR test. A second longitudinal blood sample, defined as M10 (approximately 10 months post-infection), was taken from 71 COVID-19 patients at a median number of 293 days after the initial sample collection (IQR 287,303 days). During the observation period, the Italian COVID-19 vaccine campaign started and, between January 2nd, 2021 and February 4th, 2021, 21 study subjects received a single dose of mRNA-based SARS-CoV-2 vaccines, whereas 15 obtained two doses, bringing the total number of study subjects with at least one dose to 36 (Figure 1).

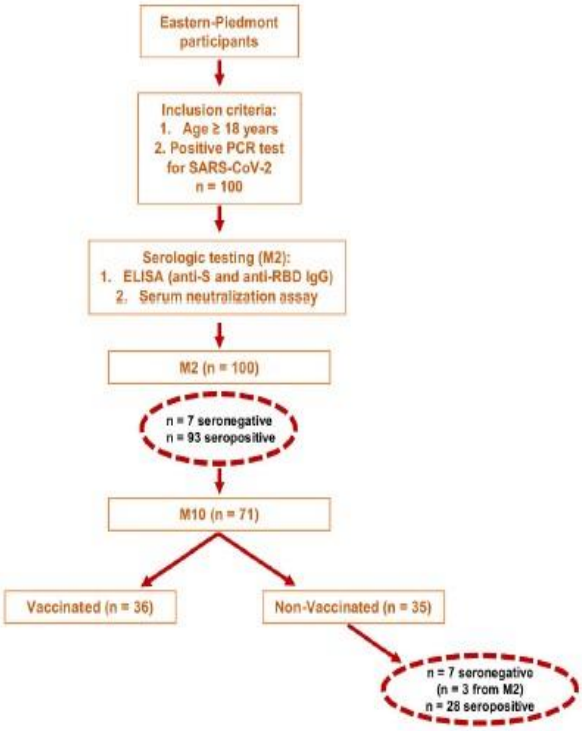

Figure 1. Study design and participants.

Circulating IgG Abs against the SARS-CoV-2 spike antigen were measured using the Kantaro Quantitative SARS-CoV-2 IgG Antibody RUO Kit, which allows detecting IgG against either the RBD or the full-length trimeric spike protein of SARS-CoV-2. At M2, 93% of the subjects showed detectable levels of IgG Abs against both RBD and total S protein, with a positive spearman correlation ($r = 0.9$, $p < 0.0001$) (Figure 2A). In addition, we identified 7 subjects, one of whom had been hospitalized for pneumonia, lacking circulating Abs to SARS-CoV-2 (Table 2). Three of them were retested at M10 but remained seronegative (Figure 1).

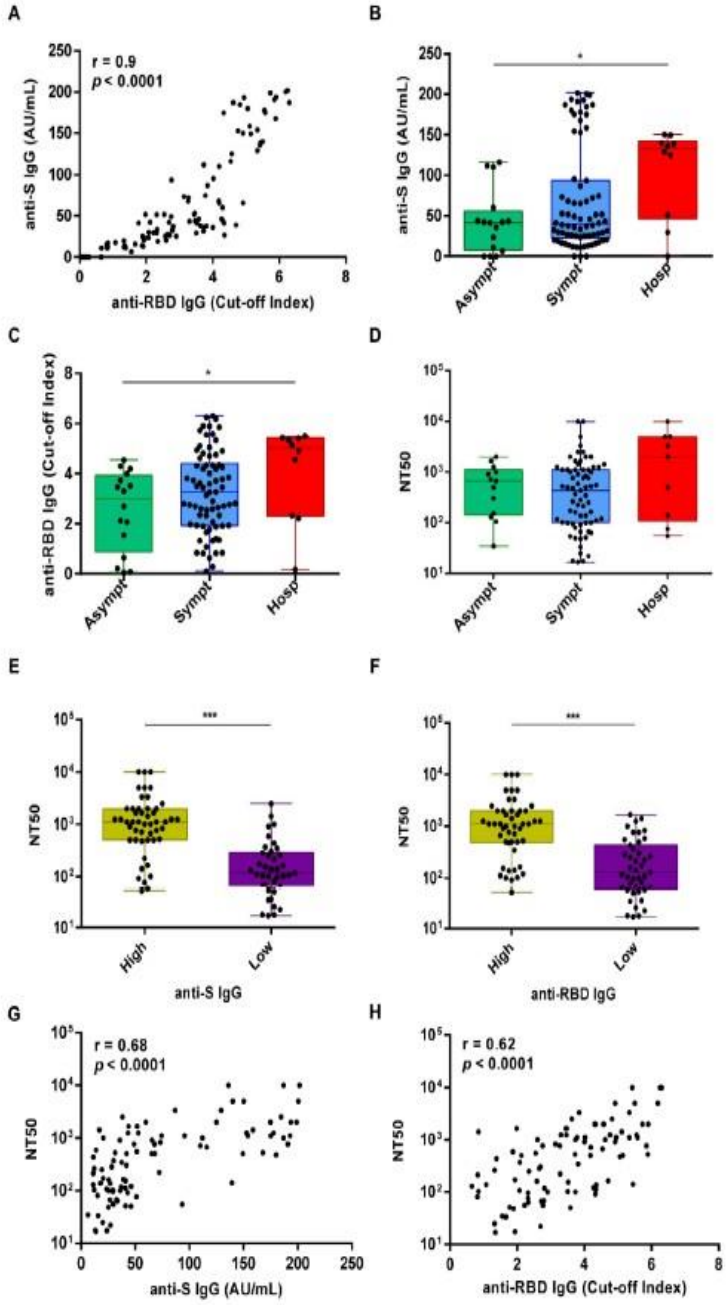

Figure 2. Antibody responses in the study cohort following SARS-CoV-2 infection at 1.5 months (M2) after the first positive PCR test. (A) Spearman's correlation between anti-S IgG AU/mL and anti-RBD IgG cut-off index as assessed by ELISA at M2. (B,C,D) The 100 study subjects were categorized into 3 groups according to disease severity (asymptomatic n = 16,

symptomatic n = 74, or hospitalized n = 10) and plotted according to anti-S IgG AU/mL (**B**) or anti-RBD IgG cut-off index (**C**) and the neutralization titer expressed as NT50 (**D**). Solid circles indicate individual values. The *p*-value among different groups was calculated by Kruskal–Wallis test * $p < 0.05$. (**E**) Box plot distribution of the neutralizing activity expressed as NT50 in the group of high or low anti-S IgG levels—above and below the median, respectively. (**F**) Box plot distribution of the neutralizing activity expressed as NT50 in the group of high or low anti-RBD IgG levels—above and below the median, respectively. In E and F, the solid circles indicate individual values. *p*-values were determined by two-sided Mann-Whitney test. *** $p < 0.001$. (**G**) Spearman correlation between the neutralization titer expressed as NT50 and the anti-S IgG levels. (**G**) Spearman correlation between the neutralization titer expressed as NT50 and the anti-RBD IgG levels.

Table 2. Clinical and laboratory characteristics of the seronegative individuals at M2.

Subject	Age	Gender	Symptoms	Comorbidities	M2	M10
1	30	F	Asymptomatic	None	55	NA
2	36	M	Symptomatic	None	50	NA
3	63	F	Symptomatic	Cancer	43	NA
4	27	F	Asymptomatic	Allergy	43	NA
5	52	F	Pneumonia	None	43	232
6	58	F	Asymptomatic	None	48	246
7	31	F	Symptomatic	None	27	254

NA, not available.

After patient stratification for COVID-19 disease severity (i.e., asymptomatic, symptomatic, or hospitalized), we observed that both anti-S and anti-RBD Ab levels were significantly higher in the group of hospitalized patients than those detected in asymptomatic cases ($p = 0.04$ and $p = 0.03$, respectively) (Figure 2B, C). A similar trend was observed for the neutralizing titers although not statistically significant ($p = 0.12$) (Figure 2D).

Given that the determination of the neutralizing effects of SARS-CoV-2 spike Abs is critical to understand the protective effects of the immune response, the same sera were also analyzed for their ability to inhibit VSV-SARS-CoV-2-SΔ21 infection of Vero E6 cells, as previously described [15,16]. The latter is a very useful BSL2 surrogate virus whose neutralization profiles strongly correlate with focus-reduction neutralization tests using SARS-CoV-2. We observed that sera with values above the median titer for both anti-S and anti-RBD IgG displayed significantly higher neutralizing activity when compared to those with values below the median value ($p < 0.0001$ for both) (Figure 2E, F), with a positive Spearman correlation r = 0.68, $p < 0.0001$ and r = 0.62, $p < 0.0001$, respectively (Figure 2G, H). The geometric mean (GeoMean) NT50 neutralization titer was 387.9 (CI 95% 280.8, 535.8) at M2, with 7% of individuals not reaching 50% neutralization at the lowest serum dilution of 1:10.

3.2. Comparative Analysis of the IgG Titers and the Neutralizing Response at Ten Months after the First Positive PCR Test (M10)

Seventy-one subjects provided additional blood samples at M10, which were assessed for the presence of both anti-S and anti-RBD IgG as described for the M2 samples. Notably, at M10, 36 study subjects had received at least one dose of mRNA-based SARS-CoV-2 vaccines.

As the objective of this study was to determine the duration of the immune response to natural infection, assessment of nAbs was only performed for those unvaccinated subjects that had positive ELISA IgG Ab test results (n = 28/35). As expected, the IgG titers against S and RBD antigens were both significantly increased in vaccinated subjects at M10 vs. M2 ($p <$ 0.0001 for both Abs) (Figure 3A, B, respectively). By contrast, in the 35 unvaccinated individuals the scenario was completely different: 28 of them remained seropositive for both anti-S and anti-RBD Ab, with a positive Spearman correlation r = 0.8, $p < 0.0001$ (Figure 3C),

while 7 turned out to be seronegative. Three of these latter were already seronegative at M2, whereas the other 4 lost their anti-S and anti-RBD IgG reactivity overtime. Specifically, the percentage of subjects seropositive for both anti-S and anti-RBD IgG within this unvaccinated cohort was 91% (32/35) at M2 vs. 80% (28/35) at M10. When we assessed the levels of the Abs over time, we found that the anti-RBD Abs had significantly decreased between M2 and M10 (p = 0.0007), while the anti-S Abs had not significantly changed (p = 0.38) (Figure 3A, B, respectively). However, when the subjects were stratified for COVID-19 symptoms, also the decrease in anti-S Abs in symptomatic patients became statistically significant (p = 0.03), while it remained unchanged in the other two subgroups (i.e., hospitalized and asymptomatic). A similar trend was also observed for the anti-RBD Ab titers (p = 0.003) (Figure 3D, E, respectively).

With regard to the neutralizing Ab titers at M10, we observed that sera displaying values above the median titer for the anti-S IgG displayed significantly higher neutralizing activity compared to that of sera with anti-S values below the median value (p = 0.0028) (Figure 4A). When we considered anti-RBD IgG titers below and above the median value, the trend was similar (p = 0.0131) (Figure 4B). The positive Spearman correlation between anti-S or anti-RBD titers and nAb titers was r = 0.59 (p = 0.001) and r = 0.51 (p = 0.005), respectively, indicating an overall lower correlation when compared to that observed at M2 (Figure 4C, D, respectively). The GeoMean NT50 neutralization titer was 163.5 (CI 95% 82.1, 325.9) at M10.

We next measured and correlated anti-S, anti-RBD IgG, and nAb levels in the sera of the 28 individuals who had not received the vaccine and remained seropositive at M10. While most of them displayed reduced anti-RBD IgG (n = 22) and nAb levels (n = 21) at M10 vs. M2, 8 unvaccinated patients still retained nAb titers above the 1:100 cut-off at M10 (48%). On the other hand, 6 subjects showed increased anti-RBD IgG levels at M10 vs. M2, and 6 displayed increased nAb titer values above the 1:100 cut-off at M10 vs. M2, while 1 subject retained low but sustained nAb titer values below the 1:100 cut-off. When we compared anti-S IgG levels at M10 with those at M2, we found them to be reduced in 16 subjects and upregulated in 12 (Figure 4E–G). Interestingly, we found that those who had increased anti-S IgG levels at M10 were older when compared to those who displayed decreased anti-S IgG levels at M10 (p = 0.01), as already reported in a series of studies conducted in healthy subjects [17–19]. Next, using the mathematical modeling approach developed by Miles P. Davenport and co-workers, which provides a quantitative prediction of the link between neutralizing antibody levels and clinical protection, we estimated the 50% protective neutralization level against SARS-CoV-2 infection in our cohort to be 78.338 in the M2 group, calculated as 20.2% of the mean level [20]. Using this predictive model and threshold, we found that 80% (28/35) of the subjects in the M2 group and 54.28% (19/35) in the M10 group were above this value. Overall, our findings show that 60% of the subjects in the unvaccinated cohort (n = 35) experienced a decline in their serum neutralizing activity at M10, while 20% did show increased nAb levels over time. The antibody levels were below the limit of detection in the remaining 20% of the subjects, indicating that 11.5% completely lost the humoral response, while 8.5% never mounted an immune response.

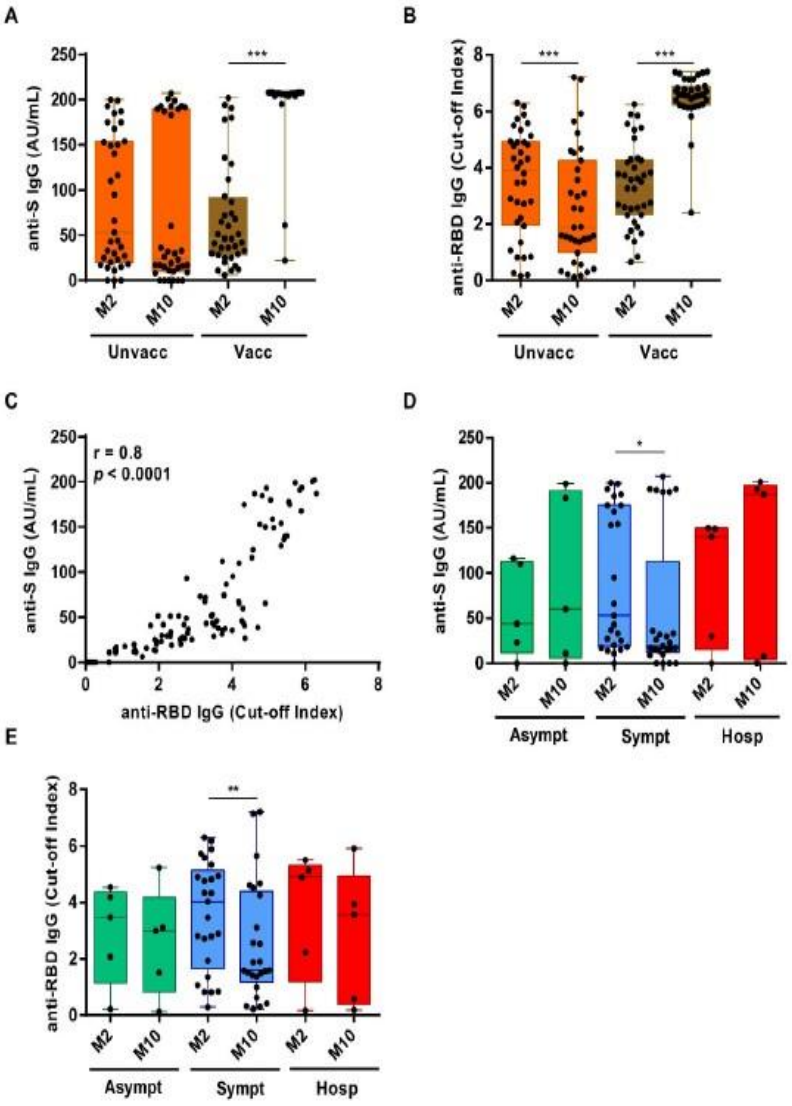

Figure 3. Dynamic changes in anti-S and anti-RBD IgG levels between M2 and M10 after the first PCR-positive test. (**A**) Box plot distribution of anti-S IgG levels or (**B**) anti-RBD IgG levels in unvaccinated (left) or vaccinated (right) subjects at M2 vs. M10. Solid circles indicate individual values. *p*-values were calculated by two-sided Wilcoxon signed-rank tests. *** $p < 0.001$. (**C**) Spearman correlation between anti-S IgG AU/mL and anti-RBD IgG cut-off index as assessed by ELISA at M10. (**D**) Comparison of anti-S IgG levels between asymptomatic (n = 16), symptomatic (n = 74), or hospitalized (n = 10) subjects at M2 and M10. *p*-values were calculated by two-sided Wilcoxon signed-rank tests. * $p < 0.05$. (**E**) Comparison of anti-RBD cut-off index between asymptomatic n = 16, symptomatic n = 74, or hospitalized n = 10 subjects at M2 or M10. *p*-values were calculated by two-sided Wilcoxon signed-rank test. ** $p < 0.01$.

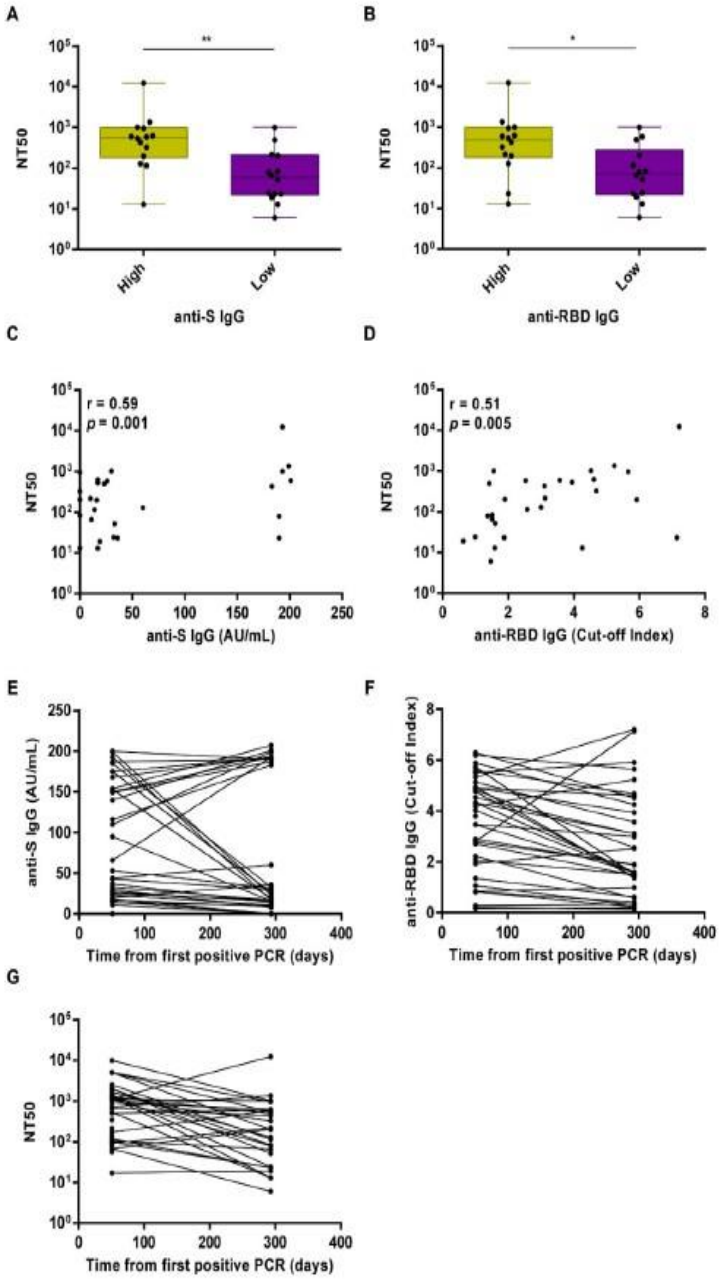

Figure 4. Longitudinal analysis of the neutralizing activity at 10 months (M10) after the first positive PCR test. (A) Box plot distribution of the neutralizing activity expressed as NT50 in the group of high or low anti-S IgG levels—above and below the median, respectively. Comparative analysis was performed by Mann-Whitney test. ** $p < 0.01$. (B) Box plot distribution of

the neutralizing activity expressed as NT50 in the group of high or low anti-RBD IgG levels—above and below the median, respectively. Comparative analysis was performed by Mann-Whitney test. * $p < 0.05$. Solid circles indicate individual values. (**C**) Spearman correlation between anti-S IgG AU/mL and the neutralizing activity expressed as NT50 at M10. (**D**) Spearman correlation between anti-RBD IgG cut-off index and the neutralizing activity expressed as NT50 at M10. (**E**) Longitudinal mapping of anti-RBD IgG cut-off index, anti-S IgG AU/mL (**F**), or neutralizing activity expressed as NT50 (**G**) in seropositive unvaccinated subjects (n = 28) at M2 and M10 after the first PCR-positive test.

4. Discussion

In this study, we have performed a longitudinal analysis of the serological responses to SARS-CoV-2 in 100 COVID-19 patients who were infected during the first wave of infection in Italy, of whom 74 were HCWs working at a hospital setting in northern Italy. In these patients, we performed quantitative determination of the anti-RBD and anti-S IgG response to SARS-CoV-2 and evaluated the neutralizing activity of their sera using an in vitro functional assay.

Both anti-RBD and anti-S antibody levels were below the detection limit of the assays in 7% of the subjects after ~50 days from the first SARS-CoV-2 positive PCR test, indicating that these patients did not seroconvert or had already lost their seroconversion at this time point [5,19,21]. At this time point, both anti-RBD and anti-S IgG levels were significantly higher in hospitalized subjects than those observed in asymptomatic or symptomatic patients. Among the 35 subjects who did not receive the vaccine between the M2 and M10 time points, 4 (11%) became seronegative with a drop in seropositivity from 91% at 2 to 80% at 10 months after SARS-CoV-2 infection. Most of the patients displayed lower IgG levels against both S and RBD at M10 vs. M2 (16/35 (42,7%) and 22/35 (62,8%), respectively). Accordingly, the GeoMean NT50 neutralizing titer dropped from 387.9 at M2 to 163.5 at M10. Likewise, the positive Spearman correlation between anti-S or anti-RBD IgG levels and the neutralizing activity of the sera decreased during the interval from M2 to M10, suggesting that the decline in anti-S and RBD IgG levels at longer time points post-infection may not faithfully reflect a similar decline in their neutralizing activity. Recent longitudinal studies aimed at investigating the duration of humoral immune response in COVID-19-recovered individuals reported similar decay kinetics. Overall, the decline appears to occur up to 7–9 months while it is thereafter stabilized at least until 12 months [19,22–24].

SARS-CoV-2 neutralizing Abs are excellent CoP because they can exert their antiviral activity by acting at the mucosal surface, which curbs the initial infection, mostly mediated by secretory IgA whose levels were shown to rise early after natural infection and neutralize the virus even to a greater extent than IgG [25]. In addition, in the bloodstream as circulating IgM or IgG, they block subsequent viral spread and protect from disease progression. Furthermore, by slowing down the growth rate of SARS-CoV-2, these nAbs may also favor the recruitment of memory B cells capable of neutralizing the infection [26]. Fittingly, vaccine-induced nAbs as well as purified IgG from convalescent animals have been shown to protect non-human primates (NHPs) from infection in a SARS-CoV-2 challenge model [1,2].

One of the major issues in assessing whether nAbs are good proxies for protection from SARS-CoV-2 infection is the determination of a titer cut-off value or range that would allow the identification of those subjects with enough neutralizing activity to make them resistant or less susceptible to reinfection. In spike-based mRNA vaccines studies among people aged 18–55, the GeoMean neutralizing titers after the second dose was 1:181 (day 85), or 1:430 (day 119) depending on the neutralization assay used, while an adenovirus-based vaccine gave an NT50 value of 1:161 or 1:193 (day 42) depending on the neutralization assay used [12]. Another study involving subjects from high attack rate events reported that neutralizing activities in the range 1:100–1:200 were strong enough to prevent infection [11]. Although direct comparisons among the aforementioned studies may suffer from some bias due to the

use of different neutralization assays [8,9,15], the emerging concept from this recent body of literature is that an NT50 neutralization titer > 100 is likely to confer protection from SARS-CoV-2 re-infection [11], [reviewed in 12]. Thus, in this context, the fact that we detected a GeoMean NT50 titer of 163.5 at 10 months after the first SARS-CoV-2 positive PCR test would indicate that a significant proportion of individuals (48%) were still within the GeoMean range observed in the vaccinated cohorts. This would suggest that the neutralizing activity elicited by the natural infection may still be effective in a large fraction of subjects (17/35 in our study) after 10 months from the initial infection, even after experiencing a very mild form of COVID-19 disease. More specifically, we found that 74/100 (74%) subjects displayed NT50 neutralizing titer >100 at M2, while in the non-vaccinated subgroup it was 26/35 at M2 (74%) and 17/35 at M10 (48%). In addition, according to the mathematical model developed by Khoury et al., 80% of the subjects at M2 and 54.2% at M10 displayed a neutralization titer that was deemed to be sufficient to provide 50% protection from symptomatic COVID-19 [20].

Our analysis is limited by the reduced sample size, particularly at M10, as half of the study participants received the vaccine in the frame of the Italian vaccination campaign which started during the observational period. However, despite the limited sample size, the availability of two longitudinal measurements, one of which up to 10 months after initial diagnosis, allowed us to achieve adequate statistical power to establish that the neutralizing antibody titer against SARS-CoV-2 were still present in 80% of the study subjects who were infected during the first wave of SARS-CoV-2 infection in Italy. Another limitation of this study is that it is possible that the trends of immune response in recovered, non-vaccinated patients might reflect re-exposure to SARS-CoV-2, particularly in those for whom titers augmented with time. We need also to point out that the requirement for fulfilling the administrative definition of recovery by COVID-19 (as previously described in Material and Methods) provided a homogenizing filter, and thus patients who had lingering detectable SARS-CoV-2 may behave differently. Another limitation is that the role of the memory B cell compartment has not been analyzed in this study. Indeed, the number of RBD-specific memory B cells has been reported to remain stable between 6 and 12 months upon natural infection [19].

Finally, the recombinant VSV expressing SARS-CoV-2 S protein was shown to behave analogously to a clinical isolate of SARS-CoV-2 and to provide comparable results to neutralization tests with the wild-type virus [15]. The r(VSV)-eGFP-based SARS-CoV-2 neutralizing Ab assay may offer utility as a diagnostic tool with which to assess patients' sera neutralizing activity. We postulate it could be predictive of the likelihood of reinfection in the general population.

Author Contributions: Conceptualization: M.G.; Data curation: G.G., S.C.; Formal analysis: D.F.; Funding acquisition: M.G.; Investigation: G.G., S.C., V.C.; Methodology: M.D.A., S.B.; Resources: D.C., V.B., C.A., S.E., A.S., A.V., M.C., T.T., G.C.; Supervision: M.G.; Writing—original draft: G.G., M.G.; Writing—review & editing: C.B., M.D.A., S.B. All authors have read and agreed to the published version of the manuscript.

Funding: This study was funded by the AGING Project, Department of Excellence (DIMET), Università del Piemonte Orientale.

Institutional Review Board Statement: The study was conducted according to the guidelines of the Declaration of Helsinki, and approved by the Ethics Committee of "Maggiore della Carità" Hospital (protocol 427/CE; study No. CE 84/20) on 15 April 2020.

Informed Consent Statement: Informed consent was obtained from all subjects involved in the study.

Acknowledgments: We thank Arabella Fontana and the Novara Health Authority for their support in patient enrollment and database creation. We are also thankful to Carmela Rinaldi and the students

from the UPO School of Nursing for their support in blood collection. We are grateful to Sean P.J. Whelan for providing the rVSV-SARS-CoV-2-SΔ21. We thank Marcello Arsura for critically reviewing the manuscript.

Data Availability Statement: The data presented in this study are available on request from the corresponding author.

Conflicts of interest: The authors declare no conflict of interest.

References

1. Mercado, N.B.; Zahn, R.; Wegmann, F.; Loos, C.; Chandrashekar, A.; Yu, J.; Liu, J.; Peter, L.; Mcmahan, K.; Tostanoski, L.H.; et al. Single-shot Ad26 vaccine protects against SARS-CoV-2 in rhesus macaques. *Nature* **2020**, *586*, 583–588, doi:10.1038/s41586-020-2607-z.
2. McMahan, K.; Yu, J.; Mercado, N.B.; Loos, C.; Tostanoski, L.H.; Chandrashekar, A.; Liu, J.; Peter, L.; Atyeo, C.; Zhu, A.; et al. Correlates of protection against SARS-CoV-2 in rhesus macaques. *Nat. Cell Biol.* **2021**, *590*, 630–634, doi:10.1038/s41586-020-03041-6.
3. Robbiani, D.F.; Gaebler, C.; Muecksch, F.; Lorenzi, J.C.C.; Wang, Z.; Cho, A.; Agudelo, M.; Barnes, C.O.; Gazumyan, A.; Finkin, S.; et al. Convergent antibody responses to SARS-CoV-2 in convalescent individuals. *Nat. Cell Biol.* **2020**, *584*, 437–442, doi:10.1038/s41586-020-2456-9.
4. Röltgen, K.; Powell, A.E.; Wirz, O.F.; Stevens, B.A.; Hogan, C.A.; Najeeb, J.; Hunter, M.; Wang, H.; Sahoo, M.K.; Huang, C.; et al. Defining the features and duration of antibody responses to SARS-CoV-2 infection associated with disease severity and outcome. *Sci. Immunol.* **2020**, *5*, 956–963, doi:10.1126/sciimmunol.abe0240.
5. Marot, S.; Malet, I.; Leducq, V.; Zafilaza, K.; Sterlin, D.; Planas, D.; Gothland, A.; Jary, A.; Dorgham, K.; Bruel, T.; et al. Rapid decline of neutralizing antibodies against SARS-CoV-2 among infected healthcare workers. *Nat. Commun.* **2021**, *12*, 844, doi:10.1038/s41467-021-21111-9.
6. Yamayoshi, S.; Yasuhara, A.; Ito, M.; Akasaka, O.; Nakamura, M.; Nakachi, I.; Koga, M.; Mitamura, K.; Yagi, K.; Maeda, K.; et al. Antibody titers against SARS-CoV-2 decline, but do not disappear for several months. *EClinicalMedicine* **2021**, *32*, 100734, doi:10.1016/j.eclinm.2021.100734.
7. Gaebler, C.; Wang, Z.; Lorenzi, J.C.C.; Muecksch, F.; Finkin, S.; Tokuyama, M.; Cho, A.; Jankovic, M.; Schaefer-Babajew, D.; Oliveira, T.Y.; et al. Evolution of antibody immunity to SARS-CoV-2. *Nature* **2021**, *591*, 639–644, doi:10.1038/s41586-021-03207-w.
8. Dan, J.M.; Mateus, J.; Kato, Y.; Hastie, K.M.; Yu, E.D.; Faliti, C.E.; Grifoni, A.; Ramirez, S.I.; Haupt, S.; Frazier, A.; et al. Immunological memory to SARS-CoV-2 assessed for up to 8 months after infection. *Science* **2021**, *371*, eabf4063, doi:10.1126/science.abf4063.
9. Pradenas, E.; Trinité, B.; Urrea, V.; Marfil, S.; Ávila-Nieto, C.; de la Concepción, M.L.R.; Tarrés-Freixas, F.; Pérez-Yanes, S.; Rovirosa, C.; Ainsua-Enrich, E.; et al. Stable neutralizing antibody levels 6 months after mild and severe COVID-19 episodes. *Med.* **2021**, *2*, 313–320.e4, doi:10.1016/j.medj.2021.01.005.
10. Levi, R.; Ubaldi, L.; Pozzi, C.; Angelotti, G.; Sandri, M.T.; Azzolini, E.; Salvatici, M.; Savevski, V.; Mantovani, A.; Rescigno, M. The antibody response to SARS-CoV-2 infection persists over at least 8 months in symptomatic patients. *Commun. Med.* **2021**, *1*, 1–9, doi:10.1038/s43856-021-00032-0.
11. Addetia, A.; Crawford, K.H.D.; Dingens, A.; Zhu, H.; Roychoudhury, P.; Huang, M.-L.; Jerome, K.R.; Bloom, J.D.; Greninger, A.L. Neutralizing antibodies correlate with protection from SARS-CoV-2 in humans during a fishery vessel outbreak with a high attack rate. *J. Clin. Microbiol.* **2020**, *58*, e02107-20, doi:10.1128/jcm.02107-20.
12. Koch, T.; Mellinghoff, S.; Shamsrizi, P.; Addo, M.; Dahlke, C. Correlates of Vaccine-Induced protection against SARS-CoV-2. *Vaccines* **2021**, *9*, 238, doi:10.3390/vaccines9030238.
13. Wu, F.; Zhao, S.; Yu, B.; Chen, Y.-M.; Wang, W.; Song, Z.-G.; Hu, Y.; Tao, Z.-W.; Tian, J.-H.; Pei, Y.-Y.; et al. A new coronavirus associated with human respiratory disease in China. *Nature* **2020**, *579*, 265–269, doi:10.1038/s41586-020-2008-3.
14. Amanat, F.; Stadlbauer, D.; Strohmeier, S.; Nguyen, T.H.O.; Chromikova, V.; McMahon, M.; Jiang, K.; Arunkumar, G.A.; Jurczyszak, D.; Polanco, J.; et al. A serological assay to detect SARS-CoV-2 seroconversion in humans. *Nat. Med.* **2020**, *26*, 1033–1036, doi:10.1038/s41591-020-0913-5.
15. Case, J.B.; Rothlauf, P.W.; Chen, R.E.; Liu, Z.; Zhao, H.; Kim, A.S.; Bloyet, L.-M.; Zeng, Q.; Tahan, S.; Droit, L.; et al. Neutralizing Antibody and Soluble ACE2 Inhibition of a Replication-Competent VSV-SARS-CoV-2 and a Clinical Isolate of SARS-CoV-2. *Cell Host Microbe* **2020**, *28*, 475–485.e5, doi:10.1016/j.chom.2020.06.021.
16. Borgogna, C.; De Andrea, M.; Griffante, G.; Lai, A.; Bergna, A.; Galli, M.; Zehender, G.; Castello, L.; Ravanini, P.; Cattrini, C.; et al. SARS-CoV-2 reinfection in a cancer patient with a defective neutralizing humoral response. *J. Med. Virol.* **2021**, *93*, 6444–6446, doi:10.1002/jmv.27200.
17. Vanshylla, K.; Di Cristanziano, V.; Kleipass, F.; Dewald, F.; Schommers, P.; Gieselmann, L.; Gruell, H.; Schlotz, M.; Ercanoglu, M.S.; Stumpf, R.; et al. Kinetics and correlates of the neutralizing antibody response to SARS-CoV-2 infection in humans. *Cell Host Microbe* **2021**, *29*, 917–929.e4, doi:10.1016/j.chom.2021.04.015.

18. Glück, V.; Grobecker, S.; Tydykov, L.; Salzberger, B.; Glück, T.; Weidlich, T.; Bertok, M.; Gottwald, C.; Wenzel, J.J.; Gessner, A.; et al. SARS-CoV-2-directed antibodies persist for more than six months in a cohort with mild to moderate COVID-19. *Infect.* **2021**, *49*, 739–746, doi:10.1007/s15010-021-01598-6.
19. Li, C.; Yu, D.; Wu, X.; Liang, H.; Zhou, Z.; Xie, Y.; Li, T.; Wu, J.; Lu, F.; Feng, L.; et al. Twelve-month specific IgG response to SARS-CoV-2 receptor-binding domain among COVID-19 convalescent plasma donors in Wuhan. *Nat. Commun.* **2021**, *12*, 1–9, doi:10.1038/s41467-021-24230-5.
20. Khoury, D.S.; Cromer, D.; Reynaldi, A.; Schlub, T.E.; Wheatley, A.K.; Juno, J.A.; Subbarao, K.; Kent, S.J.; Triccas, J.A.; Davenport, M.P. Neutralizing antibody levels are highly predictive of immune protection from symptomatic SARS-CoV-2 infection. *Nat. Med.* **2021**, *27*, 1205–1211, doi:10.1038/s41591-021-01377-8.
21. Wajnberg, A.; Amanat, F.; Firpo, A.; Altman, D.R.; Bailey, M.J.; Mansour, M.; McMahon, M.; Meade, P.; Mendu, D.R.; Muellers, K.; et al. Robust neutralizing antibodies to SARS-CoV-2 infection persist for months. *Science* **2020**, *370*, 1227–1230, doi:10.1126/science.abd7728.
22. Vacharathit, V.; Srichatrapimuk, S.; Manopwisedjaroen, S.; Kirdlarp, S.; Srisaowakarn, C.; Setthaudom, C.; Inrueangsri, N.; Pisitkun, P.; Kunakorn, M.; Hongeng, S.; et al. SARS-CoV-2 neutralizing antibodies decline after one year and patients with severe COVID-19 pneumonia display a unique cytokine profile. *Int. J. Infect. Dis.* **2021**, *112*, 227–234,, doi:10.1016/j.ijid.2021.09.021.
23. Petersen, M.S.; Hansen, C.B.; Kristiansen, M.F.; Fjallsbak, J.P.; Larsen, S.; Hansen, J.L.; Jarlhelt, I.; Pérez-Alós, L.; Steig, B.Á.; Christiansen, D.H.; et al. SARS-CoV-2 natural antibody response persists for at least 12 months in a nationwide study from the Faroe Islands. *Open Forum Infect. Dis.* **2021**, *8*, doi:10.1093/ofid/ofab378.
24. Wang, Z.; Muecksch, F.; Schaefer-Babajew, D.; Finkin, S.; Viant, C.; Gaebler, C.; Hoffmann, H.-H.; Barnes, C.O.; Cipolla, M.; Ramos, V.; et al. Naturally enhanced neutralizing breadth against SARS-CoV-2 one year after infection. *Nat. Cell Biol.* **2021**, *595*, 426–431, doi:10.1038/s41586-021-03696-9.
25. Sterlin, D.; Mathian, A.; Miyara, M.; Mohr, A.; Anna, F.; Claër, L.; Quentric, P.; Fadlallah, J.; Devilliers, H.; Ghillani, P.; et al. IgA dominates the early neutralizing antibody response to SARS-CoV-2. *Sci. Transl. Med.* **2021**, *13*, doi:10.1126/scitranslmed.abd2223.
26. Corti, D.; Lanzavecchia, A. Broadly Neutralizing Antiviral Antibodies. *Annu. Rev. Immunol.* **2013**, *31*, 705–742, doi:10.1146/annurev-immunol-032712-095916.

PART-B (Unpublished Results)

4.1 Assessment of hCoV infection in human epithelial cell

To assess the role of the innate sensor IFI16 in controlling hCoV replication, as mentioned before, we used two bat-derived viruses NL63 (alpha-CoV, low pathogenic) and SARS-CoV-2 (beta-CoV, highly pathogenic) as prototypes of hCoVs. At the same time, for the cell model, we initially decided to work with the CoV-susceptible immortalized human cell line HaCaT cells.

Different human cell lines were tested to assess their permissiveness to NL63 and SARS-CoV-2 (in collaboration with Professor Serena Delbue, *Università degli Studi di Milano La Statale*), using a replication-competent VSV-eGFP-SARS-CoV-2-$S_{\Delta 21aa}$, suitable for BSL-2 laboratories. However, only HaCaT cells were shown to be permissive to both (data not shown). HaCaT cells were a good candidate since they display a functional immune system and express high levels of ACE2 receptors (Almine, 2017). To explore the role of IFI16 in hCoV infection, we obtained WT-HaCaT and IFI16 KO-HaCaT as a kind gift from Professor Leonie Unterholzner (University of Edinburgh, UK).

Surprisingly, starting at 1d.p.i., we observed a significant reduction in viral titers in the supernatants from SARS-CoV-2-infected IFI16KO- *vs.* WT-HaCaT cells at 1 and 2d.p.i. ($P = 0.0369$, and < 0.0001, respectively) (Fig.9A), suggesting a pro-viral function of IFI16 in these cells. By contrast, no significant differences were found between the viral titers from NL63-infected IFI16KO-HaCaT and WT cells (data not shown). We also checked the protein levels of the viral nucleoprotein (NP) in both NL63 and SARS-CoV-2 infection. While we observed no differences for viral protein in WT vs. KO IFI16 with both viruses, we noticed induction of IFI16 upon infection in the WT-HaCaT cells at 2, 3, and 4d.p.i. with a decrease in protein levels at 5d.p.i. upon NL63 infection (Fig.9B). Upon SARS-CoV-2 infection, we observed a reduction in NP at 2d.p.i. An earlier induction of IFI16 protein at 6h was observed, which appeared to reduce later at1 and 2d.p.i. in WT cells (Fig.9C).

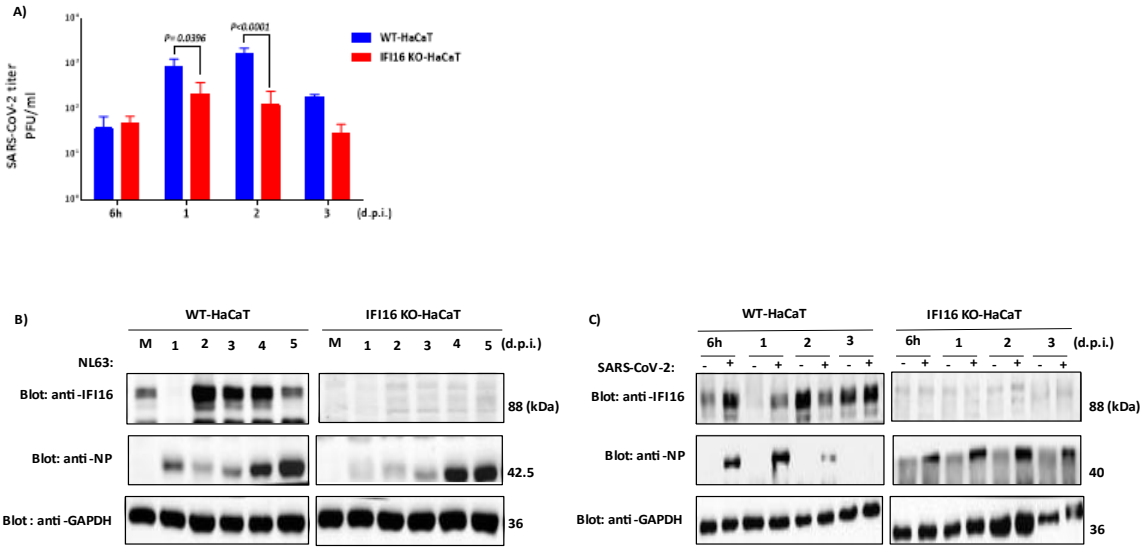

Fig.9. Coronavirus kinetics in HaCaT cells. A) Plaque assay titration of SARS-CoV-2 infected WT and IFI16 KO cells; **B-C)** WB analysis of NL63 (1, 2, 3, 4, and 5d.p.i) and SARS-CoV-2 (6h, 1, 2, and 3d.p.i.) replication kinetics in WT and IFI16 KO. NL63 titration was performed from supernatant harvest at 6d.p.i. All NL63 and SARS-CoV-2 infections were performed using MOI1 and 3, respectively. M-Mock, WB- western blot, d.p.i.- days post-infection, 6h- 6 hours post-infection, MOI- the multiplicity of infection. Bars show mean +/- SD of 3 independent experiments. Statistical significance was determined using the Bonferroni-Dunn method, with P = 0.05. For each corresponding time point, multiple comparisons t-test was performed between WT vs. IFI16 KO-HaCaT cells.

To assess viral replication and transcription in WT *vs.* KO IFI16 cells, we infected HaCaT cells and measured hCoV-mediated induction of ORF1ab and N mRNA levels as markers of virus genome replication and viral transcription, respectively. For NL63, both ORF1ab and N mRNAs started to increase at 1d.p.i. and peaked at 4d.p.i., in line with other studies showing a slow NL63 replication cycle (Herzog 2008) (Hofmann, et al., 2005) (Hoek, Pyrc, & Berkhout, 2006), with a ~10-fold increase in WT vs. IFI16 KO (Fig.10A and C), suggesting higher replication rate in the presence of IFI16. Upon SARS-CoV-2 infection, ORF1ab and N mRNA levels peaked at 1d.p.i. (Fig.10B and D), where the difference was significantly higher in WT cells than IFI16 KO-HaCaT for ORF1ab (*P<0.0001*), suggesting higher SARS-CoV-2 replication in the presence of IFI16. However, after 1d.p.i., mRNA levels dropped to basal levels, indicating an inefficient virus production in HaCaT cells.

We further tested the transcriptional induction of type-I IFNs (IFNβ) and type-III IFNs (IFNλ1) along with IFN-stimulating genes (ISGs). Upon NL63 infection, IFNβ mRNA levels were induced starting from 1d.p.i., peaking at 3-6d.p.i. and were consistently higher in IFI16 KO-HaCaT cells throughout the entire viral cycle in comparison to WT-HaCaT cells with *P<0.0001* at 3 and 6d.p.i., respectively (Fig.10E). However, for type-III IFN mRNA induction, no statistically significant distinction was observed between the two cell lines (Fig.10G). IFIT1 mRNA levels were highly induced in IFI16 KO cells upon NL63 infection (Fig.10I). On the contrary, upon SARS-CoV-2 infection, compared to WT-HaCaT cells, there was a significant reduction of IFNβ levels in IFI16 KO-HaCaT at 2d.p.i. (adjusted *P-value = 0.0022*) (Fig.10F) also reflected by reduced IFIT1 mRNA levels at that timepoint, while at 6h.p.i, a stronger induction of IFIT1 was seen in IFI16 KO-HaCaT cells compared to WT cells (Fig.10J). Some variations were seen for IFNλ1, but no statistical significance was observed among the two cell lines (Fig.10H).

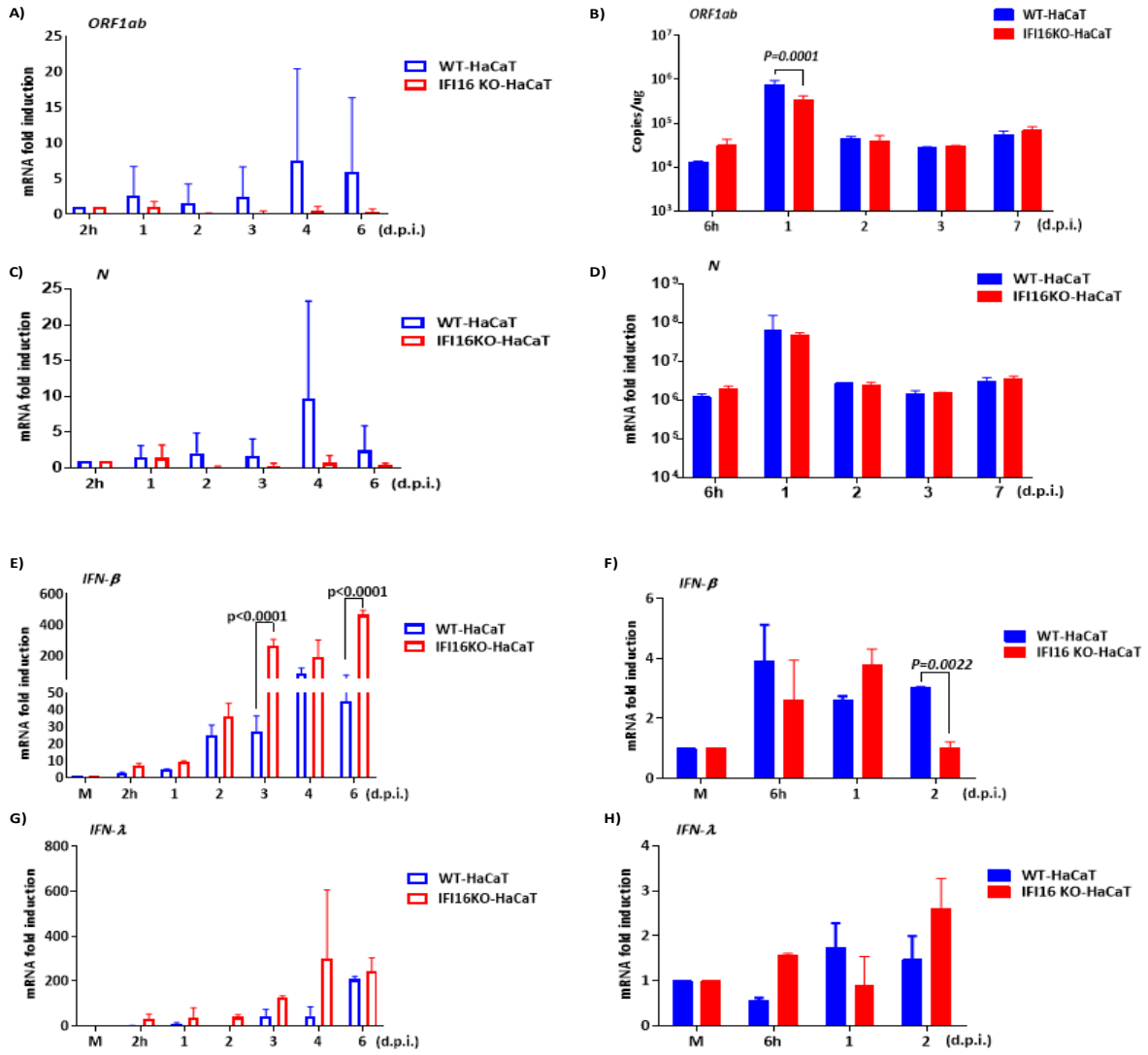

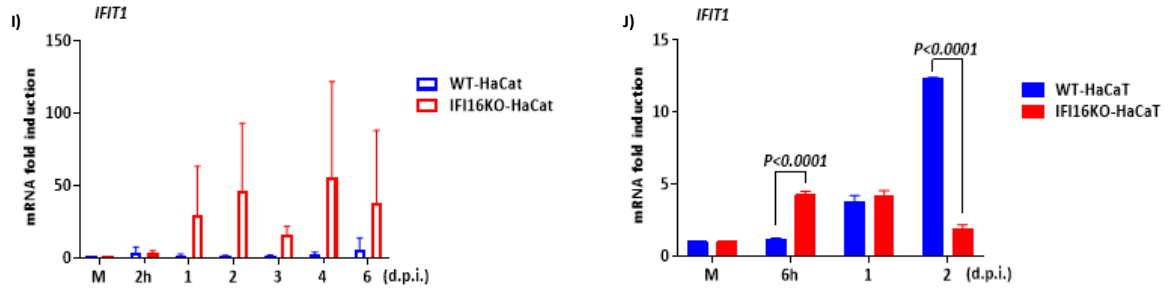

Fig.10. Assessment of viral replication and antiviral innate immune response in HaCaT cells. A-D) Relative mRNA levels of NL63 (2h, 1, 2, 3, 4, and 6d.p.i.) and SARS-CoV-2 (6h, 1,2,3, and 7d.p.i.) viral genes were quantified in infected WT and IFI16 KO-HaCaT cells. Viral NL63 mRNA levels were measured by RT-qPCR, normalized to GAPDH, and plotted as fold induction relative to 2 hpi set at 1 for NL63. For SARS-CoV-2 ORF1ab and N transcripts are quantified in copies/µg using quantitative RT-PCR; **E-F)** Relative mRNA levels of type I IFNs (IFNβ) and **(G-H)** type III IFNs (IFNλ1) were quantified for both NL63 and SARS-CoV-2; **I-J)** relative mRNA levels of ISG (IFIT1) upon NL63 and SARS-CoV-2 infection. Cellular mRNA levels were measured by RT-qPCR, normalized to GAPDH, and plotted as fold induction relative to mock-infected cells set at 1. All NL63 and SARS-CoV-2 infections were performed using MOI1 and 3, respectively. M-Mock, 2h- 2 hours post-infection, 6h- 6 hours post-infection, d.p.i.- days post-infection, MOI- a multiplicity of infection, IFNs- interferons, ISGs- IFN stimulating genes. ORF1ab-genomic RNA, N- sub-genomic RNA. Bars show means +/- SD from 3 independent experiments. Statistical significance was determined using the Bonferroni-Dunn method, with P = 0.05. For each corresponding time point, multiple comparisons t-test was performed between WT-HaCaT vs. IFI16 KO.

To finally determine the infection rate in HaCaT cells, we counted the number of infected cells by immunofluorescence analysis using antibodies against viral NP. We obtained that <1% of cells were infected with both viruses (Fig.11A). Conversely, in LLC-MK2 cells, the infection rate is much higher for both NL63 and SARS-CoV-2 when compared to that observed in HaCaT cells. (Fig.11B and C). Based on all these results, we determined that the replication rate of both NL63 and SARS-CoV-2 in HaCaT cells was shallow. Thus, these cells are not an excellent model for studying innate immune responses.

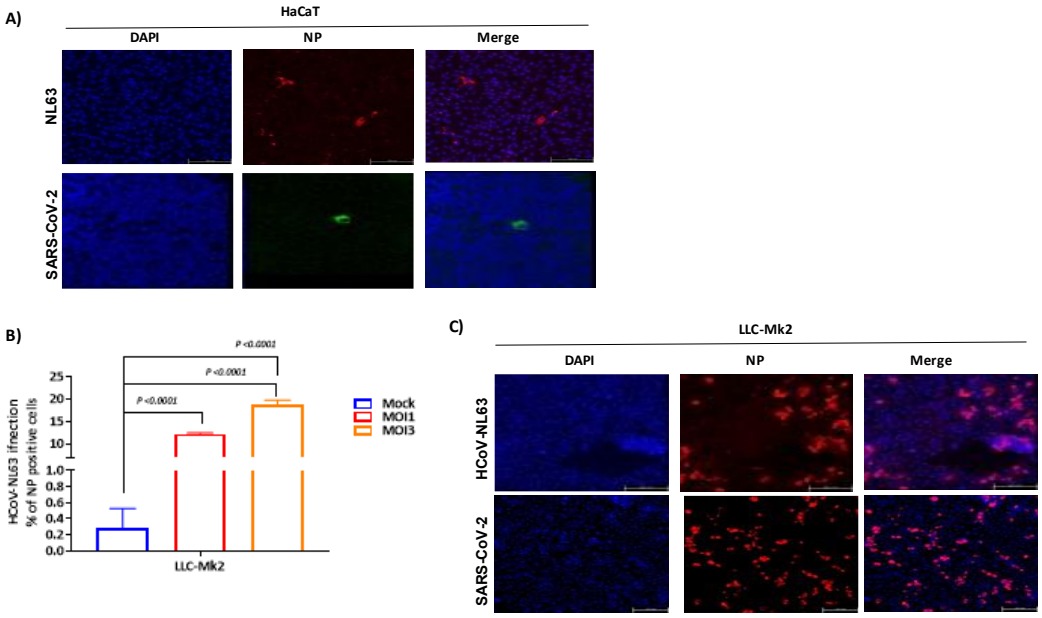

Fig.11. LLC-MK2 cell line is a suitable model for studying coronavirus pathogenesis. A) HaCaT cells were infected with NL63 (upper panels) and SARS-CoV-2 (lower panels) at MOI1 and were analyzed after 1d.p.i. (SARS-CoV-2) and 3d.p.i. (NL63). **B)** FACS analysis to quantify NL63 NP positive cells in LLC-MK2 cells at 3d.p.i., MOI1, and 3, respectively. **C)** Immunofluorescence analysis of NL63 (upper panels) and SARS-CoV-2 (lower panels) infected LLC-MK2 (MOI1). NL63 cells were analyzed after 3d.p.i. SARS-CoV-2 infected cells were analyzed after 1d.p.i. Bars show means +/- SD from 3 independent experiments. Statistical significance was determined using the Bonferroni-Dunn method, with $P = 0.05$. For each corresponding time point, multiple comparisons *t-test* was performed between Mock vs. MOI1, Mock vs. MOI3, and MOI1 vs. MOI3. Mock represents the uninfected cells.

4.2 Kinetics of SARS-CoV-2 and NL63 infection and innate response in LLC-MK2

To understand the role of the nucleic acid sensor IFI16 in hCoV replication, we sought a cell line susceptible and permissive to the replication of either SARS-CoV-2 or the low-pathogenic bat-derived NL63 virus. We decided to work with LLC-MK2, a rhesus macaque epithelial kidney that could support the efficient replication of both viruses (as shown in Fig.11B-C). LLC-MK2 cells were infected with both viruses at MOI1, and viral replication was assessed by measuring the levels of viral RNA in the culture supernatant of infected cells using RT-qPCR or ddPCR for SARS-CoV-2 and NL63, respectively. As shown in Fig.12A-B, we observed no change in viral load at 1 and 3d.p.i for NL63, which significantly increased at

6d.p.i. (*P=0.0025*), while the viral load increased at 2d.p.i. being very high at 3 and 7d.p.i for SARS-CoV-2 *(P<0.0001*).

In alignment with previous studies, western blotting analysis of the total protein extracts obtained from the same cultures using antibodies against the NP revealed that its expression was slightly delayed in NL63 compared with SARS-CoV-2. We observed NP being detectable starting from 1d.p.i. in NL63 with a peak at 3d.p.i.(Fig.12C), while in SARS-CoV-2 infected cells, it was already highly expressed at 16h.p.i that lasted until 3d.p.i. (Fig.12D) When we looked for the IFI16 expression levels in the same cell extracts, we failed to see any significant changes in IFI16 expression levels that could be related to the viral infection. Indeed, some enhancement in IFI16 expression levels was observed over time in both infected and mock-infected cells, indicating that this was mainly associated with growth density.

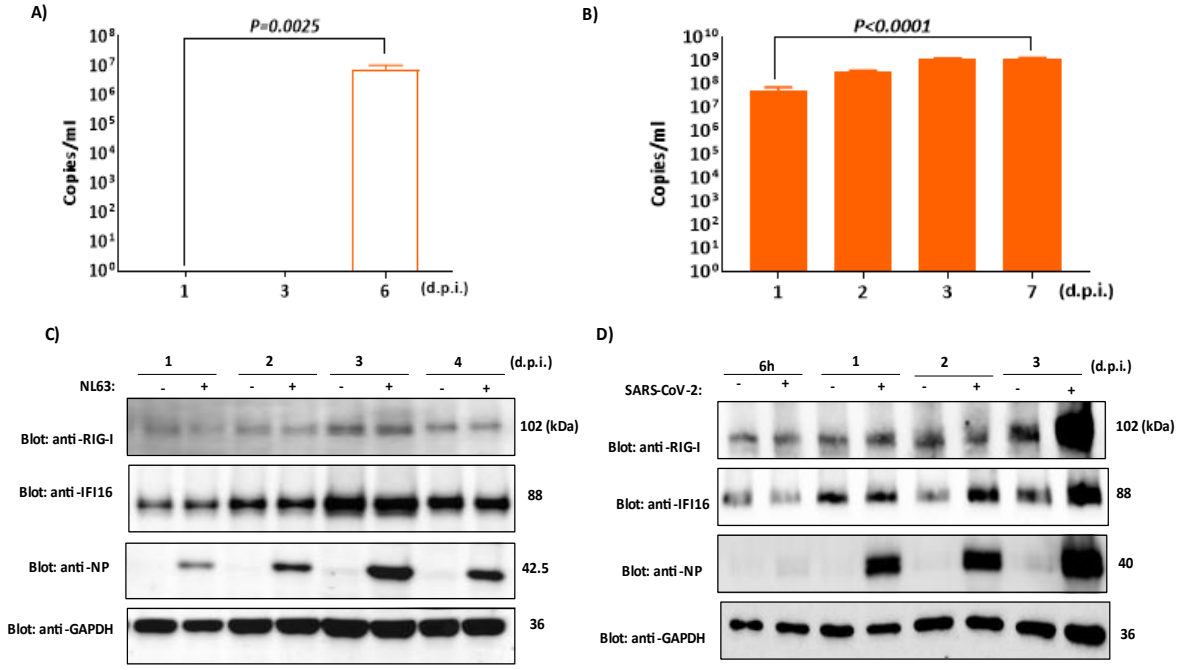

Fig.12. Coronavirus kinetics in LLC-MK2 cells A-B) Extracellular viral load in NL63 and SARS-CoV-2 infected cells was measured and expressed in copies/ml using ddPCR and quantitative RT-PCR, respectively; **C-D)** WB analysis of NL63 (1, 2, 3, and 4 d.p.i) and SARS-CoV-2 (6h, 1, 2, and 3d.p.i.) kinetics. All NL63 and SARS-CoV-2 infections were performed using MOI1. M-Mock, WB- western blot, d.p.i.- days post-infection, 6h- hours post-infection, MOI- the multiplicity of infection. Bars show means +/- SD from 3 independent experiments. A one-way ANOVA test for trend was performed, with P = 0.05 considered statistically significant.

We analyzed NL63 viral replication and transcription in LLC-MK2 cells. We noticed a significant increase (P<0.0001) in the trend for transcription of ORF1ab (genomic) and N gene (genomic and subgenomic) mRNA (Fig.13A-B). We also analyzed the innate antiviral response upon infection and found that the IFNβ mRNA levels are significantly reduced (P<0.0001) compared to the corresponding mock (Fig.13C). The mRNAs encoding for the interferon-stimulated genes (ISGs) IFIT1 and Mx1 were hardly detectable by qPCR in response to NL63 at any time points p.i. (Fig.13D-E). As internal control of the integrity of the innate response to exogenous RNA, the cells were transfected with either polyinosinic: polycytidylic acid (poly (I:C)) or the sequence optimized RIG-I agonist 5' ppp-RNA termed M8. As shown in Fig.13F, both stimuli triggered around 500-fold induction of IFIT1 mRNAs, confirming a significant induction of innate immune response to exogenous RNA was functional (*P=0.0002* and *0.0003* for poly I:C and M8, respectively). Altogether, these findings indicate that the LLC-MK2 cells are fully permissive to both viruses while poorly reacting to these viruses even though their innate response to exogenous RNA was fully functional.

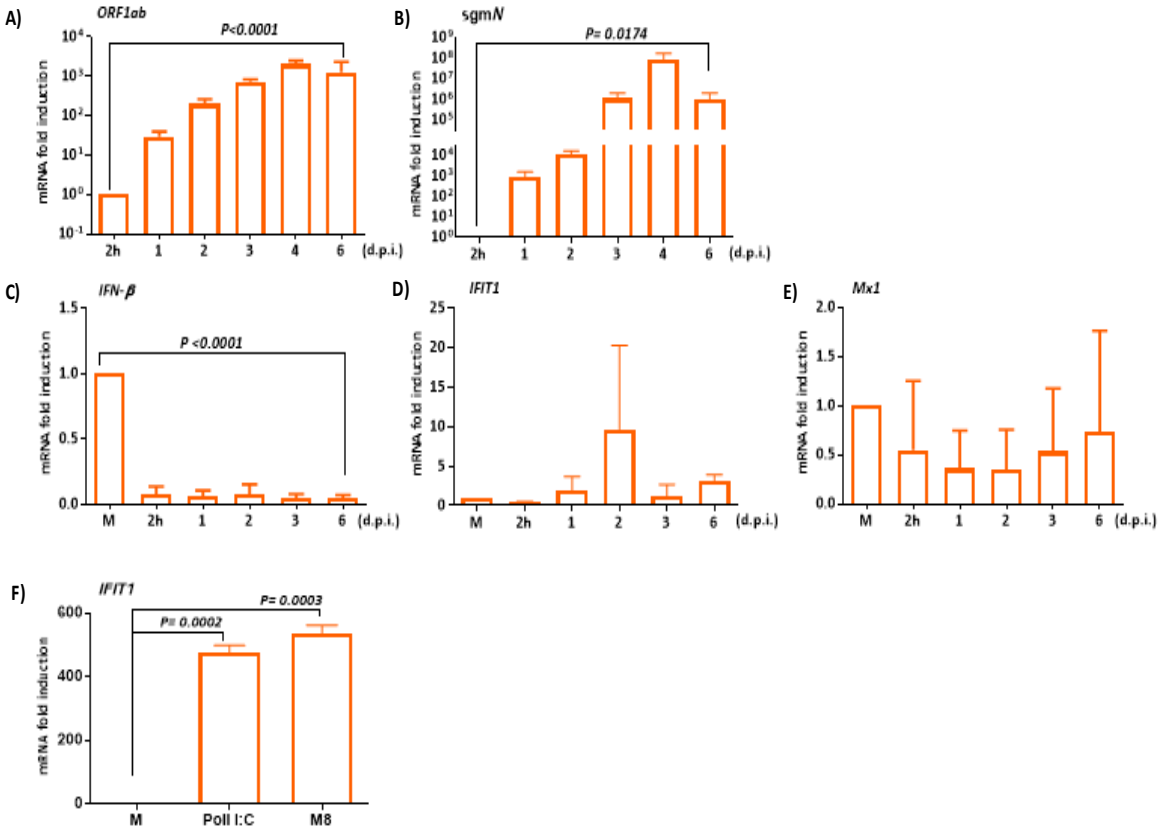

Fig.13. Viral gene transcription and antiviral innate immune response upon NL63 infection. A-B) qPCR analysis of NL63 viral genes (genomic ORF1ab and sub-genomic N) and **C-E)** type I IFNs (IFNβ) and ISGs (IFIT1 and Mx1) at 2h, 1,2,3,4, and 6d.p.i. All NL63

infections were performed using MOI1. **F)** qPCR analysis of IFIT1 mRNA expression in poly (I:C)- or M8-transfected LLC-MK2 cells at 1d post-transfection (d.p.t.). Total RNA was extracted and analyzed by qPCR. Viral mRNA levels were measured by RT-qPCR, normalized to GAPDH, and plotted as fold induction relative to 2 hpi set at 1, while cellular mRNA levels were plotted as fold induction relative to mock-infected cells set at 1. M-Mock, 2h- 2 hours, d.p.i.- days post-infection, h.p.i.- hours post-infection, MOI- a multiplicity of infection, IFNs- interferons, ISGs- IFN stimulating genes. Bars show means +/- SD from 3 independent experiments. Statistical significance was determined using the Bonferroni-Dunn method, with P = 0.05. For each corresponding time point, multiple comparisons t-test was performed.

4.3 IFI16 binds hCoV nucleoprotein

hCoVs replicate in the cytoplasm by forming double-membrane structures named replication organelles (ROs) that protect viral RNA from degradation and detection by host cellular immune sensors (Roingeard, et al., 2022). Given that IFI16 can bind to RNA viral genomes (Jiang, et al., 2021) (Kim, et al., 2020), we asked whether IFI16 could form a complex with NP, which is localized in the cytoplasm and can bind to the viral genome.

We performed an IFL analysis to assess IFI16 localization upon coronavirus infection. We infected the LLC-MK2 cells with NL63 (upper panels) and SARS-CoV-2 (middle panels) at MOI1 and performed co-staining experiments using antibodies directed against IFI16 and the viral protein NP. We observed that IFI16 was predominantly nuclear under basal conditions, but it is massively translocated to cytoplasm and co-localized with NP at 1 and 3d.p.i after SARS-CoV-2 or NL63 infection. It is worth mentioning that we have observed nuclear to cytoplasmic translocation of IFI16 even in SARS-CoV-2 infected HaCaT cells (lower panels) despite a lower percentage of infection (Fig.14).

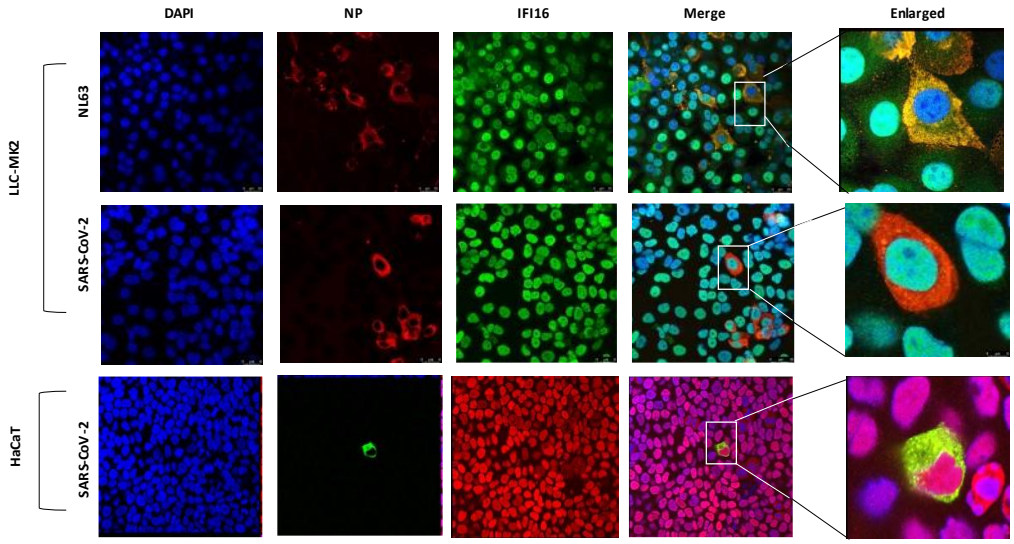

Fig.14. Nuclear translocation of IFI16 upon coronavirus infection Immunofluorescence analysis of NL63 and SARS-CoV-2-infected LLC-MK2 cells (MOI1, 3d.p.i.) (upper and middle panels) and SARS-CoV-2- infected HaCaT cells (MOI3, 16h.p.i.) (lower panels). Cells were stained with antibodies against NP and IFI16.

After finding that IFI16 translocated from the nucleus to the cytoplasm and colocalized with the NP protein upon infection, we asked whether they interacted. To this end, LLC-MK2 cells were infected with NL63 at MOI1, and at 3d.p.i, we prepared the total cell extracts to run immunoprecipitation. As shown in Fig.15, the NP protein is coimmunoprecipitated with the IFI16 protein.

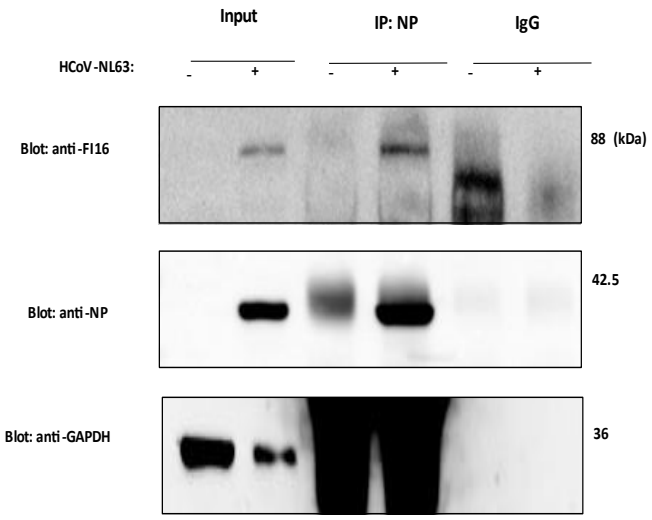

Fig.15. IFI16 binds to viral nucleoprotein. Cell lysates from NL63-infected LLC-MK2 cells were harvested at 3d.p.i and immunoprecipitated for viral NP. WB was performed to check

IFI16 binding to the immunoprecipitated NP using antibodies against IFI16 and NP. Input is a non-immunoprecipitated sample as a positive control, and IgG is a control.

These results indicate that the IFI16 protein can interact with viral NP. Further studies are being performed to gain more insight into this interaction and understand whether it depends on the binding of IFI16 to the viral RNA genome. In addition, we have recently obtained clones of LLC-MK2 whereby the IFI16 gene has been stably knocked down using the CRISPR-Cas9 gene editing technology. The availability of this cell line will help to understand the impact of IFI16 on hCoV replication and innate immune response.

5. DISCUSSION

Different factors control viral replication inside the host cell via either a positive or negative effect on the replication, varying from entry, transcription, translation, and assembly of viral progeny. Viruses transcribe and replicate their genome in the host cell by utilizing its cellular machinery and, thus, are exposed to various host cell antiviral restriction factors (Merkl, Orzalli, & Knipe, 2018). IFI16 is one such cellular host restriction factor that has been well characterized as a nuclear DNA sensor (Unterholzner, et al., 2011). IFI16 has been shown to bind to incoming viral DNA at the nuclear periphery. It has already been demonstrated that upon binding to viral DNA, IFI16 undergoes oligomerization and recruits other host factors necessary to build antiviral support to activate immune signaling and suppress transcription (Howard & Cristea, 2020). Bats have been demonstrated to host and exhibit a co-evolutionary relationship with several zoonotic DNA and RNA viruses, including coronaviruses, which have lost the entire PYHIN gene family, of which IFI16 is a member. The damage associated with DNA or RNA viruses can cause inflammasome activation, indicating the possibility that high exposure to these pathogens could be an additional evolutionary driver for the loss of the PYHIN family in bats (Ahn, Cui, Irving, & Lin-FaWang, 2016).

Based on this information, we hypothesized that IFI16, which is abundantly present in humans, might play an antiviral role in coronavirus infection. Therefore, to test our hypothesis, we used two bat-originated hCoVs, the low-pathogenic NL63 and the highly pathogenic SARS-CoV-2, to investigate the role of IFI16 during RNA virus infection in IFI16 WT and IFI16 KO-HaCaT cells. We demonstrated that IFI16 is induced upon infection of both SARS-CoV-2 and NL63 (at 6h.p.i. and 2d.p.i., respectively). Surprisingly, our data in HaCaT cells suggests that both viruses replicate more in the presence of IFI16, suggesting that IFI16 might be able to sustain viral replication directly.

Mild coronavirus induces, but pathogenic coronavirus inhibits type-I IFN induction (Fung & Liu, 2019). Supporting this statement, we have demonstrated that upon NL63 infection, HaCaT produced higher IFN-b levels that are even higher in IFI16 KO-HaCaT cells than WT-HaCaT cells, while no IFN induction was seen upon SARS-CoV-2 infection. IFI16 can induce IFNβ production through STING-TBK-1-IRF3 signaling when it is activated upon sensing of dsDNA viruses (Unterholzner, et al., 2011). Whether the induction of IFNβ in WT-HaCaT cells is induced through a similar pathway upon NL63 is not known. Unfortunately, the number of infected HaCaT cells was too low, and the same experiments are now being repeated using the LLLC-MK2 cellular model. Indeed, we have found that this monkey epithelial cell line may

be an excellent model for the following reasons: i) it is naturally infected by both NL63 and SARS-CoV-2 with a good infection efficiency (Wurtz, Penant, Jardot, Duclos, & Scola, 2021) and ii) IFI16 protein of *Macaca mulatta*, the species source of LLC-MK2, shares 88.6% similarity to *Homo sapiens* (HomoloGene, 2023). We found high viral loads for NL63 and SARS-CoV-2 in these cells. We identified that IFI16 is induced upon infection with both viruses.

Further, we characterized the active transcription of viral genomic and sub-genomic fragments in LLC-MK2 cells. Contradictory to the literature where mild coronaviruses trigger IFN response upon infection (Fung & Liu, 2019), we failed to see any induction of either IFNs or ISGs upon NL63 infection. This cell line display integrity of the innate immune response as demonstrated by a significant induction of *IFIT1*, an ISG, upon administration of exogenous RNA such as poly (I:C) or M8. These findings are coherent with the literature indicating the functional immune system in LLC-MK2 cells. Thus, the observed dampened immune response could be a viral escape mechanism, a possible explanation for the active replication of NL63 in these cells.

IFI16 is predominantly nuclear in fibroblasts, epithelial, endothelial, and lymphoid tissues, but its cytoplasmic co-localization has also been reported in macrophages in the context of DNA-induced innate immunity (Li, Diner, & Cristea, 2012). IFI16 has an evolutionarily conserved NLS, which undergoes acetylation upon pathogen invasion and initiates IFI16 translocation to the cytoplasm (Li, Diner, & Cristea, 2012). Accordingly, we observed IFI16 protein translocation from the nucleus to the cytoplasm upon both NL63 and SARS-CoV-2 infection, and it should be mostly in its acetylated form. We have also found that IFI16 colocalizes with the RNA-binding protein NP and interacts with IFI16, as demonstrated by co-immunoprecipitation. Whether this interaction may affect the hCoV viral genome sensing, the antiviral response, or its replication remains to be established.

IFI16, through its HIN200 domain, can bind to viral DNA and subsequently has been shown to sense and restrict a panel of DNA viruses (Gariano, et al., 2012) (Lo Cigno I, et al., 2015). More recently, the role of IFI16 in RNA virus sensing has also emerged. IFI16 can transcriptionally regulate type-I IFN expression during Sendai virus infection and promote MAVS-mediated production of IFNs, which inhibits the replication of porcine reproductive and respiratory syndrome (PRRSV2) (Chang, et al., 2019). IFI16 directly binds to the genomic RNA of the chikungunya virus (CHKV), thereby restricting its replication and maturation

independent of IFN-signaling (Kim, et al., 2020). Viral restriction by IFI16 has also been reported for the Zika virus (Wichit, et al., 2019) and Sindbis virus (SINV) (Garcia-Moreno M, et al., 2019). Also, IFI16, upon influenza A virus (IAV) infection, can interact with both negative-sense viral RNA and RIG-I to potentiate RIG-I-mediated IFN-I production, which inhibits IAV replication (Jiang, et al., 2021).

Despite the emerging evidence of IFI16 playing a crucial role in the control of RNA virus replication, it remains unclear whether IFI16 interacts or interferes with CoV replication directly or indirectly through crosstalk with other PRRs. From the literature, we know that IFI16 senses both DNA and RNA nucleic acids and interacts and cooperates with either the cGAS/STING or the RIG-I/MAVS signaling pathways, thereby modulating both IFN and cytokine production in different settings (Cai, Tang, Xu, & Zheng, 2021). However, its role in the hCoV-induced innate immune response is still unknown.

Although we successfully demonstrated the binding of IFI16 to NL63 NP protein, its role in viral restriction is yet to be determined. The ability of IFI16 to translocate from the nucleus to the cytoplasm following various stimuli has already been described in the literature (Costa, et al., 2011) (Dell'Oste, et al., 2014), and IFI16 activity has always been linked to the inhibition of viral infection rather than promotion. In support of the potential involvement of IFI16 in the host response to SARS-CoV-2 infection, using a COVID-19 multi-omics database (covid omics. app) (Overmyer, et al., 2021), we found that the IFI16 transcript is more abundant in leucocytes isolated from COVID-19 patients than in those from non-infected individuals, indicating a possible involvement of IFI16 in coronavirus pathogenesis.

Therefore, to test our hypothesis that IFI16 exerts an antiviral role in coronavirus infection, we are currently characterizing the active viral replication in IFI16 KO-LLC-MK2 cells through plaque assay. We are analyzing the transcriptional activation of IFN genes and ISGs in IFI16 KO-LLC-MK2 cells. We will also focus on demonstrating the nuclear to cytoplasmic localization through immunofluorescence. Further on, we would focus on characterizing the role of IFI16 and RIG-I interaction in coronavirus signaling, along with understanding the exact mechanism of IFI16 binding to the viral genome.

Overall, this study will contribute to filling the gap in knowledge about the role of the innate sensor IFI16 in controlling hCoV replication. As we are using both low- and highly pathogenic hCoVs, the project will also assess any commonalities or differences among the

two viruses that may substantially extend our insight into SARS CoV-2 enhanced pathogenicity compared to standard cold hCoVs, such as NL63.

6. REFERENCES

Abdul-Rasool, S., & Fielding, B. C. (2010). Understanding human coronavirus NL63. *Open Virol. J*, 76-84.

Adil, T., Rahman, R., Whitelaw, D., Jain, V., Al-Taan, O., Rashid, F., . . . Jambulingam, P. (2021). SARS-CoV-2 and the pandemic of COVID-19. *Postgraduate Medical Journal*, 110-116.

Ahn, M., Cui, J., Irving, A. T., & Lin-FaWang. (2016). Unique Loss of the PYHIN Gene Family in Bats Amongst Mammals: Implications for Inflammasome Sensing. *Nature*, 1-7.

Akira, S., Uematsu, S., & Takeuchi, O. (2006). Pathogen recognition and innate immunity. *Cell*, 783-801.

Almeida, J. D., Berry, D. M., & Cunningham, C. H. (1968). Coronaviruses. *Nature*, 220-650.

Almine, J. O. (2017). IFI16 and cGAS cooperate in the activation of STING during DNA sensing in human keratinocytes. . *Nat Commun*, 14392.

Al-Qaaneh, A. M., Alshammari, T., Aldahhan, R., Aldossary, H., Alkhalifah, Z. A., & Borgio, J. F. (2021). Genome composition and genetic characterization of SARS-CoV-2. *Saudi Journal of Biological Sciences*, 1978-1989.

Artika, M., Dewantari, A. K., & Wiyatno, A. (2020). Molecular Biology of Coronaviruses: Current Knowledge. *Heliyon*, e04743.

Asghari, A., Naseri, M., Safari, H., Saboory, E., & Parsamanesh, N. (2020). The Novel Insight of SARS-CoV-2 Molecular Biology and Pathogenesis and Therapeutic Options. *DNA and Cell Biology*, 1741-1753.

Banerjee, A., Kulcsar, K., Misra, V., Frieman, M., & Mossman, K. (2019). Bats and Coronaviruses. *Viruses*, 1-15.

Bawadekar, M., Andrea, M. D., Cigno, I. L., Baldanzi, G., Caneparo, V., Graziani, A., . . . Gariglio, M. (2015). The Extracellular IFI16 Protein Propagates Inflammation in Endothelial Cells Via p38 MAPK and NF-kB p65 Activation. *Journal of Interferon & Cytokine Research*, 441-453.

Bawadekar, M., de Andrea, M., Gariglio, M., & Londolfo, S. (2015). Mislocalization of the interferon-inducible protein IFI16 by environmental insults: Implications in autoimmunity. *Cytokine & Growth Factor Reviews*, 213-219.

Bayarri-Olmos, R., Idorn, M., Rosbjerg, A., Perez-Alos, L., Hansen, C., Bruun, J., . . . Garred, P. (2021). SARS-CoV-2 neutralizing antibody responses towards full-length spike protein and the receptor-binding domain. *The Journal of Immunology*, 878-887.

Beniac, D. R., Andonov, A., Grudeski, E., & Booth, T. F. (2006). Architecture of the SARS coronavirus perfusion spike. *Nature Structural and Molecular Biology*, 751-752.

Beutler, B. (2004). Inferences, questions, and possibilities in Toll-like receptor signaling. *Nature*, 257-263.

Bickler, S. W., Cauvi, D. M., Fisch, K. M., Prieto, J. M., Sykes, A. G., Thangarajah, H., . . . et. al. (2021). Extremes of age are associated with differences in the expression of selected pattern recognition receptor genes and ACE2, the receptor for SARS-CoV-2: implications for the epidemiology of COVID-19 disease. *BMC Med Genomics*, 138.

Bosso, M., & Kirchhoff, F. (2020). Emerging Role of PYHIN Proteins as Antiviral Restriction Factors. *Viruses*, 1-17.

Bosso, M., Bozzo, C. P., Hotter, D., Volcic, M., Stürzel, C. M., Rammelt, A., . . . Sau, D. (2020). Nuclear PYHIN proteins target the host transcription factor Sp1, thereby restricting HIV-1 in human macrophages and CD4+ T cells. *Plos Pathogens*, 1-30.

Cai, C., Tang, Y., Xu, G., & Zheng, C. (2021). The crosstalk between viral RNA- and DNA-sensing mechanisms. . *Cell Mol Life Sci.* , 7427-7434.

Canton, J., Fehr, A. R., Fernandez-Delgado, R., Gutierrez-Alvarez, F. J., Sanchez-Aparicio, M. T., García-Sastre, A., . . . Sola, I. (2018). MERS-CoV 4b protein interferes with the NF-κB-dependent innate immune response during infection. *Plos Pathogens*.

Carbajo-Lozoya, J., Ma-Lauer, Y., Malesevic, M., Theuerkorn, M., Kahlert, V., Prell, E., . . . von Brunn, A. (2014). Human coronavirus NL63 replication is cyclophilin A-dependent and inhibited by non-immunosuppressive cyclosporine A-derivatives including Alisporivir. *Virus Research*, 44-53.

Chang, X., Shi, X., Zhang, X., Wang, L., Li, X., Wang, A., . . . Zhan, G. (2019). IFI16 Inhibits Porcine Reproductive and Respiratory Syndrome Virus 2 Replication in a MAVS-Dependent Manner in MARC-145 Cells. *Viruses*, 1-14.

Chen, B., Tian, E.-K., He, B., Tian, L., Han, R., Wang, S., . . . Cheng, W. (2020). Overview of lethal human coronaviruses. *Signal Transduction and Targeted Therapy*, 1-16.

Costa, S., Borgogna, C., Mondini, M., Andrea, M. D., Meroni, P. L., E. Berti, M. G., & Landolfo, S. (2011). Redistribution of the nuclear protein IFI16 into the cytoplasm of

ultraviolet B-exposed keratinocytes as a mechanism of autoantigen processing. *British Journal of Dermatology*, 282-290.

Cui, J., Li, F., & Shi, Z. (2019). Origin and evolution of pathogenic coronaviruses. *Nature Reviews: Microbiology*, 181-192.

Dan, J., Mateus, J., Kato, Y., Hastie, K., Yu, E., Faliti, C., . . . Frazier, A. (2021). Immunological memory to SARS-CoV-2 assessed for up to 8 months after infection. *Science*, 371.

de Breyne, S., Vindry, C., Guillin, O., Conde, L., Mure, F., Gruffat, H., . . . Ohlmann, T. (2020). Translational Control of Coronaviruses. *Nucleic Acids Research*, 12502-12522.

Dell'Oste, V., Gatti, D., Giorgio, A. G., Gariglio, M., Landolfo, S., & Andrea, M. D. (2015). The interferon-inducible DNA-sensor protein IFI16: a key player in the antiviral response. *New Microbiologica*, 5-20.

Dell'Oste, V., Gatti, D., Gugliesi, F., Andrea, M. D., Bawadekar, M., Cigno, I. L., . . . Landolfo, S. (2014). Innate Nuclear Sensor IFI16 Translocates into the Cytoplasm during the Early Stage of In Vitro Human Cytomegalovirus Infection and Is Entrapped in the Egressing Virions during the Late Stage. *Journal of Virology*, 6970-6982.

Deng, X., & Baker, S. (2021). Coronaviruses: Molecular Biology. *Encyclopedia of Virology*, 198-207.

Doyle, N., Hawes, P. C., Simpson, J., Adams, L. H., & Maier, H. J. (2019). The porcine deltacoronavirus replication organelle comprises with Double-Membrane vesicles and zippered endoplasmic reticulum with Double-Membrane spherules. *Viruses*, 1030.

Drosten, C., Gunther, S., Preiser, W., & al., e. (2003). Identification of a novel coronavirus in patients with severe acute respiratory syndrome. *New England Journal of Medicine*, 1967-1976.

Fehr, A. R., & Perlman, S. (2015). Coronaviruses: an overview of their replication and pathogenesis. *Methods Mol. Biol.*, 1-23.

Felsenstein, S., Herbert, J. A., McNamara, P. S., & Hedrich, C. M. (2020). COVID-19:Immunology and treatement options. *Clinical Immunology*, 108448.

Fielding, B. (2011). Human coronavirus NL63: a clinically important virus? *Future Microbiol*, 153–159.

Forni, D., Cagliani, R., Clerici, M., & Sironi, M. (2017). Molecular Evolution of Human Coronavirus Genomes. *Trends Microbiology*, 35-48.

Fung, S. T., & Liu, D. X. (2019). Human coronavirus: Host-Pathogen Interaction. *Annual Review of Microbiology*, 529-557.

Garcia-Moreno M, N. M., Ni, S., Järvelin, A., González-Almela, E., Lenz, C., Bach-Pages, M., . . . al., e. (2019). System-wide Profiling of RNA-Binding Proteins Uncovers Key Regulators of Virus Infection. *Mol Cell*, 196-211.

Gariano, G., Dell'Oste, V., Bronzini, M., Gatti, D., Luganini, A., De Andrea, M., & et.al. (2012). The Intracellular DNA Sensor IFI16 Gene Acts as Restriction Factor for Human Cytomegalovirus Replication. *PLoS Pathog*, e1002498.

Gaunt, E. R., Hardie, A., Class, E. C., Simmonds, P., & Templeton, K. E. (2010). Epidemiology and clinical presentations of the four human coronaviruses 229E, HKU1, NL63, and OC43 detected over 3 years using a novel multiplex real-time PCR method. *Journal of Clinical Microbiology*, 2940.

Gaurav, A., & Al-Nema, M. (2019). Polymerases of coronaviruses: structure, function, and. *Viral Polymerases*, 271-300.

Hoek, L. v., Pyrc, K., & Berkhout, B. (2006). Human coronavirus NL63, a new respiratory virus. *FEMS Microbiological Reviews*, 760-773.

Hoek, L. v., Pyrc, K., Jebbink, M. F., Vermeulen-Oost, W., Berkhout, R. J., Wolthers, K. C., . . . Berkhout, B. (2003). Identification of a new human coronavirus. *Nature Medicine*, 368-373.

Hoek, L. v., Pyrc, K., Jebbink, M. F., Vermeulen-Oost, W., Berkhout, R. J., Wolthers, K. C., . . . Berkhout, B. (2004). Identification of a new human coronavirus. *Nature Medicine*, 368-373.

Hofmann, H., Pyrc, K., Hoek, L., Geier, M., Berkhout, B., & Pöhlmann, S. (2005). Human coronavirus NL63 employs the severe acute respiratory syndrome coronavirus receptor for cellular entry. *The National Academy of Sciences*, 7988-7993.

Hofmann, H., Pyrc, K., van der Hoek, L., Geier, M., Berkhout, B., & Pohlmann, S. (2005). Human coronavirus NL63 employs the severe acute respiratory syndrome coronavirus receptor for cellular entry. *PNAS*, 7988-7993.

Howard, T. R., & Cristea, I. M. (2020). Interrogating host antiviral environments driven by nuclear DNA sensing: A multi-omic perspective. *Biomolecules*, 1591.

Hu, B., Guo, H., Zhou, P., & Shi, Z.-L. (2021). Characteristics of SARS-CoV-2 and COVID-19. *Nature Reviews Microbiology*, 141-154.

Hu, Y., Liu, L., & Lu, X. (2021). Regulation of Angiotensin-Converting Enzyme 2: A Potential Target to Prevent COVID-19? *Frontiers in Endocrinology*, 1-10.

Huang, I.-C., Bosch, B. J., Li, F., Li, W., Lee, K. H., Ghiran, S., . . . Choe, H. (2006). SARS Coronavirus, but Not Human Coronavirus NL63, Utilizes Cathepsin L to Infect ACE2-expressing Cells. *Journal of Biological Chemistry*, 3198-3203.

Irving, A. T., Ahn, M., Goh, G., & Anderson, D. E. (2021). Lessons from the host defenses of bats, a unique viral reservoir. *Nature*, 363-370.

Islam, A., Ferdous, J., Islam, S., Sayeed, M. A., Choudhury, S. D., Saha, O., . . . Shirin, T. (2021). Evolutionary dynamics and epidemiology of endemic and emerging coronaviruses in humans, domestic animals, and wildlife. *Viruses*, 1-27.

Jiang, Z., Wei, F., Zhang, Y., Wang, T., Gao, W., Yu, S., . . . Liu, J. (2021). IFI16 directly senses viral RNA and enhances RIG-I transcription and activation to restrict influenza virus infection. *Nature Microbiology*, 932-945.

Jo, E. (2019). Interplay between host and pathogen: immune defense and beyond. *Jo Experimental & Molecular Medicine*, 149.

Kasuga, Y., Zhu, B., Jang, K.-J., & Yoo, J.-S. (2021). Innate immune sensing of coronavirus and viral evasion strategies. *Experimental & Molecular Medicine*, 723-736.

Kawai, T., & Akira, S. (2006). Innate immune recognition of viral infection. *Nature Immunology*, 131-137.

Kawai, T., & Akira, S. (2010). The role of pattern-recognition receptors in innate: update on Toll-like receptors. *Nat. Immunol*, 373–384.

Kesheh, M. M., Hosseini, P., Soltani, S., & Zandi, M. (2022). An overview on the seven pathogenic human coronaviruses. *Rev Med Virol*, e2282.

Kim, B., Arcos, S., Rothamel, K., Jian, J., Rose, K. L., McDonald, W. H., . . . Ascano, M. (2020). Discovery of Widespread Host Protein Interactions with the Pre-replicated Genome of CHIKV Using VIR-CLASP. *Molecular Cell*, 624-640.

Kirchdoerfer, R. N., Cottrell, C. A., Wang, N., Pallesen, J., Yassine, H. M., Turner, H. L., . . . al, e. (2016). Pre-fusion structure of a human coronavirus spike protein. *Nature*, 118-121.

Konno, Y., Kimura, I., Uriu, K., Fukushi, M., Irie, T., Koyanagi, Y., . . . Sato, K. (2020). SARS-CoV-2 ORF3b Is a Potent Interferon Antagonist Whose Activity Is Increased by a Naturally Occurring Elongation Variant. *Cell Reports*.

Kumar, A., Ishida, R., Strilets, T., Cole, J., Lopez-Orozco, J., Fayad, N., . . . Hobman, T. C. (2021). SARS-CoV-2 Nonstructural Protein 1 Inhibits the Interferon Response by Causing Depletion of Key Host Signaling Factors. *Journal of Virology*.

Lee, S., Channappanavar, R., & Kanneganti, T.-D. (2020). Coronaviruses: Innate Immunity, Inflammasome Activation, Inflammatory Cell Death, and Cytokines. *Trends in Immunology*, 1083-1099.

Lee, S., Lee, Y., Choi, Y., Son, A., Park, Y., Lee, K., . . . Kim, N. (2021). The SARS-CoV-2 RNA interactome. *Molecular Cell*, 2838-2850.

Li, F. (2016). Structure, function, and evolution of coronavirus spike proteins. *Annu. Rev. Virol.*, 237-261.

Li, J.-Y., Zhou, Z.-J., Wang, Q., He, Q.-N., Zhao, M.-Y., Qiu, Y., & Ge, X.-Y. (2021). Innate Immunity Evasion Strategies of Highly Pathogenic Coronaviruses: SARS-CoV, MERS-CoV, and SARS-CoV-2. *Frontiers in Microbiology*, 1-15.

Li, J.-Y., Zhou, Z.-J., Wang, Q., He, Q.-N., Zhao, M.-Y., Qiu, Y., & Ge, X.-Y. (2021). Innate Immunity Evasion Strategies of Highly Pathogenic Coronaviruses: SARS-CoV, MERS-CoV, and SARS-CoV-2. *Frontiers in Microbiology*.

Li, T., Diner, B. A., & Cristea, I. (2012). Acetylation modulates cellular distribution and DNA sensing ability of interferon-inducible protein IFI16. *PNAS*, 10558-10563.

Li, W., Sui, J., Huang, I.-C., Kuhn, J. H., Radoshitzky, S. R., Marasco, W. A., . . . Farzana, M. (2007). The S proteins of human coronavirus NL63 and severe acute respiratory syndrome coronavirus bind overlapping regions of ACE2. *Virology*, 367-374.

Li, X., Luk, H. K., Lau, S. K., & Woo, P. C. (2019). *Human Coronaviruses: General Features.* Elsevier.

Lo Cigno I, D. A., Borgogna, C., Albertini, S., Landini, M., Peretti, A., Johnson, K., . . . Gariglio, M. (2015). The Nuclear DNA Sensor IFI16 Acts as a Restriction Factor for Human Papillomavirus Replication through Epigenetic Modifications of the. *J Virol*, 7506-20.

Loo, Y.-M., & Jr, M. G. (2011). Immune signaling by RIG-I-like receptors. *Immunity*, 680-692.

Lu, R., Zhao, X., Li, J., Niu, P., Yang, B., Wu, H., & al, e. (2020). Genomic characterization and epidemiology of 2019 novel coronaviurs_ Implications for virus origins and receptor binding. *Lancet*, 565-574.

Luis, A. D., Hayman, D. T., O'Shea, T. J., Cryan, P. M., Gilbert, A. T., Pulliam, J. R., . . . & Webb, C. T. (2013). A comparison of bats and rodents as reservoirs of zoonotic viruses: are bats special? *Proc Biol Sci.*, p. 20122753.

Luis, A. D., Hayman, D. T., O'Shea, T. J., Cryan, P. M., Gilbert, A. T., Pulliam, J. R., . . . Webb, C. T. (2013, Aprile 7). A comparison of bats and rodents as reservoirs of zoonotic viruses: are bats special? *Proceedings of the Royal Society B*, pp. 1-9.

Malone, B., Urakova, N., Snijder, E. J., & Campbell, E. A. (2022). Structures and functions of coronavirus replication-transcription complexes and their relevance for SARS-CoV-2 drug design. *Nature Reviews: Molecular Cell Biology*, 21-29.

Mariana Mesel-Lemoinea, J. M.-O. (2012). A Human Coronavirus Responsible for the Common Cold Massively Kills Dendritic Cells but Not Monocytes. *American Society for Microbiology*, 7577-7587.

Marot, S., Malet, I., Leducq, V., Zafilaza, K., Sterlin, D., Planas, D., . . . Maeda, K. (2021). Rapid decline of neutralizing antibodies against SARS-CoV-2 among infected healthcare workers. *Nature Communication*, 844.

Martellucci, C. A., Flacco, M. E., Cappadona, R., Bravi, F., Mantovani, L., & Manzolib, L. (2020). SARS-CoV-2 pandemic: An overview. *Advances in Biological Regulation*, 1-13.

Masters, P. S. (2006). The Molecular Biology of Coronaviruses. *Advances in virus research*, 193-292.

Masters, P. S., & Perlman, S. (2013). *Chapter 28 Coronaviridae* (Vol. 1). (D. Knipe, & P. M. Howley, Eds.) Philadelphia: Lippincott Williams and Wilkins.

Mathewson, A. C., Bishop, A., Yao, Y., Kemp, F., Ren, J., Chen, H., . . . Jones, I. M. (2008). Interaction of severe acute respiratory syndrome-coronavirus and NL63 coronavirus spike proteins with angiotensin-converting enzyme-2. *Journal of General Virology*, 2741-2745.

Mercado, N., Zahn, R., Wegmann, F., Loos, C., Chandrashekar, A., Yu, J., . . . Peter, L. (2020). Single-shot Ad26 vaccine protects against SARS-CoV-2 in rhesus macaques. *Nature*, 583-588.

Merkl, P. E., Orzalli, M. H., & Knipe, D. M. (2018). Mechanism of host IFI16, PML, and Daxx protein restriction of Herpes Simplex Virus 1 replication. *Journal of Virology*, e00057-18.

Milewskaa, A., Nowaka, P., Owczareka, K., Szczepanskia, A., Zarebskic, M., Hoangc, A., . . . Pyrc, a. K. (2018). Entry of Human Coronavirus NL63 into the Cell. *Journal of Virology*, 1-17.

Minakshi, R., Padhan, K., Rani, M., Khan, N., Ahmad, F., & Jameel, S. (2009). The SARS Coronavirus 3a Protein Causes Endoplasmic Reticulum Stress and Induces Ligand-Independent Downregulation of the Type 1 Interferon Receptor. *Plos One*, 1-10.

Miranda, C., Silva, V., Igrejas, G., & Poeta, P. (2021). Genomic evolution of the human and animal coronavirus diseases. *Molecular Biology Reports*, 6645-6653.

Mishra, S., Raj, A. S., Kumar, A., Rajeevan, A., Kumari, P., & Kumar, H. (2022). Innate immune sensing of influenza A viral RNA through IFI16 promotes pyroptotic cell death. *iScience*, 1-16.

Mueller, S., & Rouse, B. T. (2008). Immune responses to viruses. *Clinical Immunology*, 421-431.

Nao, N., Sato, K., Yamagishi, J., Tahara, M., Nakatsu, Y., Seki, F., . . . Takeda, M. (2019). Consensus and variations in cell line specificity among human metapneumovirus strains. *PLoS One*, 1-21.

Nguyen, T., Koutsakos, M., Koutsakos, M., Druce, J., Caly, L., van de Sandt, C., . . . Cowie, B. (2020). Breadth of concomitant immune responses prior to patient recovery: a case report of non-severe COVID-19. *Nature Medicine*, 453-455.

Otieno, J. R., Cherry, J. L., Spiro, D. J., Nelson, M. I., & Trovao, N. S. (2022). Origins and Evolutions of Seasonal Human Coronaviruses. *Viruses*, 1551.

Overmyer, K., Shishkova, E., Miller, I., Balnis, J., Bernstein, M., Peters-Clarke, T., . . . et.al. (2021). Large-Scale Multi-omic Analysis of COVID-19 Severity. *Cell Syst*, 23-40.

Parisi, O. I., Dattilo, M., Patitucci, F., Malivindi, R., Delbue, S., Ferrante, P., . . . Selmin, F. (2021). Design and development of plastic antibodies against SARS-CoV-2 RBD based on molecularly imprinted polymers that inhibit in vitro virus infection. *Nanoscale*, 16821-17184.

Petrosillo, N., Viceconte , G., Ergonul, O., Ippolito, G., & Petersen, E. (2020). COVID-19, SARS, and MERS: are they closely related? *Clinical Microbiology and Infection*, 729.

Podbilewicz, B. (2014). Virus and cell fusion mechanisms. *Annu. Rev. Cell. Dev. Biol.*, 111-139.

Pradenas, E., Trinite, B., Urrea, V., Marfil, S., Avila-Nieto, C., de la Concepcion, M., . . . al, e. (2021). Stable neutralizing antibody levels 6 months after mild and severe COVID-19 episodes. *Nature Medicine*, 313-320.

Pyrc, K., Berkhout, B., & van der Hoek, L. (2007). The Novel Human Coronaviruses NL63 and HKU1. *Journal of Virology*, 3051-3057.

Pyrc, K., Jebbink, M. F., Berkhout, B., & Hoek, L. v. (2004). Genome structure and transcriptional regulation of human coronavirus NL63. *Virology Journal*, 1-11.

Raj, V. S., Mou, H., Smits, S. L., Dekkers, D. H., Muller, M. A., Dijkman, R., . . . et.al. (2013). Dipeptidyl peptidase 4 is a functional receptor for the emerging human coronavirus-EMC. *Nature*, 251-254.

Roingeard, P., Eymieux, S., Burlaud-Gaillard, J., Hourioux, C., Patient, R., & Blanchard, E. (2022). The double-membrane vesicle (DMV): a virus-induced organelle dedicated to the replication of SARS-CoV-2 and other positive-sense single-stranded RNA viruses. *Cell Mol Life Sci*, 425.

Roltgen, K., Powell, A., Wirz, O., Stevens, B., Hogan, C., Najeeb, J., . . . Huang, M. (2020). Defining the features and duration of antibody responses to SARS-CoV-2 infection associated with disease severity and outcome. *Science Immunology*, 956-963.

Shereen, M. A., Khan, S., Kazmi, A., Bashir, N., & & Siddique, R. (2020). COVID-19 infection: Origin, transmission, and characteristics of human coronaviruses. *Journal of advanced research*, 91-98.

Sun, L., Xing, Y., Chen, X., Zheng, Y., Yang, Y., Nichols, D. B., . . . Chen, Z. (2012). Coronavirus Papain-like Proteases Negatively Regulate Antiviral Innate Immune Response through Disruption of STING-Mediated Signaling. *Plos One*, 1-11.

Swanson, K. V., Deng, M., & Ting, J. P.-Y. (2019). The NLRP3 inflammasome: molecular activation and regulation to therapeutics. *Nature Reviews Immunology*, 477-489.

Tang, T., Bidon, M., Jaimes, J. A., Whittaker, G. R., & Daniel, S. (2020). Coronavirus membrane fusion mechanism offers a potential target for antiviral development. *Antivir. Res.*, 1-16.

Tang, T., Bidon, M., Jaimes, J. A., Whittaker, G. R., & Daniel, S. (2020). Coronavirus membrane fusion mechanism offers a potential target for antiviral development. *Antiviral Research*, 1-16.

Tang, T., Bidon, M., Jaimes, J. A., Whittaker, G. R., & Daniel, S. (2020). Coronavirus membrane fusion mechanism offers a potential target for antiviral development. *Antiviral Research*, 1-16.

Telenti, A., Arvin, A., Corey, L., Corti, D., Diamond, M. S., García-Sastre, A., . . . Virgin, H. W. (2021). After the pandemic: perspectives on the future trajectory of COVID-19. *Nature*, 495-504.

Unterholzner, L., Keating, S. E., Baran, M., Horan, K. A., Jensen, S. B., Sharma, S., . . . Bowie, A. G. (2011). IFI16 is an innate immune sensor for intracellular DNA. *Nature Immunology*, 1-19.

Van der Hoek, L., Pyrc, K., Jebbink, M. F., & al., e. (2004). Identification of a new human coronavirus. *Nature Medicine*, 368-373.

V'kovski, P., Kratzel, A., Steiner, S., Stalder, H., & Thiel, V. (2021). Coronavirus biology and replication: implications for SARS-CoV-2. *Nature Reviews: Microbiology*, 155-170.

Walls, A. C., Tortorici, M. A., Snijder, J., Xiong, X., Bosch , B. J., Key, F. A., & Veesler, D. (2017). Tectonic conformational changes of a coronavirus spike glycoprotein promote. *Proc. Natl. Acad.*, 11157-11162.

Wichit, S., Hamel, R., Yainoy, S., Gumpangseth, N., Panich, S., Phuadraksa, T., . . . Missé, D. (2019). Interferon-inducible protein (IFI) 16 regulates Chikungunya and Zika virus infection in human skin fibroblasts. *EXCLI J*, 46.

Woo, J., Lee, E. Y., Lee, M., Kim, T., & Cho, Y. E. (2019). An in vivo cell-based assay for investigating the specific interaction between the SARS-CoV N-protein and its viral RNA packaging sequence. *Biochem. Biophys. Res. Commun.*, 499-506.

Woo, P. C., Lau, S. K., Chu, C. M., Chan, K. H., Tsoi, H. W., Huang, Y., . . . Cai, J. J. (2005). Characterization and complete genome sequence of novel coronavirus, coronavirus HKU1, from patients with pneumonia. *Journal of Virology*, 884-895.

World Health Organization. (2022, November 10). Retrieved from COVID-19: https://covid19.who.int/region/afro/country/za

Wurtz, N., Penant, G., Jardot, P., Duclos, N., & Scola, L. (2021). Culture of SARS-CoV-2 in a panel of laboratory cell lines, permissivity, and differences in growth profile. *Eur J Clin Microbiol Infect Dis*, 477-484.

Xia, H., Cao, Z., Xie, X., Zhang, X., Chen, J. Y.-C., Wang, H., . . . Shi, P.-Y. (2020). Evasion of Type I Interferon by SARS-CoV-2. *Cell Reports*, 1-15.

Xin, L., Hayes, K. H., Susanna, K. P., & Patrick, C. Y. (2019). Human Coronaviruses: General Features. *Reference Module in Biomedical Sciences*.

Yang, L., Xie, X., Tu, Z., Fu, J., Xu, D., & Zhou, Y. (2021). The signal pathways and treatment of cytokine storm in COVID-19. *Signal Transduction and Targeted Therapy*, 1-20.

Ye, Z.-W., Yuan, S., Yuen, K.-S., Fung, S.-Y., Chan, C.-P., & Jin, D.-Y. (2020). Zoonotic origins of human coronaviruses. *International Journal of Biological Sciences*, 1686-1697.

Zhang, G., Cowled, C., Shi, Z., Huang, Z., Bishop-Lilly, K. A., Fang, X., . . . Jiang, X. (2012). Comparative Analysis of Bat Genomes Provides Insight into the Evolution of Flight and Immunity. *Science*, 456-460.

Zheng, D., Liwinski, T., & Elinav, E. (2020). Inflammasome activation and regulation: toward a better understanding of complex mechanisms. *Cell Discovery*, 1-22.

Zhuang, Z., Liu, D., Sun, J., Li, F., & Jincun, Z. (2022). Immune responses to human respiratory coronavirus infection in mouse models. *Current Opinion in Virology*, 102-111.